THESIS

# FLUORESCENT NANOSPHERE TRANSPORT: GROUNDWATER TRACING AND IMPLICATIONS FOR NANOPARTICLE MIGRATION THROUGH GROUNDWATER SYSTEMS

Submitted by

Charlene N. King

Department of Geosciences

In partial fulfillment of the requirements

For the Degree of Master of Science

Colorado State University

Fort Collins, Colorado

Fall 2015

Master's Committee:

Advisor: William E. Sanford
Co-Advisor: Yan Vivian Li

Michael J. Ronayne
Thomas Sale

# ABSTRACT

## FLUORESCENT NANOSPHERE TRANSPORT: GROUNDWATER TRACING AND IMPLICATIONS FOR NANOPARTICLE MIGRATION THROUGH GROUNDWATER SYSTEMS

Engineered nanoparticles (NPs) are being introduced to water supplies and many NPs have been shown to have deleterious effects on plants and animals; however, their behavior in natural substrates is not well characterized. In an effort to characterize nanoparticle migration through porous media a dual-tracer of fluorescent carbon nanospheres (CNP) and bromide (Br) were deployed through columns of porous media designed to be homogeneous, have dual-porosity, or be reactive. The CNP are hydrophilic, non-toxic, inert, and only 5 to 10 nm in diameter. Unlike other colloid tracers CNP are designed to be inexpensive, easy to identify, and not susceptible to pore throat filtering or settling making them an ideal particle tracer. The results of the homogeneous tests show that CNP and Br had identical breakthrough curves with retardation factors close to 1, confirming that CNP transport conservatively through silica sand. The results of the dual-porosity tests suggested that CNP may undergo slightly less transverse diffusion (mass transfer) into the immobile zone than the solute tracer Br. However the differences were less than expected because molecular diffusion was overwhelmed by the high pore velocities in the experiments. The results of the reactive media tests showed that in columns with surface-modified zeolite (SMZ) the CNP transported conservatively, while Br had a retardation factor 11 to 18 times higher, due to sorption.

This means that the CNP can function as the conservative species used in a multiple tracer test to quantify the surface area exposure of other minerals or contaminants with a surface charge along preferential flow paths. During each of these experiments the average

mass recovery for CNP was 95% indicating that there was minimal mass loss from pore throat filtering, settling, or sorption.

Not only are CNP an extremely useful new tracer for groundwater systems, but they also provide insight as to how other NPs might be transported once introduced into the subsurface. NPs with surfaces that have been functionalized to be hydrophobic or preferentially sorb to a target constituent behave differently. If NPs which sorb to a particular contaminant are introduced to the subsurface it could facilitate transport of that contaminant or facilitate sorption. Similarly the rapid transport properties of hydrophilic NPs should be considered where any toxic NP is being introduced to natural systems.

ACKNOWLEDGEMENTS

I would first like to thank my advisors Dr. William E. Sanford and Dr. Yan Vivian Li and committee members Dr. Thomas Sale and Dr. Michael Ronayne for their technical expertise and guidance throughout my research. Their combined knowledge of groundwater tracers and nanotechnology made this research possible. It has been a wonderful experience getting to design my own experiments in order to contribute to their combined vision for the overall project.

This project was also possible through the cooperation of several departments at Colorado State University. I would also like to thank Dr. Thomas Sale at the Center for Contaminant Hydrology, for providing access and use of the facilities at the Engineering Research Center. They provided additional equipment and supplies which aided in the completion of this research, as well as the skilled machinist, Bart Fink, who prepared our columns. Special thanks also goes out to Amy Nalls, Dr. Davin Henderson, and the rest or their team in the Department of Pathology for granting me the use of the microplate readers in the Hoover-Mathiason Laboratory.

My research would also not have been possible without the support from the Graduate Research Grant program at the Geological Society of America. Additional thanks are due to the CSU Water Center, who provided partial funding, including my research assistantship. And to the Department of Geosciences for providing an excellent graduate experience, as well as a summer research grant which assisted in the purchase of laboratory supplies.

Lastly I would like to recognize my husband, Ryan Graham, for coming back to graduate school with me. His loving care and commiseration has been a constant support.

TABLE OF CONTENTS

LIST OF TABLES

LIST OF FIGURES

# LIST OF UNITS

Prefix

| | |
|---|---|
| c- | centi- ($10^{-2}$) |
| m- | milli- ($10^{-3}$) |
| µ- | micro- ($10^{-6}$) |
| n- | nano- ($10^{-9}$) |

Time [T]

| | |
|---|---|
| d | days |
| min | minutes |
| s | seconds |

Length [L]

| | |
|---|---|
| m | meters |

Mass [M]

| | |
|---|---|
| g | grams |

Miscellaneous

| | |
|---|---|
| ℃ | degrees Celsius |
| eq | equivalents |
| L | liter |
| ppm | parts per million |
| V | volts |

# LIST OF PARAMETERS

Alphanumeric

| | |
|---|---|
| $c$ | concentration [$ML^{-3}$] |
| $c_0$ | initial concentration [$ML^{-3}$] |
| $c_r$ | resident concentration [$ML^{-3}$] |
| $C$ | normalized concentration, or relative concentration [dimensionless] |
| $C_0$ | normalized initial concentration, (equal to 1) [dimensionless] |
| $C_f$ | normalized flux-averaged concentration [dimensionless] |
| $C_r$ | normalized resident concentration [dimensionless] |
| $D$ | hydrodynamic dispersion coefficient [$L^2T^{-1}$] |
| $D_m$ | hydrodynamic dispersion coefficient of the mobile zone [$L^2T^{-1}$] |
| $D^*$ | molecular diffusion coefficient [$L^2T^{-1}$] |
| $K_d$ | empirical partitioning coefficient [$L^3M^{-1}$] |
| $L$ | column length [L] |
| $M_r$ | mass recovery [%] |
| $P$ | Peclet number [dimensionless] |
| $Q$ | column flow rate [$L^3/T$] |
| $r$ | column radius [L] |
| $R$ | retardation factor [dimensionless] |
| $t$ | time [T] |
| $T$ | normalized time, or pore volumes [dimensionless] |
| $T_{ap}$ | pore volumes of tracer applied [dimensionless] |
| $T_r$ | pore volumes of tracer recovered [dimensionless] |

| | |
|---|---|
| $v$ | average pore velocity [$LT^{-1}$] |
| $v_m$ | average pore velocity of the mobile zone [$LT^{-1}$] |
| $V_w$ | volume of water in porous media [$L^3$] |
| $V_v$ | volume of voids in porous media [$L^3$] |
| $V_T$ | total volume of porous media [$L^3$] |
| $x$ | longitudinal location within the column [L] |
| $Z$ | relative position within the column [dimensionless] |

Greek

| | |
|---|---|
| $\alpha$ | dispersivity [L] |
| $\beta$ | partitioning coefficient [dimensionless] |
| $\varepsilon$ | first-order kinetic rate coefficient [$T^{-1}$] |
| $\theta$ | total porosity [dimensionless] |
| $\theta_g$ | gravimetric water saturation [dimensionless] |
| $\theta_{im}$ | immobile porosity [dimensionless] |
| $\theta_m$ | mobile porosity [dimensionless] |
| $\theta_v$ | volumetric water saturation [dimensionless] |
| $\rho_b$ | bulk density of porous media [$ML^{-3}$] |
| $\omega$ | mass transfer coefficient [dimensionless] |

# CHAPTER 1: INTRODUCTION

## ENVIRONMENTAL CONCERNS ABOUT NANOPARTICLES

Colloids are particles less than 10 µm, which remain suspended in solution without settling. This particle class includes nanoparticles (NP) which range in size from 1 to 100 nm (Hofmann and von der Kammer 2009). NP can be naturally-occurring, but due to their unique properties, such as their small size and reactivity, they are also increasingly being engineered for use in industrial and household applications. The wide variety of household products includes textiles, appliances, cosmetics, and pharmaceuticals. Other industrial applications include specialized coatings, automotive parts, catalysts, and electronics. In 2010 an estimated 260,000 to 309,000 metric tons of engineered NP were produced across the globe, the majority of which are projected to end up in landfills as shown in the flow diagram in Figure 1.1 (Keller et al. 2013).

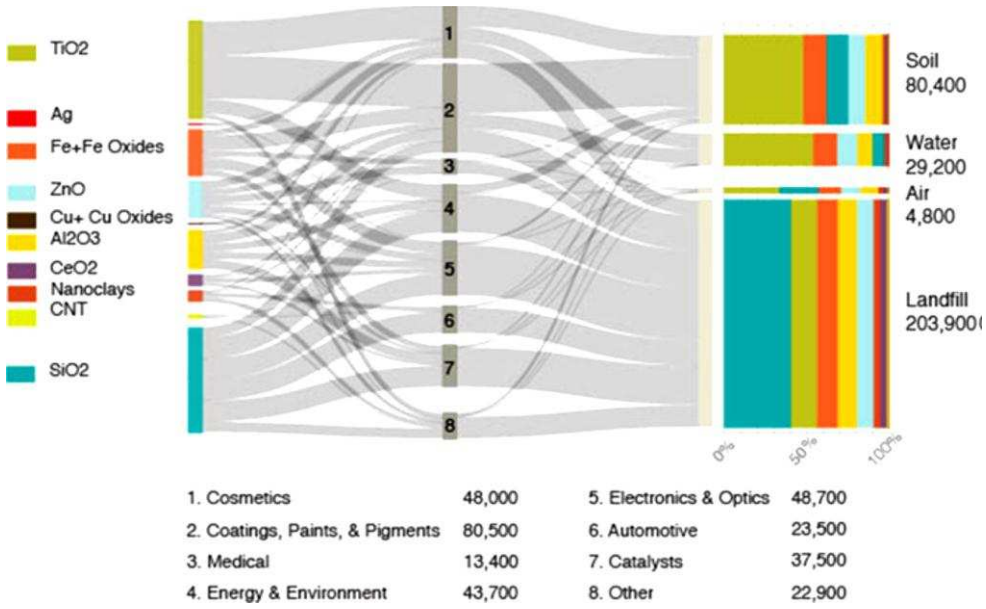


**Figure 1.1 Flow of engineered NP for 2010 in metric tons/year, from Keller et al. 2013**

Many of these consumer goods cast off NP throughout the life of the product which can enter the surface or groundwater systems. Nanomaterials that end up in landfills exuviate NP into the surrounding soil, which can infiltrate the saturated zone and leak through the liner of the landfill. The NP can also directly enter surface water bodies or detention basins through runoff from improperly discarded nanomaterials, weathering paints and coatings, or leaking, mechanically-abraded, chemically or thermally-stressed automotive parts and other nanomaterials (Wagner et al. 2014). NP can also end up in wastewater systems through household use. Silver (Ag) and zinc (Zn) NP are used as antibacterial to disinfect water in disaster relief situations, and some NP have been shown to leach out of these filters (Loo et al. 2013). If these filters are discarded improperly, the NP can enter the local environment. Ag-NP are also used to coat textiles for antibacterial clothing, and have been shown to release as much as 377 µg of NP per g of material during their first cycle in a washing machine (Geranio et al. 2009). If the household is on a septic system, the NP can remain suspended in the wastewater leaving the septic tank and will be free to migrate downward to the water table over time.

Even those NP which enter a municipal sewer systems are not all removed by wastewater treatment plants (Farkas et al. 2011; Chalew et al. 2013; Jarvie et al. 2009). One study in particular noted that under the most probable water chemistry and NP coating conditions during prefiltration stages, only between 68 to 90% of the titanium dioxide ($TiO_2$) NP were removed (Kinsinger et al. 2015). Treatment plant effluent enters the environment, either by being expelled into nearby water bodies, sprayed over infiltration fields, or injected directly into the subsurface. As a result these particles are increasingly being introduced to the subsurface and aquatic ecosystems, entering the water cycle, and potentially making it back into private and municipal drinking water supplies. This has become a cause for concern since many NP are known to have toxic effects.

Toxicology studies have indicated that Ag-NP and Zn-NP cause significant plant biomass reduction and cell death in animals as well (Lin and Xing 2008; Stampoulis et al. 2009; Som et al. 2011). $TiO_2$-NP are one of the most widely manufactured NP due to their use in sunscreens, paints, and photovoltaic cells, and experiments have demonstrated that they cause cell wall damage in benthic biofilms and planktonic organisms of streams (Fang et al. 2008; Battin et al. 2009). Impairment of DNA and degradation of hemocyte cells in gastropods has also been documented due to $TiO_2$-NP exposure as shown in Figure 1.2 (Ali et al. 2015). Other NP have also been shown to cause cell and DNA damage in bacteria, rats, fish, and humans (Oberdörster et al. 2007; Brar et al. 2009). Cells can be exposed to damage through inhalation, ingestion, and dermal contact (Wiesner et al. 2006).

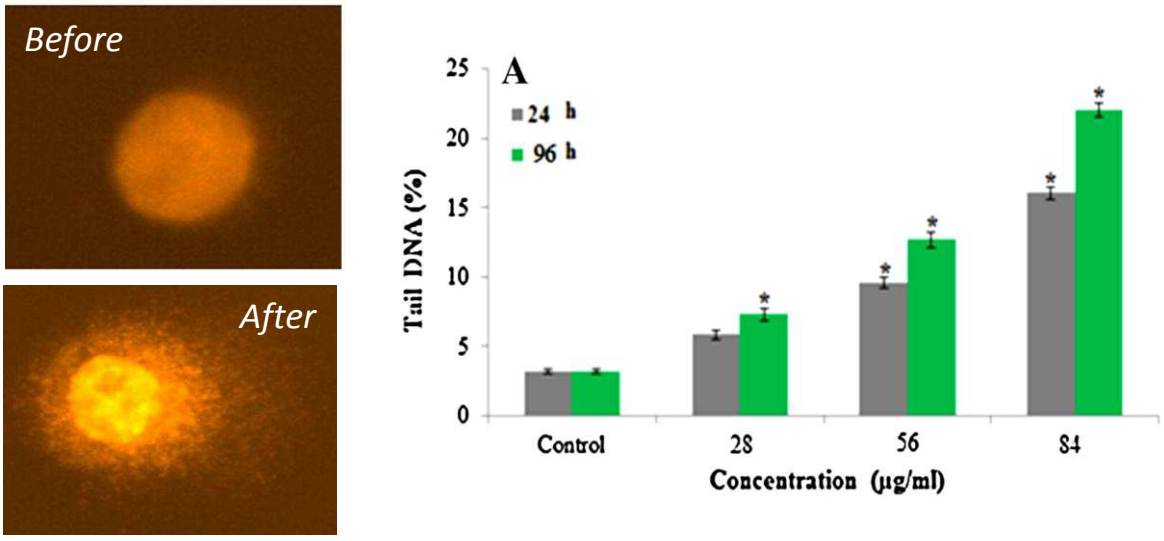


**Figure 1.2 Impairment of gastropod DNA (hemocyte cells) with increasing exposure to $TiO_2$-NP, from Ali et al. 2015**

NANOPARTICLE AND COLLOID TRANSPORT

Though NP are entering the water cycle, and subsequently ecosystems and potentially drinking-water supplies, little research has addressed how they move through the subsurface. Lecoanet et al. (2004b) conducted column experiments to study NP transport using different compositions and sizes of colloids and found that mobility in saturated porous media varies greatly. NP as well as larger colloids have different levels of mobility due to chemical reactivity, solubility, their shape and size potential for settling, dispersing, or being filtered, as well as the role of their surface charges in their propensity to sorb, aggregate, or flocculate (Huber et al. 2012). The effect that particle size has on the mobility and molecular diffusion potential of nanoparticles is demonstrated in Figure 1.3 from Skaug et al. 2015.

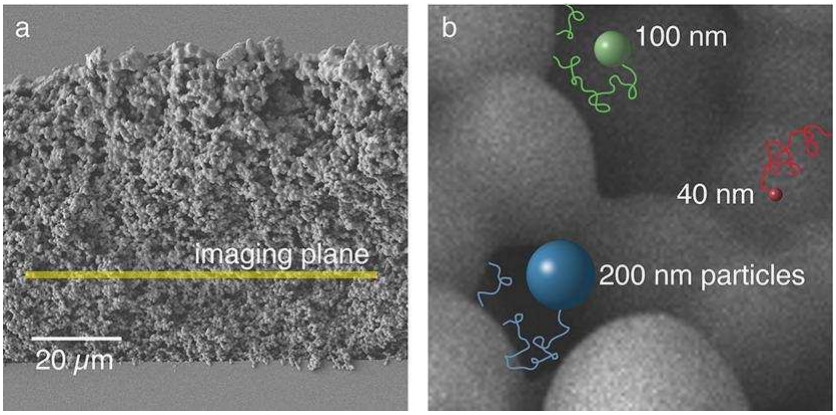


**Figure 1.3 Comparison of colloid and NP size ranges and pore throat sizes to demonstrate pore-throat limited diffusion, from Skaug et al. 2015**

Though NP can be manufactured and their surfaces can be functionalized to alter these traits, environmental characteristics such as mineral composition, fracture roughness, aqueous chemistry, and fluid velocity have a significant effect on colloid mobility (Becker et al. 1999; Crist et al. 2005; Alonso et al. 2009; Lecoanet and Wiesner 2004a). Another concern driving the

need to adequately characterize NP transport is that NP can facilitate contaminant transport through groundwater systems (Hofmann and von der Kammer 2009). Colloid-contaminant cotransport has been observed at several study sites, including radionuclide contaminated sites at Oak Ridge National Laboratory and Los Alamos National Laboratory, and when this transport mechanism is not taken into account it can result in large underestimations of contaminant spread (McCarthy and Zachara 1989; McCarthy et al. 1998a, 1998b; Penrose et al. 1990).

The reactivity of colloids and NP can make it difficult to use them to determine the flow and transport properties of a system and of the NP themselves. Due to this, non-reactive (conservative) colloids can aid the study of these characteristics, and can also be developed as a useful groundwater tracers. In the past, conservative colloids have been useful tracers to quantify preferential flow. This is due to the fact that non-reactive colloids have an earlier arrival time in effluent compared with solute tracers because solute arrival is retarded more by matrix diffusion. Solute back-diffusion can cause extreme breakthrough curve tailing after the peak concentration has passed in dual-porosity systems and this tailing is far less pronounced with colloids since it is mainly governed by desorption kinetics (McKay et al. 2000). The interest in studying the transport that largely follows flow streamlines has resulted in a large volume of research in the past where larger colloids have been used as conservative tracers. Though it was originally assumed that the greater surface area to volume ratio of small colloids, like NP, would cause them to be more reactive and sorb, the opposite mass recovery trend has been observed. This is because the recovery of larger colloids can be impacted more by gravity settling and pore-throat filtering (Reimus 1995).

Colloid transport characteristics in addition to their smaller size make inert NP attractive potential tracers which need to be characterized. Different forms of zero-valent Iron NP ($Fe^0$-NP) are currently used in groundwater remediation because they can be functionalized to sorb to target contaminants such as chromium and chlorinated solvents. They are not used to

quantify contamination however, but once attached, $Fe^0$-NP breakdown target contaminants through oxidation, and then become trapped within the subsurface (Reyhanitabar et al. 2012). This nanotechnology application takes advantage of their instability, but their magnetism causes aggregation which severely limits transport (Kanel et al. 2008). Even $Fe^0$-NP which have been surface stabilized make poor potential groundwater tracers because of their reactivity and density flow effects (Basnet et al. 2015). Ag-NP as well as Ti-NP have also been shown to attenuate in the subsurface due to aggregation and subsequent pore-throat filtering and their recovery is affected by the presence of organic matter or pH of the pore fluid, making them unsuitable for groundwater tracing (Yang et al. 2014; Sygouni & Chrysikopoulos 2015). Toxicity of metal NP also limit their potential use as tracers in the environment.

In order to characterize the transport behavior of smaller colloids a non-toxic, non-reactive NP needs to be developed for use as a groundwater tracer. Non-toxic silica NP labeled with fluorescent dye have been tested for potential as tracers, but the NP had a mean size of 88 nm in diameter, and the detection limit was as high as 5 mg/L (Vitorge et al. 2014). Carbon nanospheres (CNP) are inert and non-toxic (Li et al. 2014), have a much smaller diameter, and much lower detection limit. Due to these characteristics they have the potential to be a conservative NP tracer in order to study NP transport behavior, characterize preferential flow paths, and even track other engineered NP migration through porous media.

## THE STATE OF RESEARCH AND POTENTIAL OF CNP

Subramanian et al. (2013) used inert, fluorescent, CNP, which are 5 to 10 nm in diameter, along with a conservative tracer to determine the degree of preferential flow in columns of bimodal glass beads arranged to simulate heterogeneous porous media and fractured rock conditions. The results show that under these conditions CNP do not significantly

react, sorb, or diffuse into the matrix and immobile zones, which makes them an ideal potential groundwater tracer. A single field test, a push-pull tracer test, has also used these CNP to assess the flushing efficiency of a produced oil reservoir in carbonate-rock with groundwater conditions greater than 100℃ in temperature and 120,000 ppm in salinity (Kanj et al. 2011). The CNP remained stable with only minor adsorption. These results can be built upon for a variety of natural settings so that CNP can be applied to problems of preferential flow including fractured-rock groundwater systems. Since CNP are so stable it also has potential as a tracer in hydraulic fracturing fluid to address potential impact to local groundwater supplies. The ability to positively identify contaminant source will be instrumental in improving environmental protections as well as oil & gas production efficiencies.

Another potential use for this tracer will be to quantify target material volumes within porous media. When minerals are present in the column which react with a solute tracer, then multiple tracers (both reactive and conservative) can be used to quantify the amount of target substance present (e.g. Divine et al. 2003). If hydrophilic CNP is demonstrated to transport conservatively through natural porous media it could be used as the conservative tracer during such an experiment. It may also be feasible to functionalize CNP to be hydrophobic and preferentially sorb to target contaminants such as NAPLs. Tests using multiple tracers (reactive and conservative) have been conducted to assess the magnitude of NAPL plumes using various alcohols and solute tracers, but it may be more efficient to use NP especially in a fractured rock system when the goal is to quantify contaminant in the mobile zone only (Annable et al. 1998).

If CNP transport conservatively though groundwater systems contaminated with chlorinated solvents then they could also be used to characterize the contaminated system. In addition to this, they can be deployed with $Fe^0$-NP during remediation to assess the sweep efficiency of the NP injection to the contaminated zone.

## RESEARCH OBJECTIVES

To analyze the transport of CNP in porous media the nanospheres were tested in columns of sediments and reactive materials with homogeneous and dual-porosity designs. It was important to first verify that the CNP transport as a conservative tracer so that they can be used to assess the differences in transport with reactive NP.

In columns of homogeneous porous media the two tracers should behave similarly, since the bromide also transports conservatively through homogeneous systems. This means that the breakthrough curves for CNP and bromide should overlie each other, resulting in nearly identical retardation factors.

In dual-porosity columns the bromide should undergo greater transverse diffusion (mass transfer) into lower permeability zones or immobile zones, whereas the CNP should travel more along preferential flow paths. This means that in dual-porosity systems the breakthrough curve of bromide should be retarded and have a lower peak relative concentration than the CNP, as well as pronounced tailing due to back-diffusion.

For the reactive media columns, the reactive material used is a surface modified zeolite (SMZ), which has an internal immobile porosity and has been treated with a surfactant to have a positive surface charge. So that, in addition to diffusing into the immobile porosity, the bromide anion should also react to the positively charged mineral surfaces, while the CNP should undergo minimal diffusion into the immobile zone and no sorption. Therefore the breakthrough curve of the bromide should have a lower peak relative concentration, pronounced tailing, and a significantly retarded arrival when compared to the CNP. The CNP should continue to have a retardation factor close to one, and nearly complete mass recovery unlike the bromide. The conceptual model for tracer breakthrough in the dual-porosity and reactive porous media columns is summarized in Figure 1.4. This means that the CNP could potentially be used to

quantify the fastest colloid transport times through porous media, assess the degree of preferential flow, and to detect the presence of positively charged minerals.

I hypothesize that CNP will function as a conservative tracer with no sorption and minimal transverse diffusion into the immobile zone when compared to the solute tracer, bromide, making CNP the ideal colloid tracer.

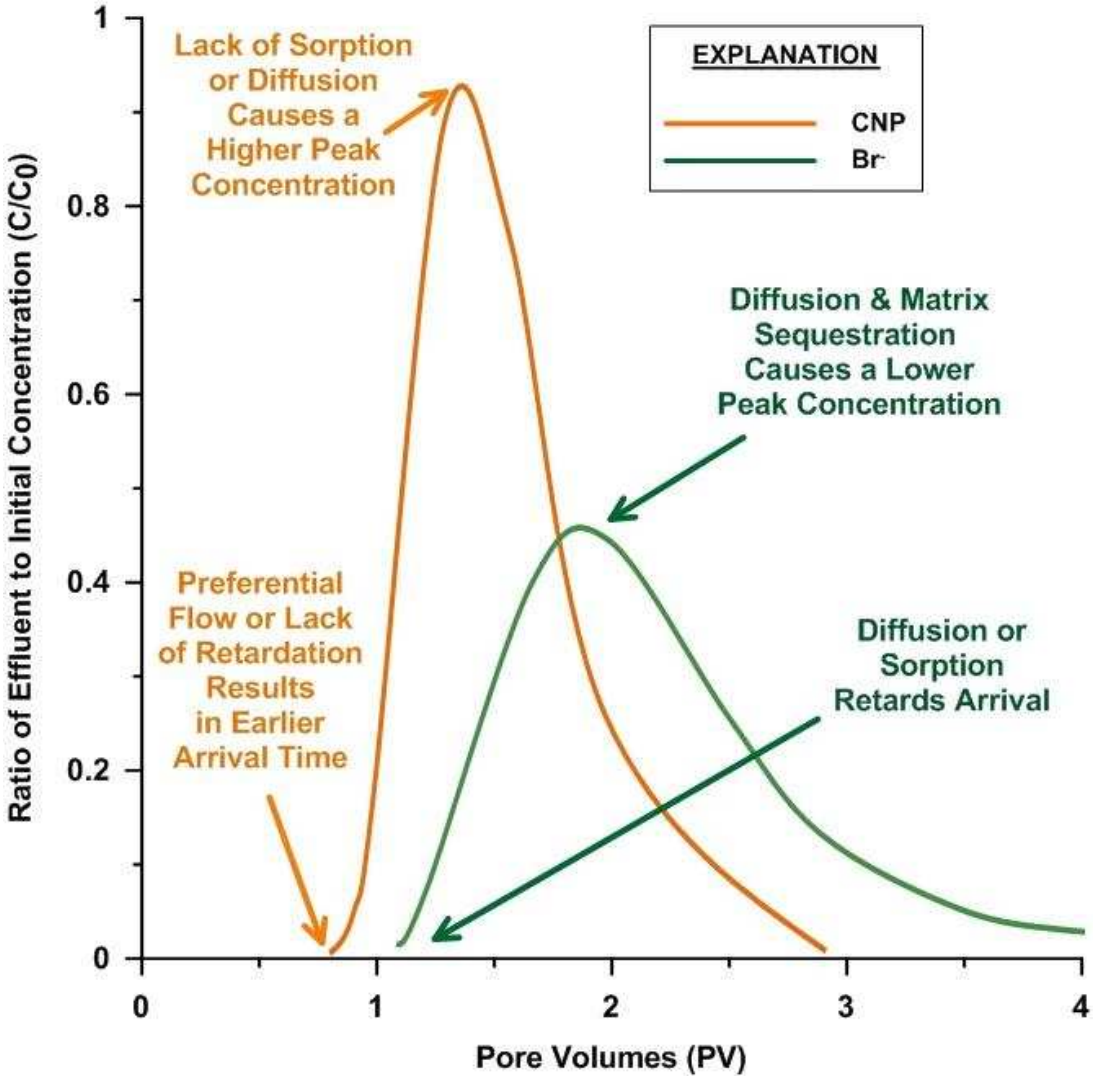


**Figure 1.4 Conceptual model for dual-porosity and reactive porous media tracer breakthrough behavior**

PAPER ORGANIZATION

This thesis is written so that CHAPTER 4 can be submitted as an independent publishable paper. A subset of tests were chosen to be included in the Results and Discussion section of the publishable paper. Lists of every Homogeneous Porous Media, Dual-Porosity, and Reactive Column test conducted are provided in Tables 1.1 through 1.3. Data sheets for all tests can be found in APPENDIX A, and all breakthrough curves and fitted parameters are provided in APPENDIX B. The publishable paper also includes an abbreviated Materials and Methods section. A more comprehensive overview of the testing materials and methods is provided in CHAPTER 2. The data processing, analysis, and curve fitting background is discussed in depth in CHAPTER 3. Within the publishable paper the pertinent details on data interpretation are included as part of the Results and Discussion section. CHAPTER 5 lists recommendations for future work with the CNP.

**Table 1.1 Tests conducted using homogeneous porous media columns**

| | **Test Details** | | | |
|---|---|---|---|---|
| **Test Name** | **Porous Media** | **Column Diameter (cm)** | **Column Length (cm)** | **Tracer Injection Method** |
| **Pulse Test #1** | coarse silica | 5.04 | 30.48 | dispersed with frit |
| **Pulse Test #2** | coarse silica | 5.04 | 30.48 | dispersed with frit |
| **Step Test** | coarse silica | 5.04 | 30.48 | dispersed with frit |

**Table 1.2 Tests conducted using dual-porosity columns**

| | Test Details | | | | | | |
|---|---|---|---|---|---|---|---|
| **Test Name** | **Core Porous Media** | **Matrix Porous Media** | **Column Diameter (cm)** | **Column Length (cm)** | **Baffle Spacing (cm)** | **Core Diameter (cm)** | **Tracer Injection Method** |
| **Design #1, Pulse Test** | coarse silica | fine silica | 5.04 | 30.48 | None | 2.54 | dispersed with frit |
| **Design #2, Pulse Test** | coarse silica | fine silica | 5.04 | 30.48 | 2.54 | 1.27 | dispersed with frit |
| **Design #3, Pulse Test #1** | coarse silica | fine silica | 5.04 | 31.76 | 2.54, with 2 extras at ends | 1.27 | directly into core |
| **Design #3, Pulse Test #2** | coarse silica | fine silica | 5.04 | 31.76 | 2.54, with 2 extras at ends | 1.27 | directly into core |
| **Design #4, Pulse Test #1** | coarse silica | fine silica | 5.04 | 31.76 | 2.54, with 2 extras at ends | 0.80 | directly into core |
| **Design #4, Pulse Test #2** | coarse silica | fine silica | 5.04 | 31.76 | 2.54, with 2 extras at ends | 0.80 | directly into core |
| **Design #3, Interruption Test** | coarse silica | fine silica | 5.04 | 31.76 | 2.54, with 2 extras at ends | 1.27 | directly into core |
| **Design #3, Long-Term Test** | coarse silica | fine silica | 5.04 | 31.76 | 2.54, with 2 extras at ends | 1.27 | directly into core |

**Table 1.3 Tests conducted using reactive porous media columns**

| | Test Details | | | |
|---|---|---|---|---|
| **Test Name** | **% Surface Modified Zeolite** | **Column Diameter (cm)** | **Column Length (cm)** | **Tracer Injection Method** |
| **Design #1, Pulse Test** | 25.0 | 5.04 | 30.48 | dispersed with frit |
| **Design #2, Pulse Test #1** | 12.5 | 5.04 | 15.24 | dispersed with frit |
| **Design #2, Pulse Test #2** | 12.5 | 5.04 | 15.24 | dispersed with frit |

# CHAPTER 2: MATERIALS AND METHODS

## POROUS MEDIA

Three types of porous media were used in the various column designs. There were two different grain sizes of silica sand, and one type of reactive media. The coarse sand which was used was 20-30 mesh Ottawa silica sand. This sand was prewashed and has grain sizes between 0.6 and 0.8 mm in diameter. The fine sand was prewashed U.S. Silica F-95 and had grain diameters between 0.1 and 0.2 mm. The porous media selected for the reactive media column tests was a surface modified zeolite (SMZ), which was prepared by the New Mexico Tech Research Foundation using zeolite sourced from St. Cloud Mine, New Mexico. It has a particle size range of 14 to 40 mesh, and mineralogical composition of 74% clinoptilolite, 12% feldspar, 12% quartz, and 5% smectite. As a result of treating the zeolite with a surfactant, it has a positive surface charge with a cation exchange capacity of 90 to 100 meq/kg of zeolite. This means it was ideally suited to react with the anion solute tracer, bromide while not reacting with the CNP.

## POROSITY CALCULATION

The packing porosity of each porous material was determined by conducting two different calculations, method A and B, using the positive displacement method. Volumes of water were measured with a graduated cylinder, and the mass of dry sand was measured with a digital scale. The water was then added to an empty 30.48 cm long, 5 cm diameter column. A known mass of sand was introduced to the column in 2 cm increments and wet-packed it with a tamping rod. Known masses of sand and volumes were added until the sediment was wet-

packed up to a height of 15.24 cm. The mass of the excess sand was then measured, as well as the volume of water above the packed sand (height times cross-sectional area) and these numbers were subtracted from the tallies to get the final volume of water ($V_w$) and final mass of sand ($M_s$). The following equations were used for the calculations:

$$\theta = \frac{\theta_A + \theta_B}{2} \tag{3.1}$$

$$\theta_A = \frac{V_w}{V_T} \tag{3.2}$$

$$\theta_B = \frac{V_v}{V_T} \tag{3.3}$$

$$V_v = V_T - V_s \tag{3.4}$$

$$V_s = M_s * \rho_s \tag{3.5}$$

Where $\theta$ is the porosity given as the average of the porosities determined from calculation A ($\theta_A$) and B ($\theta_B$), $V_T$ is the total volume of the porous media, $V_v$ is the volume of the voids, $V_s$ is the volume of the sand grains, and $\rho_s$ is the density of sand.

Once the porosity of the porous media was determined, the pore volume of that porous media was calculated. A pore volume (PV) is the volume of pore space within the amount of material which was packed into the column. By measuring flow rates as the number of pore volumes which have been flushed, time can be considered in a dimensionless form. A mobile pore volume (MPV) was calculated for any column with both an immobile and mobile zone. The MPV was used to calculate the dimensionless time where two zones were present. Results are given in Table 2.1

**Table 2.1 Porosity of packed column materials**

| Sand Type | $\theta_A$ | $\theta_B$ | $\theta$ |
|---|---|---|---|
| **Coarse Silica Sand** | 0.35 | 0.33 | 0.34 |
| **Fine Silica Sand** | 0.37 | 0.40 | 0.38 |
| **Surface-Modified Zeolite (SMZ)** | 0.50 | 0.40 | 0.45 |
| **87.5% Coarse Sand / 12.5% SMZ Mixture (by weight)** | 0.37 | 0.38 | 0.38 |
| **87.5% Coarse Sand / 12.5% SMZ Mixture (by weight) - Wetted SMZ (mobile porosity estimate)** | 0.30 | 0.28 | 0.29 |

DUAL-TRACER PREPARATION

During these tests the fluorescent carbon nanospheres (CNP) and the conservative solute tracer, bromide (as potassium bromide), were injected simultaneously into columns of well-characterized porous media. To prepare the dual-tracer we first had to manufacture the CNP. The method for preparing our CNP was documented in *Li et al. 2014*: A solution of 420 g/L citric acid monohydrate in DI water, and a solution of 367 g/L ethanolamine in DI water. Once each constituent was completely dissolved the two solutions were mixed and heated to 70 ℃ until the total volume was reduced by half. Then the solution was pyrolyzed in air, incrementally to 200 ℃, at a rate of 10 ℃/min. This results in a dense residue of solid fluorescent nanospheres which are surface functionalized to be hydrophilic, inert with a close to

neutral surface charge (zeta potential of approximately -1 to -2 mV), non-toxic, and only 5 to 10 nm in diameter. A photograph of the solid state CNP is provided in Figure 2.3.

**Figure 2.3 Solid residue of carbon nanospheres**

The CNP bulk solution was prepared by mixing 0.5 g of the solid CNP into 1 L of DI water to get a 500 ppm CNP solution. The bromide bulk solution was prepared by mixing 1 g of potassium bromide crystals into 1 L of DI water to get a 1000 ppm KBr, or 671 ppm Br solution. Bulk solutions were mixed in batches as needed and dilutions of the CNP bulk solution were prepared from each new batch for the purpose of instrument calibration. When dual-tracer was needed for a test, a mixture of 50% 500 ppm bulk CNP and 50% 671 ppm bulk Br was prepared, resulting in a dual-tracer concentration of 250 ppm CNP and 336 ppm Br.

SYSTEM DESIGN

The columns used are all 5.08 cm ID acrylic columns, machined by the Colorado State University, Engineering Research Center shop to be either 15.24 cm or 30.48 cm in length. Each end is closed by attaching a flanged end cap with screws. There are 2 different end cap types, designed to permit different uses. The 1.30 cm deep-chamber end caps are designed to accommodate a 1.3 cm thick quartz frit to evenly disperse flow across the column width. The 0.20 cm shallow-chamber end caps are designed to either accommodate a thinner frit in the future, or to secure a metal mesh under a 5.08 cm OD thick O-ring, allowing tracer to be introduced to the center of the column directly. A PTFE inlet/outlet connector was installed in the 1.27 cm NPT threaded port of each end cap, and 2.38 mm ID tygon tubing was secured using an O-ring and tightening cap.

All columns were suspended vertically with the column inlet at the bottom and outlet at the top. The outlet tubing of each column was attached to 0.5 mm ID plastic tubing using a PTFE connector, and that tubing ran to a Pharmacia Frac-100™ fraction collector programmed to collect continuous samples at 7 mL increments. The inlet tubing of each column was attached to 1 mm ID tubing using a PTFE connector, and that smaller ID tubing was installed through a Masterflex® peristaltic pump and connected to a three-way valve. The alternate inlets to the three-way valve were connected via tubing to two different reservoirs, the deionized (DI) water reservoir and the dual-tracer reservoir. A photograph of the column set up is provided in Figure 2.4.

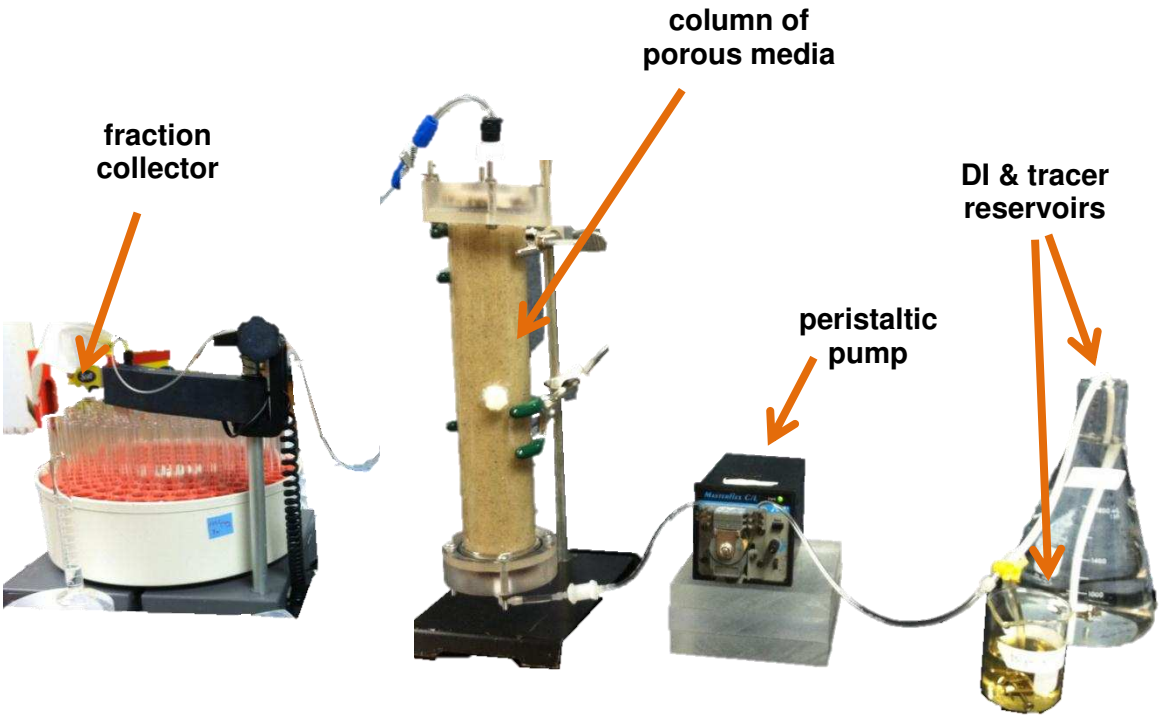


**Figure 2.4 Stitched photograph schematic of the system design for column testing**

*Homogeneous Porous Media Columns*

A 30.48 cm long column was selected for the homogeneous column tests, and the design is shown in Figure 2.5. First a deep-chamber end cap was filled with water and a 0.64 cm thick pre-wetted frit was installed, and secured with a thin 5.08 cm OD O-ring. The frit was installed to ensure that the tracer was injected evenly across the column. This end cap was installed to the inlet side of the column, and approximately 3 cm of water was poured into it. Prewashed coarse silica sand was then installed in 2 cm increments, and wet-packed with a tamping rod to a porosity of approximately 34%.

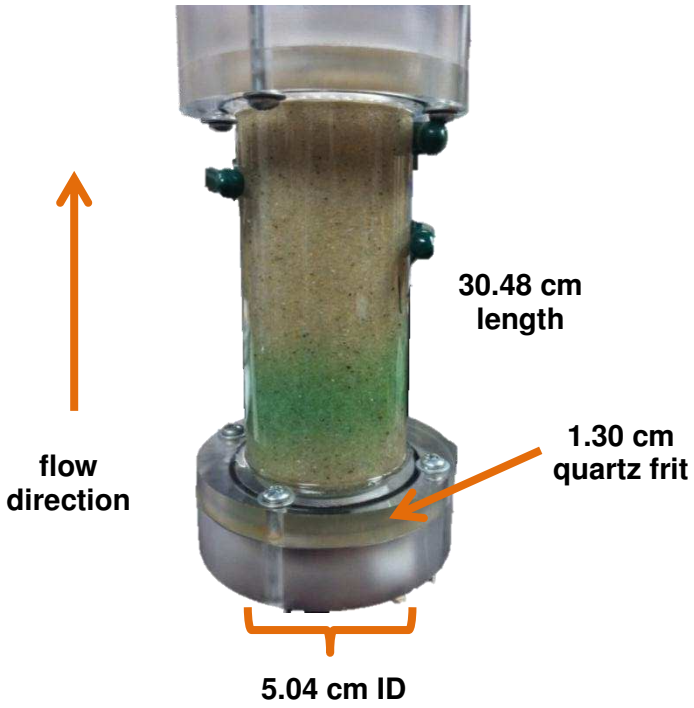


**Figure 2.5 Photograph of a homogeneous column injected with green dye to confirm that transport was occurring as an even front through the column**

*Dual-Porosity Columns*

A 30.48 cm long column was selected for the dual-porosity column tests. First a shallow-chamber end cap was filled with water and a steel mesh was installed, and secured with a thick 5.08 cm OD O-ring. The mesh was installed to prevent sand from plugging up the inlet tubing, however a frit was not installed so that the tracer would be injected directly into the core of the column. This was done so that there would be a concentration gradient between the different zones of the column. This end cap was installed to the inlet side of the column, and approximately 3 cm of water was poured into it. The column was then packed with sediment designed so that there is a lower permeability zone which is immobile and sharply separated from the preferential flow path (a coarse sediment core). To prepare the mobile zone, a removable plastic tube was placed in the center of the column, and used to install a core of

prewashed coarse silica sand, while a fine silica sand matrix was installed around it on all sides. The core was wet-packed with a tamping rod to a porosity of approximately 34%. The matrix was wet-packed with a tamping rod to a porosity of approximately 38%, and a thin plastic baffle was installed every 2.54 cm within the fine sand to make it more of an immobile zone. Three different core diameter designs were experimented with to see if a greater distinction in transverse diffusion signatures could be seen, due to higher mass transfer surface area to core volume ratios or lower pore velocities. Designs #1, #2, #3, and #4 had core diameters of 2.54, 1.27, 1.27, and 0.8 cm, respectively. Designs #1 & #2 did not utilize frits or baffles resulting in flow through the immobile zones. Only results from Design #3 are reported in CHAPTER 4, and photographs of this design are provided in Figure 2.6. All other results can be found in the Appendices.

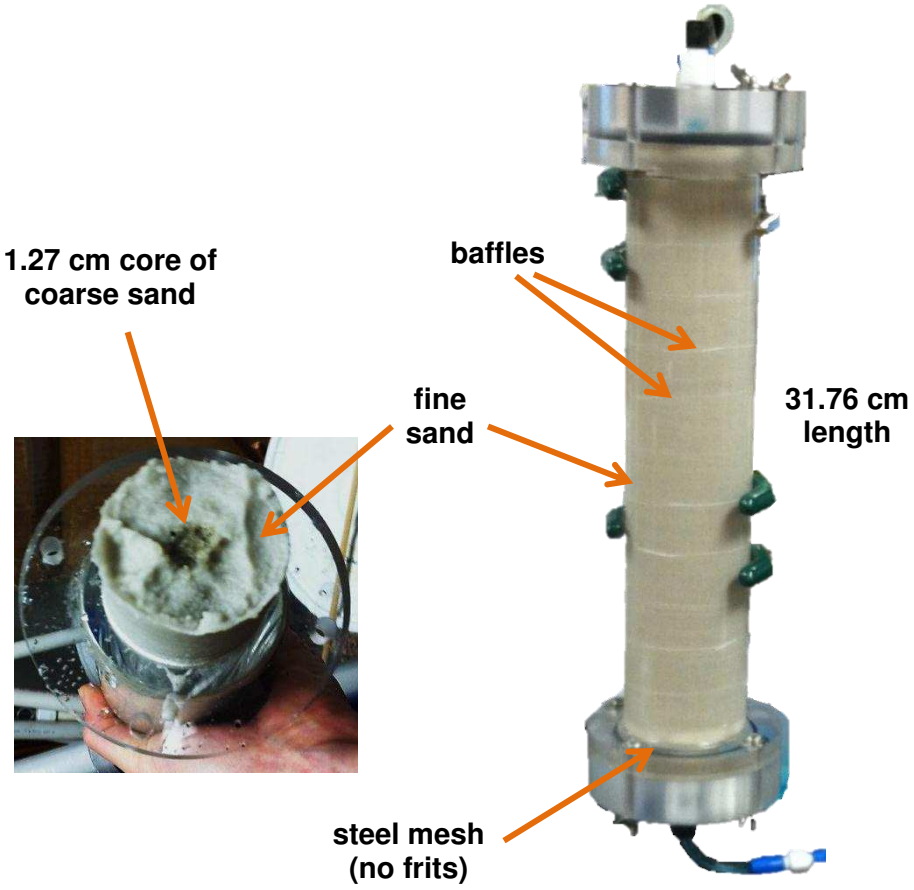


**Figure 2.6 Photographs of the dual-porosity core column design**

*Reactive Porous Media Columns*

A homogeneous mixture of prewashed coarse sand and the SMZ was prepared, and the ratio was calculated by weight. Two different designs were used for the reactive media column. Design #1 only deviated from the description below in column length (30.48 cm) and the ratio of zeolite to coarse sand (25% SMZ, by weight). Design #1 was considered unsuitable due to the near 0% bromide recovery, and results are not reported in CHAPTER 4, but can be found in the Appendices.

A 15.24 cm long column was used for Design #2 of the reactive media columns, and the design is shown in Figure 2.7. First a deep-chamber end cap was filled with water and a 0.64 cm thick pre-wetted frit was installed, and secured with a thin 5.08 cm OD O-ring. The frit was installed to disperse flow evenly across the column. This end cap was installed to the inlet side of the column, and approximately 3 cm of water was poured into it. A mixture of 12.5% SMZ by weight, and 87.5% coarse sand was then installed in 2 cm increments. It was stirred and remixed to a roughly homogeneous array, and wet-packed with a tamping rod to a mobile porosity of approximately 29%. There is also an internal immobile porosity associated with the zeolite structure itself, resulting in a total porosity of 38%.

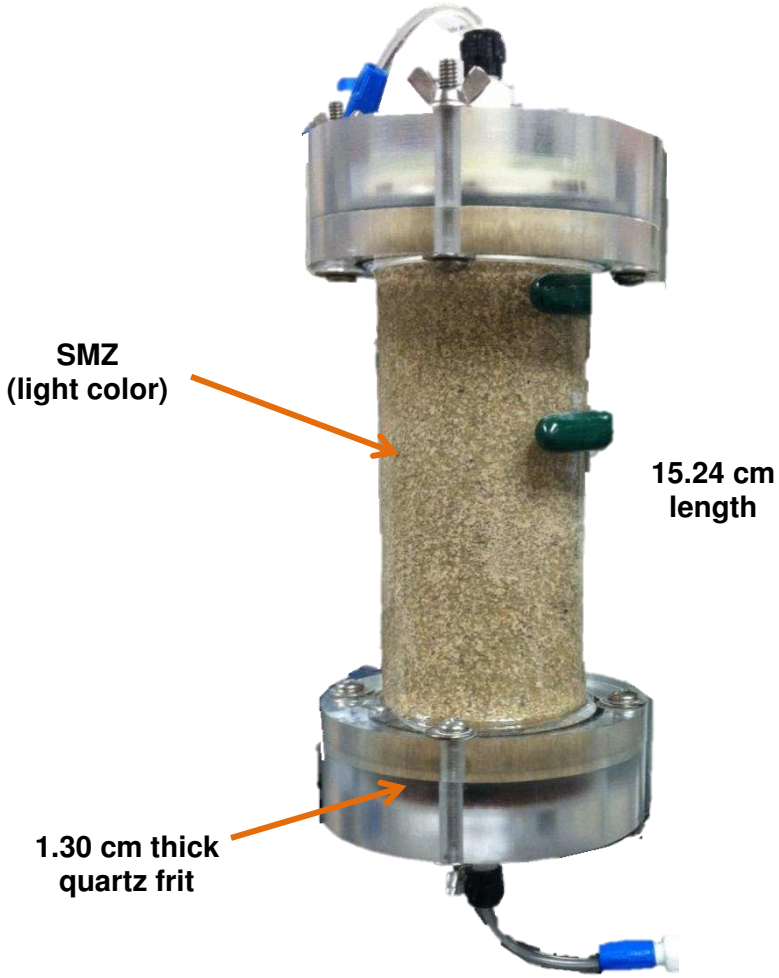


**Figure 2.7 Photograph of the reactive media column, showing the light colored areas of SMZ.**

TESTING PROCEDURE

*Preflushing*

Once each column was packed the outlet end cap was installed using the same method as the inlet. The pump was connected and DI water was flushed through the column with the PTFE outlet connector removed, until all air was removed from the outlet chamber. Then the column was preflushed with DI water at a rate of 1 to 2 mL/min for a few hours (24 hours for the reactive media to remove excess fines and surfactant). Following the preflushing period, the

pump speed was lowered and preflushed until steady-state conditions were reached. Then flow rates were measured using a stopwatch and 10-mL graduated cylinder. After several flow rates were averaged, the average flow rate was used to calculate the necessary tracer application time to achieve the desired tracer volume. Tracer application was conducted by switching the three-way valve from the DI water inlet to the dual-tracer inlet for the chosen time period.

*Pulse and Step Tests*

The tracer application time for the pulse tests was picked so that effluent concentrations should reach at least 40% of the tracer concentration at its peak. For the homogeneous tests the target tracer injection volume was ¼ of a total pore volume (TPV), but a step test was also conducted where approximately 3 TPV of tracer was injected. For the dual-porosity tests the target volumes were between 3 and 5 mobile pore volumes (MPV). And for the reactive media tests the target volumes were between 4 and 6 MPV. Effluent sample collection began at the time the tracer was turned on, and the fraction collector was programmed to collect each sample for the period of time it would take 7 mL of fluid to flow at the averaged rate. Effluent samples were collected continuously until effluent was clear of tracer or until at least 30 MPV or 4 TPV were flushed after tracer injection.

*Interruption Test*

The dual-porosity column required additional testing, due to transverse diffusion into the immobile zone which was indicated in the breakthrough curve. A second style of test, called an interruption test, was conducted where the pump was stalled for six days during tracer injection, and then stalled again for six days during the flushing period. This was done to give the tracer more time to diffuse into and then back out of the fine/immobile zone during the test.

*Long-Term Test*

Since transverse diffusion into the immobile zone of the dual-porosity column was confirmed by the interruption test, a long-term test was conducted so that the transport parameters of the bromide and CNP could be distinguished from one another. During the long-term test, tracer was injected for two weeks. Continuous samples were collected during the period of time where the effluent concentration approached the tracer concentration, then only periodic samples were collected until the tracer was shut off. Once the tracer was shut off continuous samples were collected again for a flushing period equal to approximately 50 MPV.

## EFFLUENT ANALYTICAL METHODS

Effluent samples were collected continuously in 7 mL increments in 16 cm test tubes installed in the 95 slots of the fraction collector. When it was necessary to collect additional samples to capture the breakthrough curve, a new carousel of sample tubes was installed after the 95 samples were collected. Once a carousel was removed from the fraction collector all tubes were covered and stored until analysis was conducted. A subset of the continuous samples were selected for analysis. Samples were analyzed more frequently where concentrations of either CNP or bromide were changing rapidly, and sparsely where there was little to no change occurring in the breakthrough. Samples which were not chosen for analysis, were poured into a 10-mL graduated cylinder to measure its exact volume. This volume was used to measure the change in flow rate throughout the test, since the fraction collector was filling test tubes at a known time interval.

*CNP*

CNP concentrations were measured using a FLUOstar® Omega microplate reader (spectrofluorometer). The spectrofluorometer was used to aim a specified excitation wavelength of light at the sample well of the optical bottom microplate, and then measure the intensity of a specified wavelength of light emitted by the sample in arbitrary units (a.u.). CNP emit light at a wavelength of 460 nm, and show the clearest emission signal when an excitation wavelength of 375 nm is used (Krysmann et al. 2011). The 460 nm emission filter was available on the spectrofluorometer, but the nearest excitation filter was 355 nm, which still has an acceptably strong signal, as seen in Figure 2.8 (Krysmann et al. 2011). Each microplate has 96 wells which are only 400 µL in volume, which means that a very small sample size of only 200 to 400 µL is required for analysis. First selected samples were transferred from their test tubes to clean 10-mL beakers, and then approximately 385 µL was removed from each beaker and placed in a well of the microplate, using a pipette with a fresh tip. The leftover sample was set aside for immediate bromide analysis.

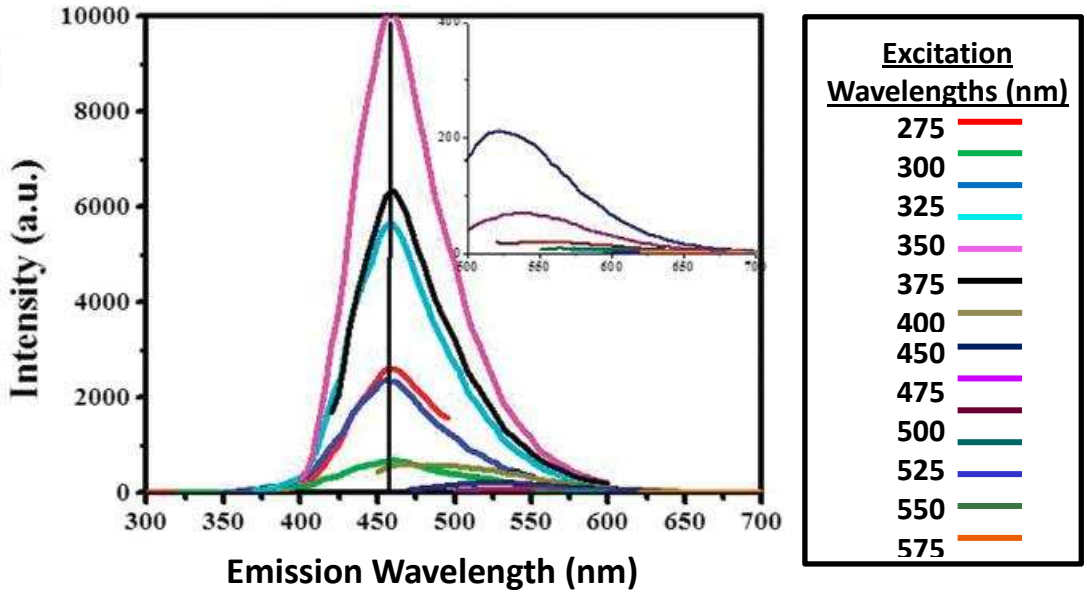


**Figure 2.8 CNP Excitation and Emission, from Krysmann et al. 2011**

Microplate sample sets were also loaded with a dilution series of bulk CNP and CNP/KBr tracer in duplicate rows for calibration purposes. Once the microplate was filled it was capped with a plastic cover, covered with plastic wrap, and stored in a Ziploc bag to protect the samples from evaporation or cross-contamination until the spectrofluorometer was available for use. Each microplate was read using a well scan protocol, where fluorescent intensity from each well was measured rapidly 308 times in a circular grid with a 4mm diameter. The fluorescent intensity measured was based on a 90% gain adjustment which was determined by the microplate reader using the well with the highest concentration of CNP in the sample set. The well scan results and averages were exported to excel, and the averages were used for data processing.

*Bromide*

Bromide concentrations were measured with a bromide ion selective electrode (ISE), using the leftover sample in each 10-mL beaker. The ISE used was an Orion™ Bromide Combination Electrode. Calibration solutions at concentrations of 5, 50, and 500 ppm bromide were prepared in 10-mL beakers using 1000 ppm bromide standard and DI water. Ionic Strength Adjuster was then added to each sample and calibration beaker at a volume equal to 0.02% of the sample volume. The ISE was then calibrated with the calibration solutions, the calibration slope was recorded, and a dilution series of the CNP/Br tracer at approximately 2.5, 25, and 250 ppm were measured and recorded. Throughout sample analysis the probe calibration was checked using the calibration solution nearest to the samples being read. When the probe reading was off by more than 5% it was recalibrated and the tracer dilutions were measured again and recorded. All bromide concentrations were recorded in ppm and comments about sample appearance, sample number, and the CNP microplate well location (rows A through H, columns 1 through 12) were noted.

# CHAPTER 3: DATA AND BREAKTHROUGH CURVE INTERPRETATION

## DATA PROCESSING

Each CNP result was divided by the highest fluorescent intensity in the sample set to get normalized values. For the Reactive Media Columns a different fluorescent intensity value had to be used to normalize the data of the effluent and the dilution samples. This was because the effluent had artificially high fluorescent intensity values due to an effect from the surfactant coming off of the SMZ. The normalized values and known concentrations of the dilution samples were graphed, and the equation of the curve-fit was used to convert all other results from normalized a.u. into concentrations in ppm. These concentrations were then divided by the measured tracer concentration of CNP to get values of relative concentration ($c/c_0$), so that they would be directly comparable to the bromide results. The bromide results were typed into the same excel file as the CNP. Each result was divided by the measured tracer concentration of bromide for that round of calibration to get values of relative concentration as well.

All relevant testing data, such as the tracer start and stop times, date of test, column design, and measured flow rates were recorded on the averages spreadsheet. The flow rates which were measured from samples taken throughout the test were averaged and this average value was used to calculate the corrected tracer volume and pore volumes (PV).

The time zero of each test was the moment when the three-way valve was turned to allow the tracer to enter the inlet tubing. The start and stop time of each sample was then determined relative to time zero. The known sampling interval from the fraction collector and recorded time of carousel switching was used to calculate the time interval of each sample. The start and stop times were averaged, and this value was used to calculate the equivalent PV

(dimensionless time) by multiplying the average sample time by the average flow rate and dividing it by the known TPV or MPV of the column. The volume of the inlet from the three-way valve to the edge of the frit in contact with sediment and the volume of the outlet from the edge of the frit in contact with the sediment to the tubing end suspended from the fraction collector arm were calculated and subtracted from the PV to get a corrected PV value. Copies of all spreadsheets are provided in APPENDIX A.

## BREAKTHROUGH CURVE ANALYSIS

The effluent relative concentrations for CNP and Br were graphed versus the corrected PV to get the breakthrough curves (BTCs). Copies of all BTCs are provided in APPENDIX B. The BTCs were first visually inspected with the conceptual model displayed in Figure 1.4 in mind. Where significant differences between the curves were seen, the relationship between the CNP and Br were tested against the conceptual model. To determine the total mass recovered, the first temporal moment analysis was conducted by directly integrating the area under each BTC using the trapezoid rule, as shown in Equation 3.1. Where $T_i$ is the dimensionless time in PV for the sample $i$, $C_i$ is the relative concentration of sample $i$, and $i-1$ refers to the prior analyzed sample.

$$T_r = \int_{t_0}^{t_f} C_i(T)dT = \sum_{i=0}^{n}(T_i - T_{i-1})\left(\frac{C_i+C_{i-1}}{2}\right) \qquad (3.1)$$

This results in the equivalent PVs of the tracer recovered ($T_r$), which was divided by the total tracer application PVs ($T_{ap}$) to get the mass recovery percentage ($M_r$) (Equation 3.2).

$$M_r = \frac{T_r}{T_{ap}} \times 100 \qquad (3.2)$$

The percent recovery was used to assess the error of the homogeneous tracer test and to assess the amount of tracer which remained sorbed to the porous media or sequestered in the immobile zone during the reactive and dual-porosity tracer tests, respectively.

## INVERSE ANALYTICAL MODELING

### *Solute and Particle Transport*

Inverse analytical modeling enables the user to estimate unknown transport parameters by fitting results of analytical models to the BTC. Each analytical model consists of a governing equation and the applicable boundary conditions, and an initial condition. The CXTFIT code, Version 2.0 was deployed using the STANMOD software to superimpose initial value problem and boundary value problem analytical solutions to fit model results to the observed column effluent concentrations (Toride et al. 1995).

The classic-advection dispersion equation (ADE) used to model solute transport is given in Equation 3.3, in terms of the resident concentration ($c_r$). The resident concentration is the volume-averaged concentration (of the liquid phase), which can be solved for at any location ($x$) and time ($t$) within the column as a function of the dispersive flux and the advective flux (van Genuchten and Alves 1982). The dispersive flux is expressed as the product of the hydrodynamic dispersion ($D$) and the derivative of the concentration gradient with respect to $x$. The advective flux is expressed in terms of the product of the average pore velocity ($v$) and the concentration gradient with respect to $x$.

Since this is a one-dimensional ADE, the hydrodynamic dispersion coefficient only describes dispersion in the direction of flow (longitudinal) and so it is a function of the

longitudinal dispersivity of the porous media ($\alpha_L$), the average pore velocity, and molecular diffusion ($D^*$), as shown in Equation 3.4.

$$\frac{\partial c_r}{\partial t} = D\frac{\partial^2 c_r}{\partial x^2} - v\frac{\partial c_r}{\partial x} \tag{3.3}$$

$$D = \alpha_L v + D^* \tag{3.4}$$

The equation is solved in CXTFIT by expressing concentration as relative concentration ($C_r$), and time in its dimensionless form as mobile pore volumes ($T$). The pore velocity parameter can be removed by converting the location within the column to a relative position ($Z$) by dividing the location $x$ by the column length ($L$) as shown in Equation 3.5. The longitudinal hydrodynamic dispersion coefficient can also be converted to the dimensionless Peclet number by using Equation 3.6. This results in the dimensionless form of the classic ADE given in Equation 3.7 (Toride et al. 1995). Terms can be added to this equation to account for tracer production, decay, retardation, mass transfer, and sorption that is limited by reactive sites.

$$Z = \frac{x}{L} \tag{3.5}$$

$$P = \frac{vL}{D} \tag{3.6}$$

$$\frac{\partial C_r}{\partial T} = \frac{1}{P}\frac{\partial^2 C_r}{\partial Z^2} - \frac{\partial C_r}{\partial Z} \tag{3.7}$$

To model the one-dimensional flow of tracer through the column boundary conditions (BC) are needed for the inlet and outlet. Since the tracer was introduced as a pulse in these experiments, it is necessary for the BC at the inlet to work for two time periods of the test; the time period where the tracer is "turned on" (injection period) and the time period once it is "turned off" (elution period). Therefore a third-type boundary condition (flux-type) must be used, which is expressed in Equation 3.8 (van Genuchten and Alves 1982). This boundary condition allows the introduced tracer concentration to vary with time, so that during injection it can be set equal to the tracer concentration and during elution it is set equal to zero. The outlet boundary condition is to assume a zero concentration gradient at some infinite distance, as shown in Equation 3.9. The initial condition for resident concentrations at any $Z$ is given in Equation 3.10, which is initially set equal to zero since the initial pore fluid is DI water with no background tracer concentrations. Each test was conducted in the same manner so that the boundary conditions and initial condition remain the same for each analytical model.

$$C_r(0,T) - \frac{1}{P}\frac{\partial C_r(0,T)}{\partial Z} = C_0(T) \tag{3.8}$$

$$\frac{\partial C_r}{\partial Z}(\infty,T) = 0 \tag{3.9}$$

$$C_r(Z,0) = C_i(Z) \tag{3.10}$$

If we were examining the tracer distribution within the column during testing the resident concentration would be all we cared about. However, the concentration data from these column tests are from the column effluent, which is the flux-averaged concentration ($C_f$). In order to fit the model results to the observed effluent concentrations, the modeled resident concentrations

must be transformed into flux-averaged concentrations using the relationship in Equation 3.11 (Toride et al. 1995).

$$C_f = C_r - \frac{1}{P}\frac{\partial C_r}{\partial Z} \tag{3.11}$$

Prior to modeling solute transport, the mechanisms governing flow were considered for each test design, a governing equation was chosen, and the unknown transport parameters were identified.

*Homogeneous Transport Model*

Solute and particle transport in a column of non-reactive (silica sand), homogeneous porous media can be described using the dimensionless classic ADE for one-dimensional transport (Equation 3.7). However the homogeneous column tests were conducted to confirm that the CNP and Br transport conservatively through silica sand, so a retardation factor ($R$) must be included and allowed to vary. Retardation here is considered as a result of linear sorption, given by Equation 3.12, where $\rho_b$ is the bulk density of the sediment and $K_d$ is the empirical linear distribution coefficient (Toride et al. 1995). This results in the governing equation shown as Equation 3.13.

$$R = 1 + \frac{\rho_b K_d}{\theta} \tag{3.12}$$

$$R\frac{\partial C_r}{\partial T} = \frac{1}{P}\frac{\partial^2 C_r}{\partial Z^2} - \frac{\partial C_r}{\partial Z} \tag{3.13}$$

$$v = \frac{Q}{\pi r^2 \theta} \tag{3.14}$$

Since the average flow rate ($Q$), column radius ($r$), and porosity ($\theta$) are known, the average pore velocity can be calculated using Equation 3.14. So the only unknown parameters which need to be solved for are the longitudinal dispersion coefficient and retardation factor. The analytical solution to this model is expressed in the terms of these dimensional transport parameters in Equation 3.15 (from van Genuchten and Alves 1982), though CXTFIT uses the dimensionless form to simplify the calculations.

$$c(x,t) = \frac{1}{2} erfc\left[\frac{Rx-vt}{2(DRt)^{1/2}}\right] + \left(\frac{v^2 t}{\pi DR}\right)^{1/2} exp\left[\frac{(Rx-vt)^2}{4DRt}\right] - \frac{1}{2}\left(1 + \frac{vx}{D} + \frac{v^2 t}{DR}\right) exp\left(\frac{vx}{D}\right) erfc\left[\frac{Rx+vt}{2(DRt)^{1/2}}\right] \quad (3.15)$$

*Dual-Porosity Transport Model*

Additional processes must be considered for solute and particle transport through a dual-porosity column. The dual-porosity column consists of two distinct zones; there is a coarse silica sand core (the mobile zone) which is surrounded by fine silica sand matrix with baffles (the immobile zone). During tracer injection preferential flow will occur through the higher permeability core, transporting the solute and particles very quickly, while the concentration gradient between the pore fluids in the core and matrix will drive mass transfer of solute and to a lesser extent the particles into the immobile zone at a much slower rate. The concentration of tracer in the immobile zone will continue to climb until it is at equilibrium with the core or until the tracer is shut off. During the elution period DI will flush the core, reversing the concentration gradient, driving tracer back out of the immobile zone, resulting in a pronounced tail on the breakthrough curve. The mobile porosity ($\theta_m$) and immobile porosity ($\theta_{im}$) are defined such that Equation 3.16 is true.

$$\theta = \theta_m + \theta_{im} \tag{3.16}$$

Due to the mass transfer process between the mobile zone and immobile zone a two-region nonequililbrium ADE, or transient storage model, must be used to model transport in the mobile and mobile zones (Equations 3.17 and 3.18). These equations include two new terms: a partitioning term which consists of the dimensionless partitioning coefficient ($\beta$), and a mass transfer term which is the product of the dimensionless mass transfer coefficient ($\omega$) and the difference in relative concentration between the mobile ($C_m$) and immobile ($C_{im}$) zones. The parameter $\beta$ is defined in Equation 3.19 which includes the fraction of adsorption sites ($f$) at equilibrium with the mobile zone, the bulk density ($\rho_b$), and the partitioning coefficient ($K_d$). The parameter $\omega$ is defined in Equation 3.20 which includes the first-order kinetic rate coefficient ($\varepsilon$) and column length ($L$). The first-order kinetic rate coefficient, $\varepsilon$, is a measure of exchange between the mobile and immobile zones, and has dimensions of inverse time. Since the grain size distribution is different from the homogeneous column the longitudinal dispersion coefficient may be different it is also an unknown parameter. However, if it is confirmed that both the Br and CNP transport conservatively through silica sand during the homogeneous test, then the retardation factor should be equal to 1 and can be disregarded. If the solutes are non-reactive this also means that $\beta$ represents the fraction of mobile water and can be expressed using Equation 3.21 instead (Toride et al. 1995). The resident concentration of both the mobile and immobile zones must be added to get the total resident concentration, as shown in Equation 3.22 and this value must be used in Equation 3.23 to get the flux-averaged concentration.

$$\beta R \frac{\partial C_r}{\partial T} = \frac{1}{P} \frac{\partial^2 C_r}{\partial Z^2} - \frac{\partial C_r}{\partial Z} - \omega(C_m - C_{im}) \tag{3.17}$$

$$(1-\beta)R\frac{\partial C_{im}}{\partial T} = \omega(C_m - C_{im}) \quad (3.18)$$

$$\beta = \frac{\theta_m + f\rho_b K_d}{\theta + \rho_b K_d} \quad (3.19)$$

$$\omega = \frac{\varepsilon L}{\theta v} \quad (3.20)$$

$$\beta = \frac{\theta_m}{\theta} \quad (3.21)$$

$$C_T = \beta R C_m + (1-\beta)RC_{im} \quad (3.22)$$

$$C_f = C_T - \frac{1}{P}\frac{\partial C_T}{\partial Z} \quad (3.23)$$

Since the flow rate, radius of the mobile zone ($r_m$), and porosity of the mobile zone are known, an average mobile zone pore velocity ($v_m$) can be calculated assuming zero flow through the immobile zone, using Equation 3.24. However this value cannot be entered directly into the two-region model because it does not reflect the velocity of both the mobile and immobile regions. Therefore the mobile zone velocity should be multiplied by the ratio of the mobile porosity to the total porosity, as shown in Equation 3.25, in order to calculate an initial estimate of an average pore velocity. Similarly, an initial estimate of the longitudinal dispersion coefficient can be made using Equation 3.26. Since $v$ and $\beta$ should be the same for both CNP and Br, by using our initial estimates and taking the average of the solution that each model converged on, we could set both $v$ and $\beta$ as known parameters during subsequent model runs in order to better solve for differences in $D$ and $\omega$.

$$v_m = \frac{Q}{\pi {r_m}^2 \theta_m} \tag{3.24}$$

$$v = \frac{\theta_m}{\theta} v_m \tag{3.25}$$

$$D = \frac{\theta_m}{\theta} D_m \tag{3.26}$$

*Reactive Transport Model*

Transport of solute and particles through the reactive porous media column must be considered in detail. The reactive media, SMZ, has an internal porosity associated with it and theoretically there could be mass transfer and partitioning taking place between the mobile porosity outside of the zeolite and the immobile porosity within the zeolite. Due to this consideration the dimensionless two-region nonequilibrium ADE was used to model transport in the reactive columns, with retardation included due to the expected reactivity (Equations 3.17 and 3.18). If the solute or particles are reactive the partitioning coefficient, $\beta$, will be defined by Equation 3.19, which includes the mobile porosity and the fraction of adsorption sites at equilibrium with the mobile zone (Toride et al. 1995).

Since the average flow rate, radius of the column, and porosity of the mobile zone are known, an average pore velocity for the mobile zone can be calculated assuming zero flow through the immobile porosity, using Equation 3.27. This value can be used to calculate the average velocity of the entire system using Equation 3.25 so that this parameter can be set as known. Additionally, since the sand and zeolite are homogeneously mixed throughout the column, any change in the longitudinal dispersion coefficient should be negligible, and the longitudinal dispersion of the mobile zone can be set equal to the results of the homogeneous

tests, so that Equation 3.26 can be used to calculate an initial estimate of $D$. So the unknown parameters which need to be solved for are the retardation factor, longitudinal hydrodynamic dispersion coefficient, partitioning coefficient, and mass transfer coefficient.

$$v_m = \frac{Q}{\pi r^2 \theta_m} \tag{3.27}$$

# CHAPTER 4: PROFESSIONAL PAPER

In an effort to characterize nanoparticle migration through porous media a dual-tracer of fluorescent carbon nanospheres (CNP) and bromide (Br) was deployed through columns of porous media designed to be homogeneous, have dual-porosity, or be reactive. The CNP are hydrophilic, non-toxic, inert, and only 5 to 10 nm in diameter. The results of the homogeneous test show that CNP and Br had identical breakthrough curves with retardation factors close to 1, confirming that CNP transport conservatively through silica sand. The results of the dual-porosity test suggested that CNP may undergo less transverse diffusion (mass transfer) into the immobile zone than the solute tracer Br. However the differences were less than expected because molecular diffusion was overwhelmed by the high pore velocities in the experiments. The results of the reactive tests showed that in columns with surface-modified zeolite (SMZ), the CNP transported conservatively, while Br had a retardation factor of 11 to 18 times higher, due to sorption. This means that the CNP can function as the conservative species used with multiple tracers to quantify the surface area exposure of other minerals or contaminants with a surface charge. During each of these experiments the average mass recovery for CNP was 95% indicating that there was minimal mass loss from pore throat filtering, settling, or sorption. These results identify CNP as a useful new fluid tracer, and their transport can inform modelling of other NP transport through the subsurface. CNP's rapid transport properties and propensity to diffuse in systems with larger pore throats should be considered where any toxic NP which is also hydrophilic is being introduced to natural systems.

# INTRODUCTION

## *Context of Research*

It is important to understand how nanoparticles (NP) are transported through porous media because they are being introduced to the environment by manufactured materials. Nanoparticles (NP) are increasingly being engineered for use in industrial and household goods including: textiles, appliances, cosmetics, pharmaceuticals, specialized coatings, automotive parts, catalysts, and electronics. In 2010 an estimated 260,000 to 309,000 metric tons of engineered NP were produced across the globe, the majority of which are projected to end up in landfills (Keller et al. 2013). Many of these consumer goods cast off NP throughout the life of the product which can enter surface and groundwater systems, through direct runoff from stressed, weathered, or improperly disposed products, leachate from landfills, and infiltration of septic system effluent (Wagner et al. 2014).

Even those NP which enter a municipal sewer systems are not all removed by wastewater treatment plants (Farkas et al. 2011; Chalew et al. 2013; Jarvie et al. 2009). One study in particular noted that under the most probable water chemistry and NP coating conditions during prefiltration stages, only between 68 to 90% of the titanium dioxide ($TiO_2$) NP were removed (Kinsinger et al. 2015). As a result these particles are increasingly being introduced to the subsurface and aquatic ecosystems, entering the water cycle, and potentially making it back into private and municipal drinking water supplies.

This has become a cause for concern since many NP are known to have toxic effects. $TiO_2$-NP are one of the most widely manufactured NP due to their use in sunscreens, paints, and photovoltaic cells, and experiments have demonstrated that they cause cell wall damage in benthic biofilms and planktonic organisms of streams (Fang et al. 2008; Battin et al. 2009).

Other NP have also been shown to cause cell and DNA damage in bacteria, rats, fish, and humans (Oberdörster et al. 2007; Brar et al. 2009).

Though NP are entering the water cycle, and subsequently ecosystems and potentially drinking-water supplies, research has only recently addressed how they move through the subsurface. NP as well as larger colloids have different levels of mobility due to chemical reactivity, solubility, their size potential for settling, dispersing, or being filtered, as well as the role of their surface charges in their propensity to sorb, aggregate, or flocculate (Huber et al. 2012). Another concern driving the need to adequately characterize NP transport is that NP can facilitate contaminant transport through groundwater systems (Hofmann and von der Kammer 2009). Colloid-contaminant cotransport has been observed at several study sites, including radionuclide contaminated sites at Oak Ridge National Laboratory and Los Alamos National Laboratory, and when this transport mechanism is not taken into account it can result in large underestimations of contaminant spread (McCarthy and Zachara 1989; McCarthy et al. 1998a, 1998b; Penrose et al. 1990).

The reactivity of colloids and NP can make it difficult to use them to determine the flow and transport properties of a system and of the NP themselves. Conservative NP can aid the study of these characteristics, and can also be developed as a useful groundwater tracers. Though it was originally assumed that the greater surface area to volume ratio of small colloids, like NP, would cause them to be more reactive and sorb, the opposite mass recovery trend has been observed. This is because the recovery of larger colloids can be impacted more by gravity settling and pore-throat filtering (Reimus 1995). In addition to size the NP surface charge is very important to predicting transport. Colloid transport characteristics in addition to their smaller size make inert NP attractive potential tracers to characterize.

In order to characterize the transport behavior of smaller colloids a non-toxic, non-reactive NP needs to be developed for use as a groundwater tracer. Fluorescent carbon nanospheres (CNP) which are surface-functionalized to be hydrophilic are also inert with a close to neutral surface charge (zeta potential of -1 to -2 mV), non-toxic, and only 5 to 10 nm in diameter. Subramanian et al. 2013 demonstrated that CNP transport conservatively through columns of bimodal glass beads arranged to simulate heterogeneous conditions and they calculated the molecular diffusion coefficient of CNP as $1.5X10^{-6}$ $cm^2/s$. A single field test, a push-pull tracer test, has also used these CNP to assess the flushing efficiency of a produced oil reservoir in carbonate-rock with groundwater conditions greater than 100°C in temperature and 120,000 ppm in salinity (Kanj et al. 2011). The CNP remained stable with only minor adsorption. These results can be built upon for a variety of natural settings so that CNP can be applied to problems of preferential flow including fractured-rock groundwater systems.

Another potential use for this tracer will be to quantify target material volumes within porous media. When minerals are present in the column which react with a solute tracer, multiple tracers may be used to quantify the amount of target substance present (e.g., Divine et al. 2003). If hydrophilic CNP is demonstrated to transport conservatively through porous media it could be used as the conservative tracer during such an experiment. It may also be feasible to functionalize CNP to be hydrophobic and preferentially sorb to target contaminants such as NAPLs.

*Research Objectives*

To analyze the transport of CNP in porous media these nanospheres were tested along with the conservative tracer, bromide, in columns of sediments and reactive materials with homogeneous and heterogeneous designs. It was important to first verify that the CNP transport as a conservative tracer so that they can be used to assess the differences in

transport with reactive NP. The breakthrough curve (graph of relative tracer concentration measured in the column effluent) can be analyzed to provide insight on how the CNP transport through the column compared to bromide. The conceptual model presented in Figure 4.1 demonstrates how the properties of the breakthrough curve can be interpreted to determine transport characteristics.

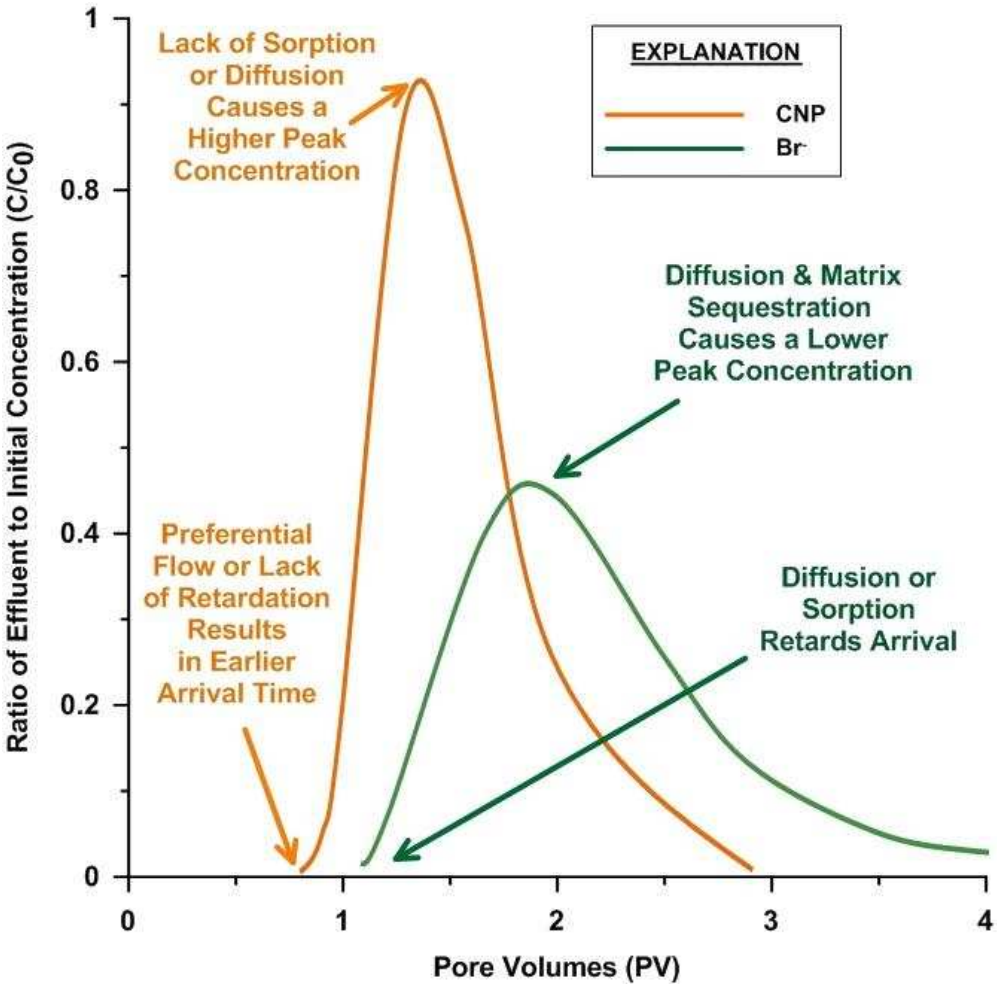


**Figure 4.1 Hypotheses for dual-porosity and reactive porous media tracer breakthrough**

In columns of homogeneous porous media the two tracers should behave similarly, since the bromide also transports conservatively through homogeneous systems. This means

that the breakthrough curves for CNP and bromide should overlie each other, resulting in nearly identical retardation factors.

In columns of porous media with mobile and immobile zones the bromide should undergo more transverse diffusion into lower permeability or immobile zones, whereas the CNP should travel more along preferential flow paths. This means that in dual-porosity systems the breakthrough curve of bromide should have a lower peak relative concentration than the CNP, as well as pronounced tailing due to back-diffusion, as seen in Figure 4.1.

For the reactive media columns, the reactive material used is a surface modified zeolite (SMZ), which has an internal immobile porosity and has been treated with a surfactant to have a positive surface charge. So that, in addition to diffusing into the immobile porosity, the bromide anion should also react to the positively charged mineral surfaces, while the CNP should undergo minimal diffusion into the immobile zone with little to no sorption. Therefore, the breakthrough curve of the bromide should have a lower peak relative concentration, pronounced tailing, and a significantly retarded arrival when compared to the CNP (Figure 4.1). The CNP should continue to have a retardation factor close to one, and nearly complete mass recovery unlike the bromide. This means that the CNP along with other tracers could potentially be used to quantify the fastest transport times through porous media, assess the degree of preferential flow, and to detect the presence of positively charged minerals.

## MATERIALS

### *Porous Media*

Three types of porous media were used in the various column designs. There were two different grain sizes of silica sand, and one type of reactive media. The coarse sand which was

used was 20-30 mesh Ottawa silica sand. This sand was prewashed and has grain sizes between 0.6 and 0.8 mm in diameter. The fine sand was prewashed U.S. Silica F-95 and had grain diameters between 0.1 and 0.2 mm. The porous media selected for the reactive media column tests was a surface modified zeolite (SMZ), which was prepared by the New Mexico Tech Research Foundation using zeolite sourced from St. Cloud Mine, New Mexico. It has a particle size range of 14 to 40 mesh, and mineralogical composition of 74% clinoptilolite, 12% feldspar, 12% quartz, and 5% smectite. As a result of treating the zeolite with a surfactant, it has a positive surface charge with a cation exchange capacity of 90 to 100 meq/kg of zeolite.

*Particle and Solute Dual-Tracer Preparation*

During these tests the fluorescent carbon nanospheres (CNP) and the conservative solute tracer, bromide (as potassium bromide), were injected simultaneously into columns of well-characterized porous media. To prepare the dual-tracer we first had to manufacture the CNP. The method for preparing our CNP was documented as the procedure for "CNP-3" in the supplementary materials of *Li et al. 2014*. When dual-tracer was needed for a test, a mixture of 50% 500 ppm bulk CNP and 50% 671 ppm bulk Br was prepared, resulting in a dual-tracer concentration of 250 ppm CNP and 336 ppm Br.

*System and Column Design*

The columns used are all 5.08 cm ID acrylic columns either 15.24 cm or 30.48 cm in length. All columns were suspended vertically with the column inlet at the bottom and outlet at the top. The outlet tubing of each column was attached to a fraction collector and the inlet tubing of each column was attached to a peristaltic pump and connected to a three-way valve. The alternate inlets to the three-way valve were connected via tubing to two different reservoirs, a deionized (DI) water reservoir and a dual-tracer reservoir.

A 30.48 cm long column was selected for the homogeneous column tests and was filled with coarse sand, wet-packed with a tamping rod to a porosity of 34%. A quartz frit was installed in both end caps to ensure that the tracer would transport evenly across the column.

A 30.48 cm long column was selected for the dual-porosity column tests and was wet-packed with sediment designed so that there is a lower permeability matrix which is immobile and sharply separated from the preferential flow path (a coarse sediment core). To prepare the dual-porosity core column, a removable plastic tube was placed in the center of the column, and used to install a 1.27 cm diameter core of prewashed coarse silica sand, while a fine silica sand matrix was installed around it on all sides. The core was wet-packed with a tamping rod to a porosity of approximately 34%. The matrix was wet-packed with a tamping rod to a porosity of approximately 38%, and a thin plastic baffle was installed every 2.54 cm within the fine sand to minimize flow through the matrix. No frit was installed in the end caps, so that the tracer was injected directly into the core of the column in order to create a concentration gradient from the mobile to immobile zones which could drive transverse diffusion. Since there was no frit the actual length of sediment into the column was 31.76 cm.

For the reactive media test a 15.24 cm long column was selected. A mixture of 12.5% SMZ by weight, and 87.5% coarse sand was then installed in 2 cm increments. It was stirred and remixed to a homogeneous distribution, and wet-packed with a tamping rod to a mobile porosity of approximately 29%. The total porosity, including the immobile porosity within the zeolite, was 38%. A quartz frit was installed in each end cap to ensure that tracer was transported evenly across the width of the column.

## METHODS

### *Pulse and Step Tests*

Testing of each column was conducted by pumping DI water through each column at a steady flow rate and introducing the dual-tracer as a pulse. The breakthrough concentrations of each tracer was measured in the effluent for the period of dual-tracer injection and elution. The tracer application time for the pulse tests was picked so that effluent concentrations should reach at least 40% of the tracer concentration at its peak. For the homogeneous tests the target tracer injection volume was 25% of a total pore volume (TPV), but a step test was also conducted where approximately 3 TPV of tracer was injected. For the dual-porosity tests the target volumes were between 3 and 5 mobile pore volumes (MPV). A mobile pore volume is the volume of pore space within the column's core (the mobile zone). And for the reactive media tests the target volumes were between 4 and 6 TPV. Effluent samples were collected continuously until effluent was clear of tracer or until at least 30 MPV or 4 TPV were flushed after tracer injection.

### *Flow Interruption Test*

To maximize the effects of transverse diffusion in the dual-porosity column, a flow interruption test was conducted where the pump was stopped for six days during tracer injection, and then stopped again for six days during the flushing period. This was done to give the tracers more time to diffuse into and out of the immobile zone during the test.

### *Long-Term Test*

A long-term test was conducted for the dual-porosity column so that the transport parameters of the bromide and CNP could be distinguished from one another more easily.

During the long-term test tracer was injected for 14 days. Samples were collected continuously until the effluent concentration reached the influent concentration. Afterwards samples were collected periodically until the injection period ended. Samples were again collected continuously for a flushing period equal to approximately 50 MPV.

*Effluent Analytical Methods*

CNP concentrations were measured using a FLUOstar® Omega microplate reader (spectrofluorometer). CNP emit light at a wavelength of 460 nm, and show the clearest emission signal when an excitation wavelength of 375 nm is used. The 460 nm emission filter was available on the spectrofluorometer, but the nearest excitation filter was 355 nm, which still results in an acceptably strong fluorescence (Krysmann et al. 2011). Approximately 385 µL of each selected sample was placed in a well of the microplate. Each microplate was read using a well scan protocol, where fluorescent intensity in arbitrary units (a.u.) was measured rapidly 308 times in a circular grid with a 4mm diameter over each well and then averaged.

Bromide concentrations were measured with a bromide ion selective electrode (ISE). The ISE used was an Orion™ Bromide Combination Electrode. Throughout sample analysis the probe calibration was checked using the calibration solution nearest to the samples being read. When the probe reading was off by more than 5% it was recalibrated.

*Data Processing*

CNP results were normalized and converted to concentrations using the calibration curve for that run of tracer. These concentrations were then divided by the measured dual-tracer concentration of CNP to get values of relative concentration ($C/C_0$), so that they would be directly comparable to the bromide results. Each bromide result was divided by the measured dual-tracer concentration of bromide for that round of calibration to get values of relative

concentration as well. The flow rate was measured periodically and the average was multiplied by the time and divided by the known PV of the column to calculate the equivalent PV (dimensionless time).

*Solute and Particle Curve Fitting*

STANMOD is a publicly available software package which allows you to run multiple transport codes in order to predict or fit the transport of tracers through various systems. The CXTFIT code, Version 2.0, was selected to model transport behavior within the column. This code was selected because it utilizes equilibrium and nonequilibrium solutions to the advection-dispersion equation (ADE) for one dimensional flow. This code was used to set up analytical solutions and fit model results to the observed column effluent concentrations. This program optimizes parameter estimates by using a nonlinear least-squares optimization approach (Toride et al. 1995). Prior to modeling solute transport, the mechanisms governing flow were considered for each test design, a governing equation and set of boundary conditions were chosen, and the unknown transport parameters were identified.

## RESULTS & DISCUSSION

*Homogeneous Transport*

Three transport tests were conducted: two pulse tests, and one step test. The effluent results for CNP and Br from Homogeneous Pulse Test #1 are shown as open circles in Figure 4.2. The BTCs directly overlie each other, indicating that both the CNP and Br transported similarly through the column. The initial breakthrough of the tracers are sharp and the elution portion of the curve shows no pronounced tailing, indicating that transport of CNP and Br

through the homogeneous column was conservative. The total mass recovered ($M_r$) was calculated by integrating under the breakthrough curve, and this value was expressed as a percentage of the total mass injected. In this test the mass recovery for the Br was 96.2% and the CNP was 96.4%, demonstrating that a negligible amount of tracer remained in the column.

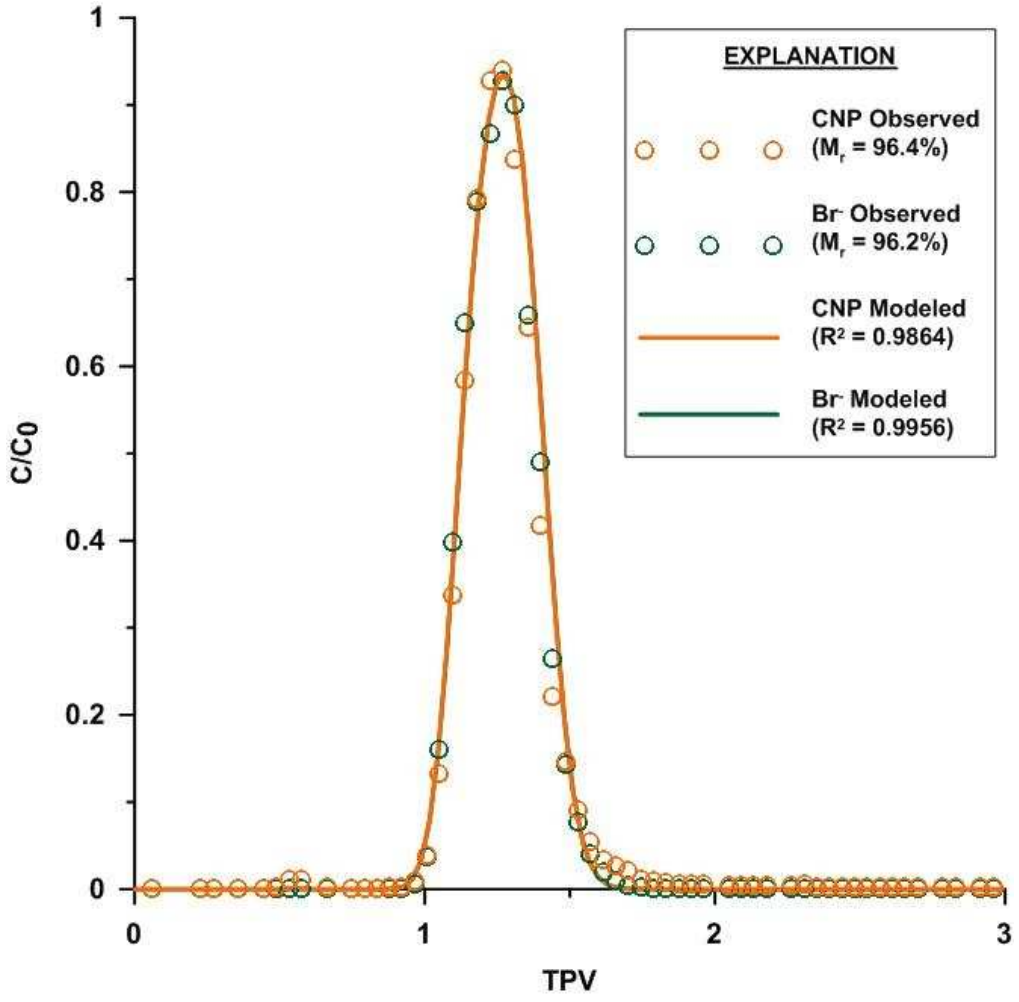


**Figure 4.2 Homogeneous Pulse Test #1 BTC**

To confirm this assertion transport through the homogeneous column was modeled for both CNP and Br using the equilibrium model in CXTFIT. And any reactions were modeled using the retardation factor ($R$). The equilibrium model uses a superposition of initial and

boundary value problem analytical solutions to the one-dimensional classic-advection dispersion equation (ADE) (Toride et al. 1995). The governing equation is given in its dimensionless forms in Equation 4.1. CNP and Br concentrations are all expressed in resident relative concentration ($C_r$) and converted to the flux-averaged concentration ($C_f$) as measured in effluent, using the relationship in Equation 4.2. To model the one-dimensional flow of tracer through the column boundary conditions are needed for the inlet and outlet. Since the tracer was introduced as a pulse in these experiments, it is necessary for the BC at the inlet to work for two time periods of the test; the time period where the tracer is "turned on" (injection period) and the time period once it is "turned off" (elution period). Therefore a third-type boundary condition (flux-type) must be used, which is expressed in Equation 4.3 (van Genuchten and Alves 1982). This boundary condition allows the introduced tracer concentration to vary with time, so that during injection it can be set equal to the tracer concentration and during elution it is set equal to zero. The outlet boundary condition is to assume a zero concentration gradient at some infinite distance, as shown in Equation 4.4. The initial condition for resident concentrations at any $Z$ is given in Equation 4.5, which is initially set equal to zero since the initial pore fluid is DI water with no background tracer concentrations. Each test was conducted in the same manner so that the boundary conditions and initial condition remain the same for each analytical model.

$$R\frac{\partial C_r}{\partial T} = \frac{1}{P}\frac{\partial^2 C_r}{\partial Z^2} - \frac{\partial C_r}{\partial Z} \tag{4.1}$$

$$C_f = C_r - \frac{1}{P}\frac{\partial C_r}{\partial Z} \tag{4.2}$$

$$C_r(0,T) - \frac{1}{P}\frac{\partial C_r(0,T)}{\partial Z} = C_0(T) \tag{4.3}$$

$$\frac{\partial C_r}{\partial Z}(\infty, T) = 0 \tag{4.4}$$

$$C_r(Z, 0) = C_i(Z) \tag{4.5}$$

Dimensionless time ($T$) is equivalent to the number of pore volumes of column effluent. Dimensionless distance ($Z$) is equivalent to the proportional distance through the column (Equation 4.6) where $x$ is the distance from the inlet and $L$ is the column length. The dispersive flux in Equation 4.1 is expressed as the product of the inverse Peclet number and the derivative of the concentration gradient with respect to $Z$. The Peclet number ($P$) is a ratio of advective to dispersive transport and is defined in terms of the hydrodynamic dispersion coefficient ($D$), average pore velocity ($v$), and column length in Equation 4.7. Since this is a one-dimensional ADE, the hydrodynamic dispersion coefficient only describes dispersion in the direction of flow (longitudinal) and so it is a function of the longitudinal dispersivity of the porous media ($\alpha_L$), the average pore velocity, and molecular diffusion ($D^*$), as shown in Equation 4.8. The advective flux in Equation 4.1 is expressed in terms of the concentration gradient with respect to $Z$.

$$Z = \frac{x}{L} \tag{4.6}$$

$$P = \frac{vL}{D} \tag{4.7}$$

$$D = \alpha_L v + D^* \tag{4.8}$$

Since the average flow rate ($Q$), column radius ($r$), and total porosity ($\theta$) are known, the average pore velocity was calculated, using Equation 4.9. So the only unknown parameters which needed to be solved for were the longitudinal dispersion coefficient and retardation factor.

$$v = \frac{Q}{\pi r^2 \theta} \tag{4.9}$$

Parameter results of three independent homogeneous column tests are given in Table 4.1. It can be seen that the modeled retardation factor was close to 1 for each run, and was nearly identical for bromide and CNP, indicating that no retardation occurred. Since there was no retardation it is shown that CNP and Br transported conservatively through the homogeneous column with an average dispersion coefficient equal to $2.56X10^{-4}$ $cm^2/s$.

**Table 4.1 Homogeneous pulse test parameters**

| | | Parameters | | | |
|---|---|---|---|---|---|
| | | Known | | Fitted | |
| **Test Name** | **Tracer** | **Pore Velocity, v (m/d)** | **Application Time (min)** | **Dispersion Coefficient, D ($cm^2/s$)** | **Retardation Factor, R** |
| **Pulse Test #1** | **CNP** | 2.55 | 50.00 | $2.18X10^{-4}$ | 1.11 |
| | **Br** | | | $2.18X10^{-4}$ | 1.11 |
| **Pulse Test #2** | **CNP** | 1.97 | 55.73 | $2.36X10^{-4}$ | 1.16 |
| | **Br** | | | $1.74X10^{-4}$ | 1.15 |
| **Step Test** | **CNP** | 2.74 | 608.89 | $2.89X10^{-4}$ | 1.14 |
| | **Br** | | | $2.85X10^{-4}$ | 1.13 |

*Dual-Porosity Transport*

The effluent results for CNP and Br from Dual-Porosity Column Design #3, Pulse Test #1 are shown as open circles in Figure 4.3. The BTCs nearly overlie each other, indicating that both the CNP and Br transported similarly through the column, though it is apparent that the CNP peaked at a higher relative concentration and the Br experienced a slightly more pronounced tail. The advective front of each BTC is sharp however the elution portion of the curve shows pronounced tailing, indicating that Br and to a lesser extent CNP, are diffusing into the immobile zone of the column. The tailing is also exacerbated by some flow through the cells in between the baffles. The mass recovery for the Br was 103.5% and the CNP was 96.0%. The slightly higher peak relative concentration of CNP and the slightly less pronounced tail also indicates that the CNP are being transported more rapidly through the mobile core of the column. Additionally, the higher concentration of bromide in the tail of the breakthrough indicates that bromide is diffusing back out of the immobile zone at a faster rate.

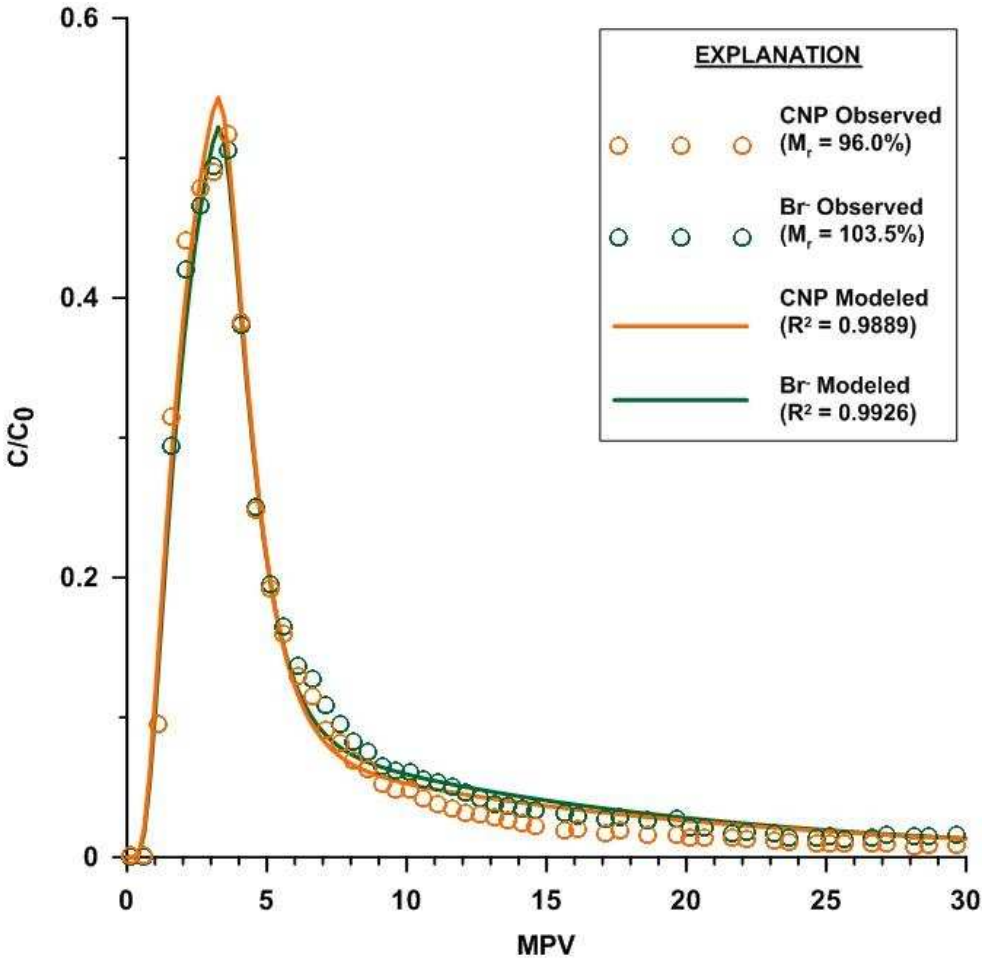


**Figure 4.3 Dual-Porosity Column, Pulse Test #1 BTC**

Additional processes must be considered for solute and particle transport through a dual-porosity column. The dual-porosity column consists of two distinct zones; there is a coarse silica sand core (the mobile zone) which is surrounded by fine silica sand matrix with baffles (the immobile zone). Preferential flow occurred through the higher permeability core, transporting the solute and particles very quickly, while the concentration gradient between the pore fluids in the core and fine sand matrix drove mass transfer of solute and to a slightly lesser extent the nanoparticles into the immobile zone at a much slower rate. The mobile porosity ($\theta_m$) and immobile porosity ($\theta_{im}$) are defined such that Equation 4.10 is true.

$$\theta = \theta_m + \theta_{im} \quad (4.10)$$

Due to the mass transfer process between the mobile porosity zone and immobile zone a two-region nonequililbrium ADE was used to model transport (Toride et al. 1995). This model is an analog of the transient storage model, so it uses multiple parameters to model the occurrence of transverse diffusion as temporary mass storage of tracer. Equations 4.11 and 4.12 include two new terms: a partitioning term which consists of the dimensionless partitioning coefficient ($\beta$), and a mass transfer term which is the product of the dimensionless mass transfer coefficient ($\omega$) and the difference in relative resident concentration between the mobile ($C_m$) and immobile ($C_{im}$) zones. The boundary conditions and initial condition remain the same as for the equilibrium model (given in Equations 4.3 through 4.5). Equation 4.11 models the change in resident concentration over time in the mobile zone and Equation 4.12 model the change in resident concentration over time in the immobile zone. The total resident concentration is found using Equation 4.13 and then converted to the flux-averaged concentration using Equation 4.14. The parameter $\beta$ is defined in Equation 4.15 which includes the fraction of adsorption sites ($f$) at equilibrium with the mobile zone, the bulk density ($\rho_b$), and the partitioning coefficient ($K_d$). The parameter $\omega$ is defined in Equation 4.16 which includes the first-order kinetic rate coefficient ($\varepsilon$) and column length ($L$). Since it was confirmed that both the Br and CNP transport conservatively through silica sand during the homogeneous test, then the retardation factor should be equal to 1 and can be disregarded. Since the solutes are non-reactive this also means that $K_d = 0$, so that $\beta$ represents the fraction of mobile water and can be expressed using Equation 4.17 instead (Toride et al. 1995).

$$\beta R \frac{\partial C_m}{\partial T} = \frac{1}{P}\frac{\partial^2 C_m}{\partial Z^2} - \frac{\partial C_m}{\partial Z} - \omega(C_m - C_{im}) \quad (4.11)$$

$$(1-\beta) R \frac{\partial C_{im}}{\partial T} = \omega(C_m - C_{im}) \quad (4.12)$$

$$C_T = \beta R C_m + (1-\beta) R C_{im} \quad (4.13)$$

$$C_f = C_T - \frac{1}{P}\frac{\partial C_T}{\partial Z} \quad (4.14)$$

$$\beta = \frac{\theta_m + f\rho_b K_d}{\theta + \rho_b K_d} \quad (4.15)$$

$$\omega = \frac{\varepsilon L}{\theta v} \quad (4.16)$$

$$\beta = \frac{\theta_m}{\theta} \quad (4.17)$$

Since the average flow rate, radius of the mobile zone ($r_m$), and porosity of the mobile zone are known, an average mobile zone pore velocity ($v_m$) can be calculated assuming zero flow through the immobile zone, using Equation 4.18. However this value cannot be entered directly into the two-region model because it does not reflect the velocity of both the mobile and immobile regions. Therefore Equation 4.19 should be used to calculate an initial estimate of an average pore velocity for the column. Though the dispersion coefficient is known from the homogeneous columns for transport through the coarse silica core, it is evident that transport is also taking place through the fine silica matrix which may affect the longitudinal dispersivity and therefore the longitudinal dispersion coefficient in the dual-porosity column. Due to this the

longitudinal dispersion coefficient is also an unknown parameter. Therefore an initial estimate of the longitudinal dispersion coefficient can be made using Equation 4.20, where $D_m$ is the mobile zone longitudinal dispersion coefficient.

$$v_m = \frac{Q}{\pi {r_m}^2 \theta_m} \tag{4.18}$$

$$v = \frac{\theta_m}{\theta} v_m \tag{4.19}$$

$$D = \frac{\theta_m}{\theta} D_m \tag{4.20}$$

The initial estimates of four independent dual-porosity column tests are given in Table 4.2. Since both tracers were shown to be non-reactive to the silica sand in the homogeneous column, the $\beta$ values were calculated using Equation 4.17. The initial estimates for the average pore velocity and average dispersion coefficient were calculated from Equations 4.19 and 4.20, respectively. The value of the mobile zone longitudinal dispersion coefficient (for the coarse sand core) came from the average of the dispersion coefficients from the homogeneous tests. The mobile zone pore velocity was calculated using Equation 4.18. Since the core size and packing porosities are the same for each test with Design #3 the initial estimates of $D$ and $\beta$ are identical.

**Table 4.2 Dual-Porosity Column Design #3, initial parameter estimates**

| | | Known | | Initial Estimates | | |
|---|---|---|---|---|---|---|
| **Test Name** | **Tracer** | **Mobile Dispersion Coeff. $D_m$ ($cm^2/s$)** | **Mobile Pore Velocity $v_m$ (m/d)** | **Average Pore Velocity v (m/d)** | **Average Dispersion Coeff. D ($cm^2/s$)** | **Partitioning Coeff., β** |
| **Pulse Test #1** | **Both** | $2.56X10^{-4}$ | 18.64 | 0.98 | $1.35X10^{-5}$ | $5.26X10^{-2}$ |
| **Pulse Test #2** | **Both** | $2.56X10^{-4}$ | 12.79 | 0.67 | $1.35X10^{-5}$ | $5.26X10^{-2}$ |
| **Interrupt Test** | **Both** | $2.56X10^{-4}$ | 14.56 | 0.77 | $1.35X10^{-5}$ | $5.26X10^{-2}$ |
| **Long-Term Test** | **Both** | $2.56X10^{-4}$ | 15.85 | 0.83 | $1.35X10^{-5}$ | $5.26X10^{-2}$ |

Parameter results of four independent dual-porosity column tests are given in Table 4.3. Once each model converged on a solution these parameters were averaged between the CNP and Br runs since they should not vary depending on the tracer. These values were then set as known parameters so that the longitudinal dispersion coefficients and mass transfer coefficients (indicator of transverse diffusion into the immobile zone) could be compared more easily once the model converged on a subsequent run.

**Table 4.3 Dual-Porosity Column Design #3, test parameters**

| | | Parameters | | | | | |
|---|---|---|---|---|---|---|---|
| | | Known | | Fitted | | | |
| Test Name | Tracer | Length (cm) | Tracer Application Time (min) | D ($cm^2/s$) | v (m/d) | Partitioning Coeff., β | Mass Transfer Coeff., ω |
| Pulse Test #1 | CNP | 31.76 | 67.74 | $1.87X10^{-2}$ | 2.29 | 0.29 | 0.58 |
| | Br | | | $1.76X10^{-2}$ | 2.29 | 0.29 | 0.65 |
| Pulse Test #2 | CNP | 31.76 | 177.43 | $2.61X10^{-2}$ | 1.56 | 0.53 | 0.29 |
| | Br | | | $2.42X10^{-2}$ | 1.56 | 0.53 | 0.28 |
| Interrupt Test | CNP | 31.76 | 175.17 | $6.86X10^{-3}$ | 0.87 | 0.13 | 0.77 |
| | Br | | | $5.23X10^{-3}$ | 0.87 | 0.13 | 0.86 |
| Long-Term Test | CNP | 31.76 | 20,162 | $1.72X10^{-2}$ | 1.22 | 0.30 | 0.51 |
| | Br | | | $1.69X10^{-2}$ | 1.22 | 0.30 | 0.50 |

As shown in Table 4.3, the values of $v$ and $\beta$ are an order of magnitude higher than the initial estimate. This is likely due to flow occurring within the individual cells of the column, as illustrated in Figure 4.4. Since some of the column which had been calculated as immobile zone was actually mobile this drove up the ratio of mobile porosity to total porosity, which in turn drove up the value of $\beta$ and the effective average pore velocity, $v$. As a result of flow occurring through the finer-grained matrix and the resulting spread in tracer concentration down the core, the longitudinal dispersion coefficient was three orders of magnitude higher than its initial estimate.

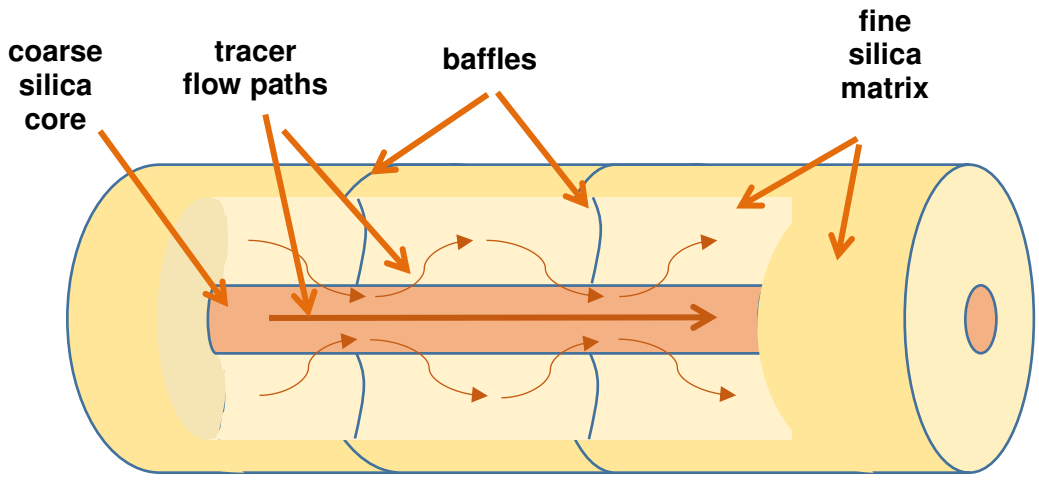


**Figure 4.4 Cross-sectional illustration of flow of tracer through the individual cells of the immobile zone in the dual-porosity column, indicated by the higher $\beta$ values**

Before examining the difference in the results between CNP and Br, it is important to recognize that as $\omega$ approaches 0 there is less mass transfer occurring, and this parameter is used to simulate the occurrence of transverse dispersion. It is evident that the CNP and Br transported through the dual-porosity column similarly, likely because the fine sand matrix had pore throats which were still large enough to allow the CNP to enter. Since pore throat filtering was not a problem two of the experiments showed no significant difference in the mass transfer coefficients, indicating that the occurrence of transverse diffusion was similar, or that the difference was masked due to the flow occurring in each immobile zone cell. However, where there was a significant difference in the mass transfer coefficients, the value for bromide was higher, indicating that more transverse dispersion occurred for bromide than CNP because CNP has a lower molecular diffusion rate. Even when the transverse dispersion was noticeably different the hydrodynamic dispersion coefficients for each tracer were still very similar, because the equilibrium model is one-dimensional, so $D$ is only the dispersion occurring longitudinally.

Though the molecular diffusion coefficients should be lower for CNP than the Br, the magnitude of the average pore velocity and longitudinal dispersivity in these experiments was too great to be able to recognize the relatively small contribution of molecular diffusion ($D^*$) to the hydrodynamic dispersion equation.

Due to the evidence of molecular diffusion and the difficulty in modeling the difference in the longitudinal dispersion coefficient and mass transfer coefficient (indicates of transverse diffusion) for the pulse tests, a flow-interruption test was conducted. The results of the interruption test confirmed graphically that molecular diffusion was driving mass transfer of CNP into the immobile zone as seen in Figure 4.5.

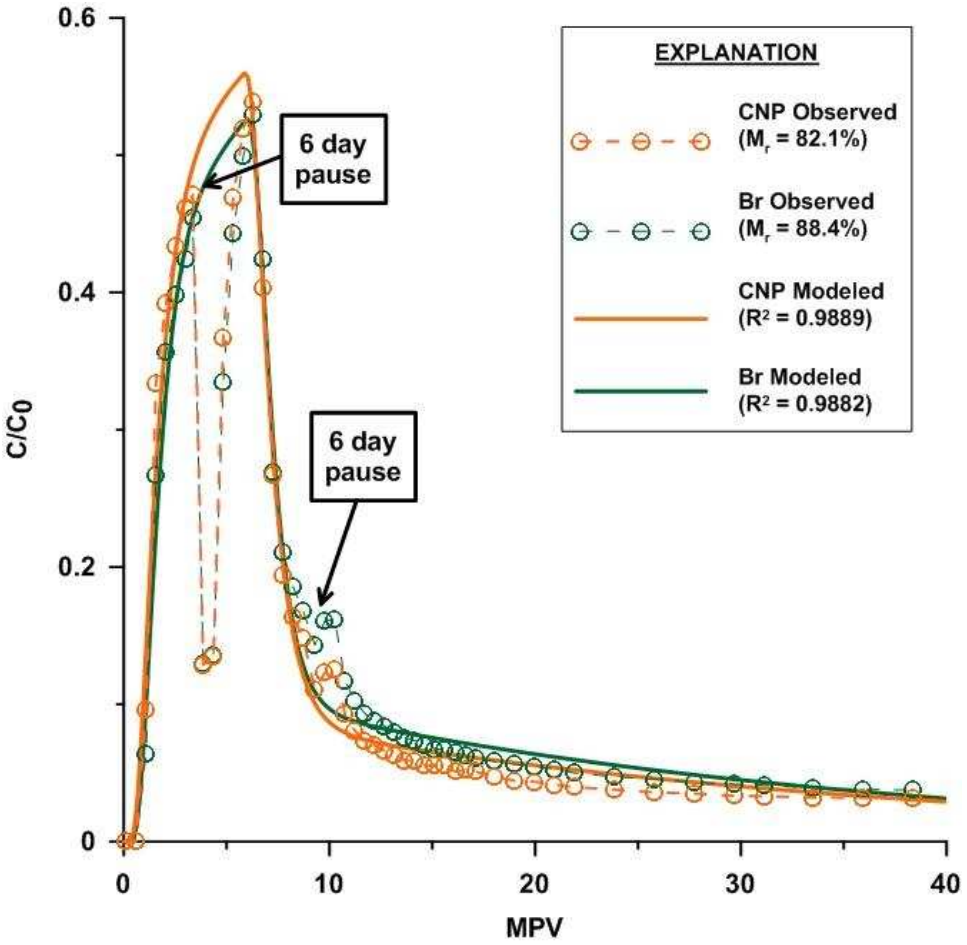

**Figure 4.5 Dual-Porosity Column Design #3, Interruption Test BTC**

During the injection period, flow was stopped after approximately four MPV of tracer. It was stopped for six days, after which flow and sample collection resumed. The first two samples after the pump was turned back on showed a significant drop in relative concentration of both CNP and Br. The effluent concentration of each dropped as a result of the solute and particles diffusing into the immobile zone during the six-day interruption. Transverse diffusion was driven by the concentration gradient between the mobile and immobile zones, and both tracers appear to have behaved in a similar way. It is important to note that since the effluent concentration had not reached 1 there would have also been a slight concentration gradient along the mobile core, which would drive longitudinal diffusion. However if the longitudinal diffusion had been dominant then the first sample after the interruption period would have had a higher concentration instead of the lower concentration which was observed. Though longitudinal diffusion was minor it may have limited the apparent magnitude of transverse diffusion in the experiment.

Once flow was resumed 2 MPV of tracer were injected, followed by 4 MPV of DI water before the pump was stalled again for six days. During the elution period, the samples that follow the second interruption show an increased concentration of both the CNP and Br. This is a result of the Br and CNP diffusing back out of the immobile zone and into the mobile zone due to the reversal of the concentration gradient during flushing. The elution interruption resulted in higher Br effluent concentrations than CNP, which appears to indicate that CNP was less able to diffuse back out of the finer immobile zone, possibly due to the lower molecular diffusion coefficient of CNP (Subramanian et al. 2013). The overall mass recovery for CNP was again less than that of the Br, further indicating that transverse diffusion is a slower process for CNP.

It is evident that the CNP was peaking at a higher concentration than the bromide, which

may indicate that bromide was undergoing more transverse diffusion. During the first interruption the concentration of both tracers dropped off dramatically, indicating that the additional contact time was successful in allowing the concentration gradient of each tracer to drive mass transfer into the immobile zone. Once the pump was turned back on six days later the CNP again peaked at higher concentration than the Br, indicating that bromide was still undergoing more transverse diffusion into the immobile zone. Once the tracer was shut off the concentration of both tracers dropped quickly, but bromide concentrations remained higher. The higher bromide concentrations also indicated that bromide was undergoing transverse diffusion at a faster rate, this time back out of the immobile zone. This is further supported by how much higher the bromide concentration rose than the CNP concentration during the second interruption. CNP concentration did not rise as much because it diffuses at a much slower rate, and likely had less mass in the immobile zone, resulting in a lower concentration gradient driving exchange. After the interruption, bromide concentrations remained high due to its faster rate of transverse diffusion out of the immobile zone. In order to model the transport behavior during the experiment, the spikes which occurred during interruptions were removed, before parameters were fit to the overall curve. The mass transfer coefficients were higher for the interruption test than the pulse tests, due to the increase in contact time which allowed the concentration gradient to drive more exchange into the immobile zone. Though the results graphically demonstrate the relationships and the occurrence of CNP transverse diffusion, the variable flow rate prevented this test from being modeled accurately in CXTFIT. Therefore a long-term test was conducted to model the difference in transverse diffusion between the two tracers. The results of the long-term test are shown in Figure 4.6.

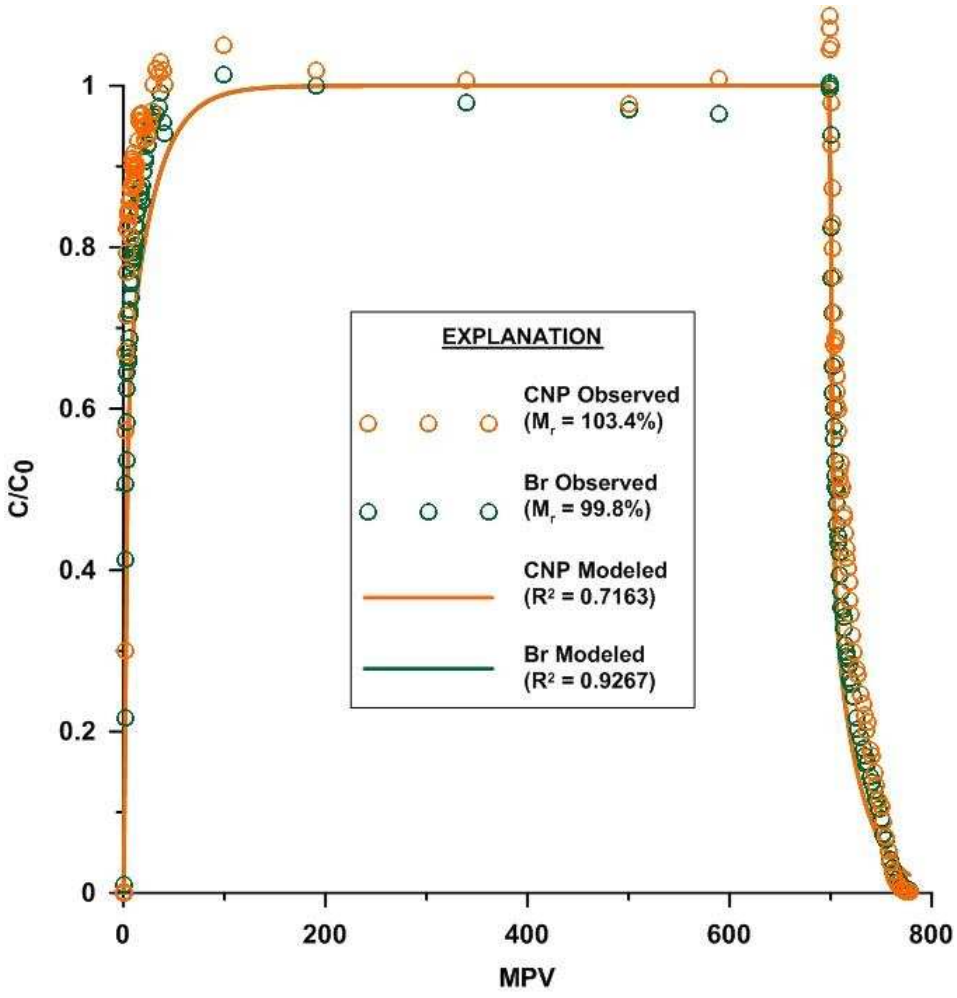


**Figure 4.6 Dual-Porosity Column Design #3, Long-Term Test BTC**

The tracer was injected for 14 days during the long-term tracer test. This allowed more time for the slow process of diffusion to take place. As shown by the BTC in Figure 4.6, CNP still underwent only slightly less transverse diffusion into the immobile zone than the Br during the injection period, resulting in higher peak relative concentrations. The elution curve however was nearly identical for each tracer, which may have been the result of cross flow in the cells between baffles minimizing and masking the effects of transverse diffusion on the long-term scale. The mass recovery for CNP was actually higher than Br during this test, but the average pore velocity was still too high to adequately see obvious differences in the longitudinal

dispersion coefficients resulting from the difference in molecular diffusion between CNP and Br. Results of the long-term test are also provided in Table 4.3.

*Reactive Transport*

The effluent results for CNP and Br from one of the reactive media pulse test are shown as open circles in Figure 4.7. The BTC are drastically different, indicating that the CNP and Br transported very differently through the columns. The CNP broke through after 1 MPV with virtually no retardation, indicating that the CNP transported conservatively through the column. During elution the CNP concentration dropped in the effluent rapidly supporting the conclusion that little to no reversible sorption took place. In contrast the Br did not break through until approximately 6 MPV, showing significant retardation as a result of reactivity with the SMZ. The Br also peaked at a much lower relative concentration compared to the CNP, due to bromide mass loss to the reactive SMZ. The elution portion of the Br curve also shows pronounced tailing, indicating that Br underwent desorption very slowly, and some degree of irreversible sorption may have occurred. In this example the overall mass recovery after 30 TPV for the Br was only 71.3% while 92.7% of the CNP was recovered. Since CNP does have a very slight surface charge of -1 to -2 mV, a minimal amount of sorption may have occurred.

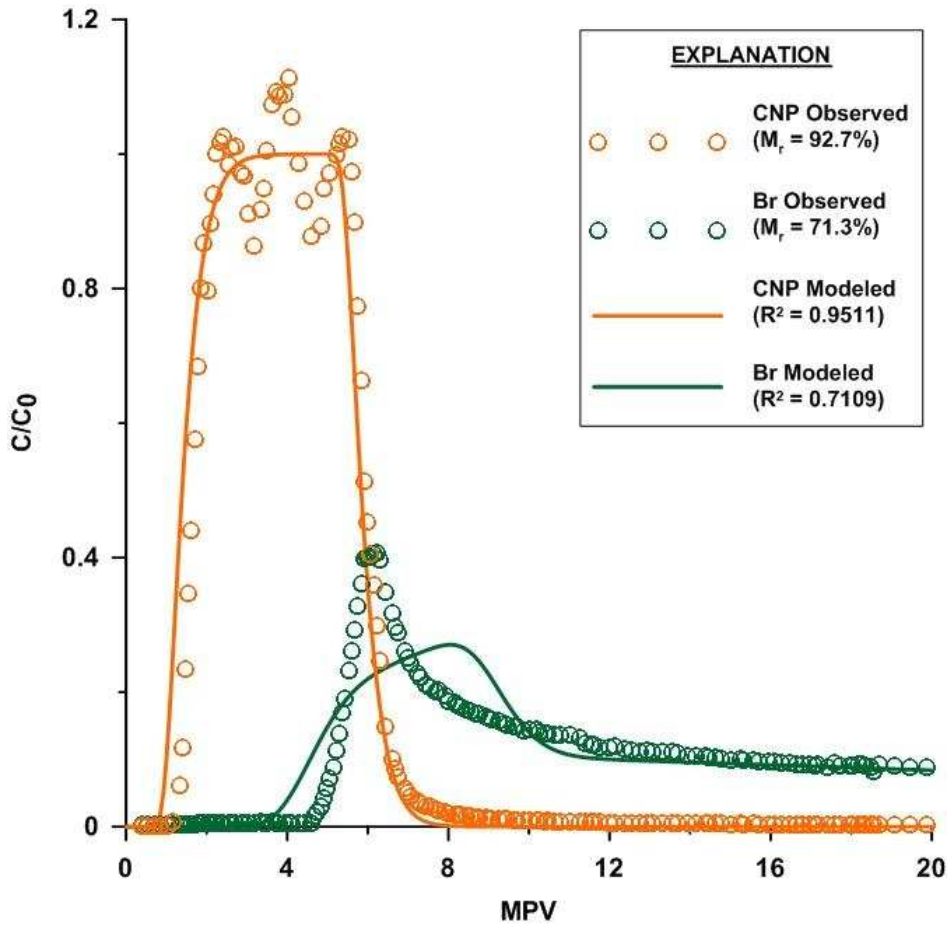


**Figure 4.7 Reactive Column Design #2, Pulse Test #1 BTC**

To determine the difference in transport parameters for the CNP and Br, transport of solute and particles through the reactive porous media column must be considered in detail. The reactive media, SMZ, has an internal porosity associated with it and theoretically there could be mass transfer and partitioning taking place between the mobile porosity outside of the zeolite and the immobile porosity within the zeolite. Due to this consideration the dimensionless two-region nonequilibrium ADE was used to model transport in the reactive columns (Equations 4.11 through 4.14). The boundary conditions and initial condition remained the same (Equations 4.3 through 4.5).

Since the average flow rate, radius of the column, and porosity of the mobile zone are known, an average mobile zone pore velocity was calculated assuming zero flow through the immobile porosity, using Equation 4.21. However this value cannot be entered directly into the two-region model because it does not reflect the velocity of both the mobile and immobile regions. Therefore Equation 4.19 was used to calculate an initial estimate of an average pore velocity for the column. Additionally, since the sand and zeolite are homogeneously mixed throughout the column, any change in the longitudinal dispersion coefficient should be negligible, and the hydrodynamic dispersion of the mobile zone can be set equal to the results of the homogeneous tests, so that Equation 4.20 can be used to calculate $D$. So the unknown parameters which need to be solved for are the retardation factor, partitioning coefficient, and mass transfer coefficient.

$$v_m = \frac{Q}{\pi r^2 \theta_m} \tag{4.21}$$

Parameter results of two independent reactive column pulse tests are given in Table 4.4. The average pore velocity was fitted based on the initial estimate from Equations 4.19. Once each model converged on a solution $v$ was averaged between the CNP and Br runs since it should not vary depending on the tracer. Since the transport was shown to be conservative for CNP, the partitioning coefficient for CNP was calculated from Equation 4.17. These values were then set as known parameters so that the retardation, dispersion coefficients, and mass transfer coefficients could be compared more easily.

The retardation factor is 11 to 18 times higher for bromide, showing that it reacts significantly with the SMZ. The bromide also shows significantly lower $\beta$ values than those calculated for CNP, indicating that far more partitioning was occurring due to the higher $K_d$ of

Br. Since the CNP was shown to be conservative, it's $K_d$ should have been equal to zero, so that $\beta$ was defined and calculated by Equation 4.17. For Pulse Test #1 the mass transfer coefficient of Br and CNP was very similar, indicating that the immobile porosity of the SMZ still had pore throats large enough to permit CNP to enter. In addition, the velocities may have been too high for the difference in transverse dispersion into the immobile zone to be noticeable, and since transverse dispersion is modeled using the mass transfer coefficient, this resulted in very similar values of $\omega$. Pulse Test #2 had a very poorly constrained $\omega$ value, since the model would converge on solutions with non-unique $\omega$, so it cannot be compared to the Br value for that experiment. In general, the model was very insensitive to changes in $\omega$.

**Table 4.4 Reactive Column Design #2, pulse test parameters**

| | | **Parameters** | | | | | | |
|---|---|---|---|---|---|---|---|---|
| | | **Known** | | | **Fitted** | | | |
| **Test Name** | **Tracer** | **Mobile Pore Velocity $v_m$ (m/d)** | **Tracer Application Time (min)** | **D ($cm^2/s$)*** | **R** | **v (m/d)** | **β** | **ω** |
| **Pulse Test #1** | **CNP** | 1.05 | 930.23 | $1.95X10^{-4}$ | 1.13 | 0.80 | 0.77** | 1.72 |
| | **Br** | | | $1.95X10^{-4}$ | 20.76 | 0.80 | 0.18 | 1.65 |
| **Pulse Test #2** | **CNP** | 1.08 | 983 | $1.95X10^{-4}$ | 1.21 | 1.08 | 0.77** | 3.00 |
| | **Br** | | | $1.95X10^{-4}$ | 13.87 | 1.08 | 0.22 | 0.85 |

* Set equal to the average of D from the homogeneous tests multiplied the factor of $\theta_m/\theta$.
** Value was set equal to the calculated β (as $\theta_m/\theta$) since CNP was shown to be non-reactive

SUMMARY

The CNP were demonstrated to transport conservatively through both silica and the reactive media, SMZ. In the dual-porosity columns there appeared to be less transverse diffusion (mass transfer) of CNP into the immobile zone than Br, but the results of the two tracers were more similar than expected due to the high pore velocities. Subramanian et al. 2013 calculated the molecular diffusion coefficient of CNP, from their experiments as $1.5X10^{-6}$ $cm^2/s$. This value was within the range determined using the diameter of the particle and the Stokes-Einstein equation, and is one order of magnitude less than the molecular diffusion coefficient of Br (1.0X10-5 $cm^2/s$). CNP's smaller molecular diffusion coefficient agrees with the apparently lower mass transfer coefficients that were fitted, and the slightly lower concentrations of CNP in the elution portion of the dual-porosity breakthrough curves. However, the large pore velocities overwhelmed the contribution of molecular diffusion to the longitudinal hydrodynamic dispersion equation, resulting in nearly equal D values. This has important implications for the migration of environmental nanoparticles. In a coarse homogeneous or heterogeneous aquifer, the spreading of environmental nanoparticles could be a much larger problem than anticipated. Very fine NP, such as CNP, could disperse similarly to a solute into materials with large enough pore throats.

The other important result of this study, was to show that CNP are almost perfectly inert. Though they have a small surface charge of -1 to -2 mV, they barely reacted to the positive surface charge of the SMZ. In these experiments CNP had a retardation factor nearly equal to 1, while the retardation factor or Br was 11 to 18 times that value. This means that CNP would be very useful as the conservative tracer deployed with a reactive solute to detect the presence of other minerals or contaminants with either positive or negative surface charges.

# CHAPTER 5: RECOMMENDATIONS FOR FUTURE WORK

The process of fully developing CNP as a groundwater tracer through transport characterization has been started with this work, but there is much more which needs to be accomplished. CNP transport needs to be tested in a wider variety of porous media and pore fluid chemistries. Transport should also be studied in 2 and 3 dimensional space in addition to this 1 dimensional transport study. Since one of the main goals in the overall project is to understand how NP move through the subsurface it will also be important to work with different surface-functionalized CNP. And though the precursors to these CNP indicate that they should be non-toxic this should be confirmed. With these aims in mind, I suggest the following future work be conducted.

## ADDITIONAL COLUMN TESTS

- A randomly-arrayed heterogeneous column should be designed to mimic vertical flow around and partially through lenses of finer material in the subsurface.
- Finer material such as non-swelling clays should be experimented with in heterogeneous columns to determine whether CNP diffusion is inhibited by material with even lower permeability than the fine sand tested in these experiments.
- To test reactivity under more natural conditions, laboratory-grade organic matter, such as Suwannee River Humic Acid, should be used as the reactive media instead of SMZ.
- Locally-collected sediment should be characterized with grain-size analyses and fraction of organic carbon, so that they can be used in column testing.
- Locally-collected water samples should be analyzed for their common and trace ion chemistry, so that they can be used in column testing.

- Additional sediment types and water chemistries, including a range of ionic strengths, from other regions should be considered for testing.

SAND TANK EXPERIMENTS

- Homogeneous sand tank experiments should be conducted to assess the impact of density-driven flow at various tracer concentrations.
- Heterogeneous sand tanks should be designed with lenses of finer material, to examine mass transfer between the mobile and immobile zones.
- During these tests time-lapse photography and/or videos of transport can be taken under black-light conditions to view CNP flow paths.

GROUNDWATER TRACER TESTS

- Short-range push-pull field tests should be conducted first to assess mass recovery and necessary injection concentrations and volumes in aquifers with various hydrogeologic conditions.
- Longer-range interwell field test should be conducted to test CNP recovery and transit times relative to solute tracers in heterogeneous aquifers with likely preferential flow paths.
- CNP should be used as a groundwater tracer in a harsh environments to confirm their stability and suitability, such as salt flats or hydraulic fracturing operations.
- CNP should be co-deployed with $Fe^0$-NP at a contaminated site to test the ability of CNP to assess the sweep efficiency of a remediation effort.

## SURFACE WATER TRACER TESTS

- CNP should be co-deployed with a salt or dye tracer to assess their applicability as a surface water tracer.
- Recovery of the CNP should be compared to standard tracers to determine if they increase the understanding of transient storage stream processes.
- Real time recording of CNP flow paths under black-light conditions at night could further illuminate differences such as hyporheic exchange versus eddying.

## DIFFERENT SURFACE FUNCTIONALIZATION

- Hydrophobic CNP should be engineered and tested in the same way as the hydrophilic CNP to assess differences in transport properties.
- CNP targeted to sorb to subsurface contaminants such as NAPL or heavy metals should be engineered to test the viability of CNP as the partitioning tracer, instead of the conservative tracer used to assess amount of the target in the subsurface.

## TOXICOLOGY

- An effort should be made to reach out to the College of Veterinary Medicine and Biomedical Sciences, Department of Environmental and Radiological Health Sciences, which runs the Toxicology program at CSU.
- The identified collaborator(s) may want to start with similar studies to those which have been cited in CHAPTER 1, focusing on aquatic life.

SUGGESTED EQUIPMENT OR PROCEDURAL CHANGES

- Concentrations of column effluent between CNP and $Br^-$ could be directly comparable if identical concentrations of each were in the dual-tracer.
- Numerical modeling methods should be considered in order to analyze the 2D and 3D transport experiments.
- A microplate sealer should be purchased to better protect the CNP samples from cross-contamination or evaporation.
- More accurate $Br^-$ analyses could be conducted, much more quickly, if funding for ion-chromatography analysis was available.
- Barring the availability for ion-chromatography, the process of analyzing samples could be streamlined with the addition of another ISE probe and meter.
- A slower flow rate could be achieved, particularly in the heterogeneous columns, if a syringe pump was available.
- The additional fraction collector which was procured for the carousels should be brought online to allow multiple column tests to be conducted at the same time.
- If the second fraction collector is put into service, the purchase of three more carousels and two more boxes of test tubes should be made.
- Swage-lock PTFE connectors and more quartz frits should be purchased to allow more columns to be built at the same time.
- A variety of porous and/or reactive media should be considered for purchase.
- A laboratory assistant or two should be hired to cover 10 to 20 hours a week in order to stay on top of analyzing samples, washing lab ware, and maintaining equipment.

# REFERENCES


Ali, D., Ali, H., Alarifi, S., Kumar, S., Serajuddin, M., Mashih, A.P., Ahmed, M., Khan, M., Adil, S.F., Shaik, M.R., and Ansari, A.A., 2015, Impairment of DNA in a freshwater gastropod (Lymnea luteola L.) after exposure to titanium dioxide nanoparticles: Archives of Environmental Contamination and Toxicology, v. 68, p. 543-552.

Alonso, U., Missana, T., Patelli, A., Ceccato, D., Alabarran, N., García-Gutiérrez, M., Lopez-Torrubia, T., and Rigato, V., 2009, Quantification of Au nanoparticles retention on a heterogeneous rock surface: Colloids and Surfaces A: Physiochemical and Engineering Aspects, v. 347, p. 230-238.

Annable, M.D., Rao, P.S.C, Hatfield, K., Graham, W.D., Wood, A.L., and Enfield, C.G., 1998, Partitioning tracers for measuring residual NAPL: Field-scale test results: Journal of Environmental Engineering, v. 124, no. 6, p. 498-503.

Basnet, M., Tommaso, C.D., Ghoshal, S., and Tufenkji, N., 2015, Reduced transport potential of a palladium-doped zero valent iron nanoparticle in a water saturated loamy sand: Water Research, v. 68, p. 354-363.

Battin, T.J., von der Kammer, F., Weilhartner, A., Ottofuelling, S., and Hofmann, T., 2009, Nanostructured TiO2: transport behavior and effects on aquatic microbial communities under environmental conditions: Environmental Science & Technology, v. 43, p. 8098-8104.

Becker, M.W., Reimus, P.W., and Vilks, P., 1999, Transport and attenuation of carboxylate-modified latex microspheres in fractured rock laboratory and field tracer tests: Ground Water, v. 37, no. 3, p. 387-395.

Brar, S.K., Verma, M., Tyagi, R.D., Surampalli, R.Y., 2009, Engineered nanoparticles in wastewater and wastewater sludge – evidence and impacts: Waste Management, v. 30, p. 504-520.

Chalew, T.E., Ajmani, G.S., Huang, H., and Schwab, K.J., 2013, Evaluating nanoparticle breakthrough during drinking water treatment: Environmental Health Perspectives, v. 121, no. 10, p. 1161-1166.

Crist, J.T., Zevi, Y., McCarthy, J.F., Throop, J.A., and Steenhuis, T.S., 2005, Transport and retention mechanisms of colloids in partially saturated porous media, v. 4, p. 184-195.

Divine, C.E., Sanford, W.E., and McCray, J.E., 2003, Helium and neon groundwater tracers to measure residual DNAPL: Laboratory investigation: Vadose Zone Journal, v. 2, p. 382-388.

Fang, J., Shan, X-q., Wen, B., Lin, J-m., and Owens, G., 2008, Stability of titania nanoparticles in soil suspensions and transport in saturated homogeneous soil columns: Environmental Pollution, v. 157, p. 1101-1109.

Farkas, J., Peter, H., Christian, P., Urrea, J.A.G., Hassellöv, M., Tuoriniemi, J., Gustafsson, S., Olsson, E., Hylland, K., and Thomas, K.V., 2011, Characterization of the effluent from a nanosilver producing washing machine: Environment International, v. 37, p. 1057-1062.

Geranio, L., Heuberger, M., and Nowack, B., 2009, The behavior of silver nanotextiles during washing: Environment Science and Technology, v. 43, p. 8113-8118.

Hofmann, T. and von der Kammer, F., 2009, Estimating the relevance of engineered carbonaceous nanoparticle facilitated transport of hydrophobic organic contaminants in porous media: Environmental Pollution, v. 157, p. 1117-1126.

Huber, F., Enzmann, F., Wenka, A., Bouby, M., Dentz, M., and Shafer, T., 2012, Natural micro-scale heterogeneity induced solute and nanoparticle retardation in fractured crystalline rock: Journal of Contaminant Hydrology, v. 133, p. 40-52.

Jarvie, H.P., Al-Obaidi, H., King, S.M., Bowes, M.J., Lawrence, M.J., Drake, A.F., and Dobson, P.J., 2009, Fate of silica nanoparticles in simulated primary wastewater treatment: Environment Science & Technology, v. 43, p. 8622-8628.

Kanel, S.R., Goswami, R.R., Clement, T.P., Barnett, M.O., and Zhao, D., 2008, Two dimensional transport characteristics of surface stabilized zero-valent iron nanoparticles in porous media: Environmental Science & Technology, v. 42, p. 896-900.

Kanj, M.Y., Rashid, H., and Giannelis, E.P., 2011, Industry first field trial of reservoir nanoagents: Society of Petroleum Engineers International, Middle East Oil and Gas Show and Conference, paper 142592.

Keller, A.A., McFerran, S., Lazareva, A., and Suh, S., 2013, Global life cycle releases of engineered nanomaterials: Journal of Nanoparticle Research, v. 15, 17 p.

Kinsinger, N., Honda, R., Keene, V., and Walker, S.L., 2015, Titanium dioxide nanoparticle removal in primary prefiltration stages of water treatment: role of coating, natural organic matter, source water, and solution chemistry: Environmental Engineering Science, v. 32, no. 4, p. 292-300.

Krysmann, M.J., Kelarakis, A., Dallas, P., and Giannelis, E.P., 2011, Formation mechanism of carbogenic nanoparticles with dual photoluminescence emission: Journal of the American Chemistry Society, v. 134, n. 2, p. 747-750.

Lecoanet, H.F. and Wiesner, M.R., 2004a, Velocity effects on fullerene and oxide nanoparticle deposition in porous media: Environmental Science & Technology, v. 38, p. 4377-4382.

Lecoanet, H.F., Bottero, J., Wiesner, M.R., 2004b, Laboratory assessment of the mobility of nanomaterials in porous media: Environmental Science & Technology, v. 38, p. 5164-5169.

Li, Y.V., Cathles L.M., and Archer, L.A., 2014, Nanoparticle tracers in calcium carbonate porous media: Journal of Nanoparticle Research, v. 16, 14 p.

Lin, D. and Xing, B., 2008, Root uptake and phytotoxicity of ZnO nanoparticles. Environmental Science & Technology, v. 42, p. 5580-5585.

Loo, S-L., Fane, A.G., Lim, T-T., Krantz, W.B., Liang, Y-N., Liu, X., and Hu, X., 2013, Superabsorbent cryogels decorated with silver nanoparticles as a novel water technology for point-of-use disinfection: Environmental Science & Technology, v. 47, p. 9363-9371.

McCarthy, J.F. and Zachara, J.M., 1989, Subsurface transport of contaminants: Environmental Science and Technology, v. 23, no. 5, p. 496-502.

McCarthy, J.F., Czerwinski, K.R., Sanford, W.E., Jardine, P.M., and Marsh, J.D., 1998a, Mobilization of transuranic radionuclides from disposal trenches by natural organic matter: Journal of Contaminant Hydrology, v. 30, p. 49-77.

McCarthy, J.F., Sanford, W.E., and Stafford, P.L., 1998b, Lanthanide field tracers demonstrate enhanced transport of transuranic radionuclides by natural organic matter: Environmental Science & Technology, v. 32, no. 24, p. 3901-3906.

McKay, L.D., Sanford, W.E., and Strong, J.M., 2000, Field-scale migration of colloidal tracers in a fractured shale saprolite: Groundwater, v. 38, no. 1, p. 139-147.

Oberdörster, G., Stone, V., and Donaldson, K., 2007, Toxicology of nanoparticles: a historical perspective: Nanotoxicology, v. 1, no. 1, p. 2-25.

Penrose, W.R., Polzer, W.L., Essington, E.H., Nelson, D.M., and Orlandini, K.A., 1990, Mobility of plutonium and americium through a shallow aquifer in a semiarid region: Environmental Science & Technology, v. 24, p. 228-234.

Reimus, P.W., 1995, Transport of synthetic colloids through single saturated fractures: a literature review: Los Alamos National Laboratory Report LA-12707-MS.

Reyhanitabar, A., Alidokht, L., Khataee, A.R., and Oustan, S., 2012, Application of stabilized $Fe^0$ nanoparticles for remediation of Cr(VI)-spiked soil: European Journal of Soil Science, v. 63, p. 724-732.

Som, C., Wick, P., Krug, H., Nowack, B., 2011, Environmental and health effects of nanomaterials in nanotextiles and façade coatings: Environmental International, v. 37, p. 1131-1142.

Stampoulis, D., Sinha, S.K., White, J.C., 2009, Assay-dependent phytotoxicity of nanoparticles to plants: Environmental Science & Technology, v. 43, p. 9473-9479.

Subramanian, S.K., Li, Y., Cathles, L.M., 2013, Assessing preferential flow by simultaneously injecting nanoparticle and chemical tracers: Water Resources Research, v. 49, p. 29-42.

Sygouni, V., and Chrysikopoulos, C.V., 2015, Characterization of TiO2 nanoparticle suspensions in aqueous solutions and TiO2 nanoparticle retention in water-saturated columns packed with glass beads: Chemical Engineering Journal, v. 262, p. 823-830.

Toride, N., Leij, F.J., and van Genuchten, M.Th., 1995, The CXTFIT code for estimating transport parameters from laboratory or field tracer experiments, version 2.0: U.S. Department of Agriculture, Agricultural Resource Service, U.S. Salinity Laboratories, research report no. 137, 117 p.

van Genuchten, M.Th., and Alves, W.J., 1982, Analytical solutions of the one-dimensional convective-dispersion solute transport equation: U.S. Department of Agriculture, technical bulletin no. 1661, 151 p.

Vitorge, E., Szenknect, S., Martins, J.M.F., Barthès, V., Auger, A., Renard, O., and Gaudet, J-P., 2014, Comparison of three labeled silica nanoparticles used as tracers in transport experiments in porous media. Part I: synthesis and characterizations: Environmental Pollution, v. 184, p. 605-612.

Wagner, S., Gondikas, A., Neubauer, E., Hofmann, T., and von der Kammer, F., 2014, Spot the difference: engineered and natural nanoparticles in the environment – release, behavior, and fate: Angewandte Chemie, International Edition, v. 53, p. 12398-12419.

Wiesner, M.R., Lowry, G.V., Alvarez, P., Dionysiou, D., and Biswas, P., 2006, Assessing the risks of manufactured nanomaterials: Environmental Science & Technology, July, p. 4336-4345.

Yang, X., Lin, S., and Wiesner, M.R., 2014, Influence of natural organic matter on transport and retention of polymer coated silver nanoparticles in porous media: Journal of Hazardous Materials, v. 264, p. 161-168.

# APPENDIX A: EFFLUENT CONCENTRATION DATA

**Column Type:** Homogeneous Porous Media
**Experiment Name:** Pulse Test #1; Page 1 of 2
**Experiment Date:** 30-Dec-14
**Media Length (cm):** 30.48
**Pore Volume (mL):** 210.04
**Design Details / Problems:** with 1.30 cm thick quartz frits; pore velocity could be lower

**Tracer Pulse Time (min):** 50
**Flow Rate (mL $min^{-1}$):** 1.22
**Application Volume (mL):** 61.06
**Pore Velocity (m $d^{-1}$):** 2.55

| T (PV) | Br ($C/C_0$) | CNP ($C/C_0$) |
|---|---|---|
| 0.061 | 0.000 | 0.000 |
| 0.228 | 0.000 | 0.002 |
| 0.271 | 0.000 | 0.002 |
| 0.358 | 0.000 | 0.002 |
| 0.445 | 0.000 | 0.002 |
| 0.488 | 0.000 | 0.002 |
| 0.531 | 0.000 | 0.010 |
| 0.575 | 0.000 | 0.011 |
| 0.661 | 0.000 | 0.002 |
| 0.748 | 0.000 | 0.002 |
| 0.791 | 0.000 | 0.002 |
| 0.835 | 0.000 | 0.002 |
| 0.878 | 0.000 | 0.002 |
| 0.921 | 0.000 | 0.003 |
| 0.965 | 0.006 | 0.009 |
| 1.008 | 0.037 | 0.039 |
| 1.051 | 0.161 | 0.133 |
| 1.095 | 0.398 | 0.337 |
| 1.138 | 0.651 | 0.584 |
| 1.181 | 0.789 | 0.792 |
| 1.225 | 0.867 | 0.928 |
| 1.268 | 0.928 | 0.940 |
| 1.311 | 0.901 | 0.838 |
| 1.355 | 0.660 | 0.645 |

**Continued**

| T (PV) | Br ($C/C_0$) | CNP ($C/C_0$) |
|---|---|---|
| 1.398 | 0.491 | 0.417 |
| 1.441 | 0.264 | 0.221 |
| 1.485 | 0.144 | 0.147 |
| 1.528 | 0.077 | 0.091 |
| 1.571 | 0.040 | 0.055 |
| 1.615 | 0.019 | 0.034 |
| 1.658 | 0.009 | 0.027 |
| 1.701 | 0.005 | 0.021 |
| 1.745 | 0.002 | 0.011 |
| 1.788 | 0.000 | 0.010 |
| 1.831 | 0.000 | 0.008 |
| 1.875 | 0.000 | 0.006 |
| 1.918 | 0.000 | 0.006 |
| 1.961 | 0.000 | 0.005 |
| 2.048 | 0.000 | 0.004 |
| 2.091 | 0.000 | 0.004 |
| 2.135 | 0.000 | 0.004 |
| 2.178 | 0.000 | 0.004 |
| 2.265 | 0.000 | 0.005 |
| 2.308 | 0.000 | 0.005 |
| 2.351 | 0.000 | 0.003 |
| 2.395 | 0.000 | 0.003 |
| 2.438 | 0.000 | 0.003 |

**Column Type:** Homogeneous Porous Media
**Experiment Name:** Pulse Test #1; Page 2 of 2

**Continued**

| T (PV) | Br ($C/C_0$) | CNP ($C/C_0$) |
|---|---|---|
| 2.481 | 0.000 | 0.003 |
| 2.525 | 0.000 | 0.003 |
| 2.568 | 0.000 | 0.003 |
| 2.611 | 0.000 | 0.003 |
| 2.655 | 0.000 | 0.003 |
| 2.698 | 0.000 | 0.003 |
| 2.785 | 0.000 | 0.003 |
| 2.828 | 0.000 | 0.003 |
| 2.915 | 0.000 | 0.003 |
| 2.958 | 0.000 | 0.003 |
| 3.001 | 0.000 | 0.003 |
| 3.045 | 0.000 | 0.003 |
| 3.131 | 0.000 | 0.002 |
| 3.175 | 0.000 | 0.002 |
| 3.218 | 0.000 | 0.002 |
| 3.261 | 0.000 | 0.002 |
| 3.305 | 0.000 | 0.002 |
| 3.391 | 0.000 | 0.002 |

**Column Type:** Homogeneous Porous Media
**Experiment Name:** Pulse Test #2
**Experiment Date:** 24-Jan-15
**Media Length (cm):** 30.48
**Pore Volume (mL):** 210.04
**Design Details / Problems:** with 1.30 cm thick quartz frits

**Tracer Pulse Time (min):** 55.73
**Flow Rate (mL $min^{-1}$):** 0.94
**Application Volume (mL):** 61.06
**Pore Velocity (m $d^{-1}$):** 1.97

| T (PV) | Br ($C/C_0$) | CNP ($C/C_0$) |
|---|---|---|
| 0.006 | 0.000 | 0.000 |
| 0.112 | 0.000 | 0.002 |
| 0.145 | 0.000 | 0.002 |
| 0.210 | 0.000 | 0.002 |
| 0.275 | 0.000 | 0.002 |
| 0.307 | 0.000 | 0.001 |
| 0.405 | 0.000 | 0.001 |
| 0.470 | 0.000 | 0.002 |
| 0.535 | 0.000 | 0.002 |
| 0.567 | 0.000 | 0.002 |
| 0.664 | 0.000 | 0.002 |
| 0.762 | 0.000 | 0.002 |
| 0.794 | 0.000 | 0.002 |
| 0.859 | 0.000 | 0.002 |
| 0.924 | 0.000 | 0.001 |
| 0.957 | 0.000 | 0.001 |
| 0.989 | 0.000 | 0.002 |
| 1.022 | 0.012 | 0.020 |
| 1.054 | 0.053 | 0.086 |
| 1.087 | 0.146 | 0.176 |
| 1.119 | 0.319 | 0.342 |
| 1.152 | 0.509 | 0.537 |
| 1.184 | 0.653 | 0.663 |
| 1.217 | 0.782 | 0.780 |
| 1.249 | 0.877 | 0.833 |
| 1.282 | 0.877 | 0.792 |
| 1.314 | 0.801 | 0.761 |
| 1.347 | 0.666 | 0.671 |
| 1.379 | 0.571 | 0.577 |

**Continued**

| T (PV) | Br ($C/C_0$) | CNP ($C/C_0$) |
|---|---|---|
| 1.412 | 0.433 | 0.463 |
| 1.444 | 0.289 | 0.373 |
| 1.477 | 0.195 | 0.278 |
| 1.509 | 0.118 | 0.189 |
| 1.542 | 0.061 | 0.135 |
| 1.574 | 0.026 | 0.082 |
| 1.607 | 0.009 | 0.047 |
| 1.639 | 0.008 | 0.023 |
| 1.671 | 0.001 | 0.015 |
| 1.704 | 0.000 | 0.007 |
| 1.736 | 0.000 | 0.004 |
| 1.769 | 0.000 | 0.002 |
| 1.834 | 0.000 | 0.068 |
| 1.899 | 0.000 | 0.024 |
| 1.931 | 0.000 | 0.001 |
| 2.029 | 0.000 | 0.001 |
| 2.061 | 0.000 | 0.001 |
| 2.094 | 0.000 | 0.001 |
| 2.159 | 0.000 | 0.001 |
| 2.191 | 0.000 | 0.001 |
| 2.289 | 0.000 | 0.001 |
| 2.354 | 0.000 | 0.001 |
| 2.419 | 0.000 | 0.001 |
| 2.484 | 0.000 | 0.001 |
| 2.549 | 0.000 | 0.001 |
| 2.581 | 0.000 | 0.001 |

**Column Type:** Homogeneous Porous Media
**Experiment Name:** Step Test; Page 1 of 2
**Experiment Date:** 16-Jan-15
**Media Length (cm):** 30.48
**Pore Volume (mL):** 210.04
**Design Details / Problems:** with 1.30 cm thick quartz frits

**Tracer Pulse Time (min):** 463.5
**Flow Rate (mL $min^{-1}$):** 1.31
**Application Volume (mL):** 608.89
**Pore Velocity (m $d^{-1}$):** 2.74

| T (PV) | Br ($C/C_0$) | CNP ($C/C_0$) |
|---|---|---|
| 0.010 | 0.000 | 0.000 |
| 0.119 | 0.000 | 0.001 |
| 0.150 | 0.000 | 0.005 |
| 0.244 | 0.000 | 0.001 |
| 0.275 | 0.000 | 0.006 |
| 0.337 | 0.000 | 0.013 |
| 0.368 | 0.000 | 0.003 |
| 0.462 | 0.000 | 0.001 |
| 0.493 | 0.000 | 0.002 |
| 0.524 | 0.000 | 0.001 |
| 0.555 | 0.000 | 0.001 |
| 0.618 | 0.000 | 0.002 |
| 0.680 | 0.000 | 0.001 |
| 0.711 | 0.000 | 0.006 |
| 0.742 | 0.000 | 0.004 |
| 0.805 | 0.000 | 0.002 |
| 0.836 | 0.001 | 0.002 |
| 0.898 | 0.001 | 0.002 |
| 0.930 | 0.000 | 0.002 |
| 0.961 | 0.001 | 0.005 |
| 0.992 | 0.005 | 0.014 |
| 1.023 | 0.030 | 0.047 |
| 1.054 | 0.083 | 0.113 |
| 1.085 | 0.185 | 0.212 |
| 1.117 | 0.349 | 0.368 |
| 1.148 | 0.521 | 0.512 |
| 1.179 | 0.714 | 0.719 |
| 1.210 | 0.780 | 0.797 |
| 1.241 | 0.873 | 0.862 |

**Continued**

| T (PV) | Br ($C/C_0$) | CNP ($C/C_0$) |
|---|---|---|
| 1.273 | 0.901 | 0.897 |
| 1.304 | 0.931 | 0.863 |
| 1.335 | 0.937 | 0.888 |
| 1.366 | 0.994 | 0.877 |
| 1.397 | 0.961 | 0.957 |
| 1.429 | 0.940 | 0.974 |
| 1.460 | 0.955 | 0.991 |
| 1.491 | 0.964 | 0.947 |
| 1.522 | 0.910 | 0.993 |
| 1.553 | 0.973 | 0.996 |
| 1.584 | 1.012 | 0.923 |
| 1.616 | 1.000 | 0.944 |
| 1.647 | 0.978 | 0.937 |
| 1.678 | 0.987 | 0.857 |
| 1.740 | 0.975 | 0.839 |
| 1.772 | 1.003 | 0.958 |
| 1.865 | 1.000 | 1.018 |
| 1.896 | 0.990 | 0.952 |
| 1.927 | 1.038 | 0.961 |
| 1.959 | 1.022 | 0.997 |
| 1.990 | 0.994 | 0.984 |
| 2.052 | 1.006 | 0.971 |
| 2.083 | 0.987 | 0.974 |
| 2.115 | 0.994 | 0.913 |
| 2.146 | 1.038 | 0.933 |
| 2.239 | 1.016 | 0.999 |
| 2.270 | 1.000 | 1.012 |
| 2.333 | 0.994 | 1.012 |

**Column Type:** Homogeneous Porous Media

**Experiment Name:** Step Test; Page 2 of 2

**Continued**

| T (PV) | Br ($C/C_0$) | CNP ($C/C_0$) |
|---|---|---|
| 2.395 | 1.006 | 1.034 |
| 2.426 | 1.000 | 1.030 |
| 2.520 | 0.990 | 0.986 |
| 2.582 | 1.016 | 0.979 |
| 2.614 | 1.006 | 1.000 |
| 2.676 | 1.019 | 1.035 |
| 2.769 | 0.981 | 1.026 |
| 2.801 | 1.013 | 1.003 |
| 2.832 | 0.976 | 0.997 |
| 2.863 | 0.976 | 0.910 |
| 2.957 | 0.997 | 0.918 |
| 2.988 | 0.985 | 0.942 |
| 3.019 | 1.009 | 0.998 |
| 3.081 | 1.000 | 0.964 |
| 3.112 | 1.012 | 1.026 |
| 3.144 | 0.997 | 1.034 |
| 3.175 | 0.974 | 1.037 |
| 3.206 | 0.944 | 1.016 |
| 3.300 | 1.003 | 0.987 |
| 3.393 | 0.929 | 0.998 |
| 3.424 | 0.921 | 0.977 |
| 3.518 | 0.985 | 0.912 |
| 3.580 | 0.891 | 0.949 |
| 3.611 | 0.932 | 0.980 |
| 3.643 | 0.928 | 0.990 |
| 3.736 | 0.928 | 0.979 |
| 3.799 | 0.936 | 1.048 |
| 3.830 | 0.908 | 1.035 |
| 3.861 | 0.902 | 1.044 |
| 3.892 | 0.893 | 0.979 |
| 3.923 | 0.728 | 0.853 |
| 3.954 | 0.630 | 0.719 |
| 3.986 | 0.497 | 0.559 |
| 4.017 | 0.355 | 0.393 |
| 4.048 | 0.233 | 0.254 |
| 4.079 | 0.127 | 0.201 |
| 4.110 | 0.068 | 0.148 |

**Continued**

| T (PV) | Br ($C/C_0$) | CNP ($C/C_0$) |
|---|---|---|
| 4.142 | 0.038 | 0.108 |
| 4.173 | 0.022 | 0.076 |
| 4.204 | 0.009 | 0.055 |
| 4.235 | 0.004 | 0.041 |
| 4.266 | 0.001 | 0.034 |
| 4.297 | 0.001 | 0.029 |
| 4.329 | 0.001 | 0.026 |
| 4.360 | 0.001 | 0.022 |
| 4.391 | 0.001 | 0.019 |
| 4.422 | 0.001 | 0.018 |
| 4.453 | 0.001 | 0.017 |
| 4.485 | 0.001 | 0.016 |
| 4.547 | 0.000 | 0.014 |
| 4.641 | 0.000 | 0.013 |
| 4.703 | 0.000 | 0.012 |
| 4.734 | 0.000 | 0.012 |
| 4.765 | 0.000 | 0.011 |
| 4.859 | 0.000 | 0.010 |
| 4.890 | 0.000 | 0.010 |
| 4.921 | 0.000 | 0.009 |
| 4.952 | 0.000 | 0.009 |
| 5.015 | 0.000 | 0.008 |
| 5.077 | 0.000 | 0.007 |
| 5.108 | 0.000 | 0.008 |
| 5.139 | 0.000 | 0.008 |
| 5.202 | 0.000 | 0.007 |
| 5.264 | 0.000 | 0.007 |
| 5.295 | 0.000 | 0.007 |
| 5.327 | 0.000 | 0.007 |
| 5.358 | 0.000 | 0.007 |
| 5.389 | 0.000 | 0.007 |
| 5.420 | 0.000 | 0.006 |

**Column Type:** Dual-Porosity
**Experiment Name:** Design #1, Pulse Test; Page 1 of 2
**Experiment Date:** 26-Jan-15
**Media Length (cm):** 30.48
**Mobile Pore Volume (mL):** 52.51
**Design Details / Problems:** 2.54cm diameter core, with frits, no baffles
flow paths through fines results in double peak of BTC
**Tracer Pulse Time (min):** 55.05
**Flow Rate (mL $min^{-1}$):** 0.95
**Application Volume (mL):** 52.5
**Mobile Pore Velocity (m $d^{-1}$):** 7.97

| T (PV) | Br ($C/C_0$) | CNP ($C/C_0$) |
|---|---|---|
| 0.082 | 0.003 | 0.003 |
| 0.341 | 0.002 | 0.003 |
| 0.462 | 0.002 | 0.003 |
| 0.704 | 0.002 | 0.003 |
| 0.946 | 0.002 | 0.003 |
| 1.101 | 0.002 | 0.003 |
| 1.343 | 0.002 | 0.003 |
| 1.585 | 0.003 | 0.003 |
| 1.827 | 0.003 | 0.003 |
| 1.947 | 0.002 | 0.003 |
| 2.068 | 0.002 | 0.003 |
| 2.189 | 0.003 | 0.006 |
| 2.310 | 0.015 | 0.026 |
| 2.431 | 0.055 | 0.089 |
| 2.552 | 0.114 | 0.172 |
| 2.673 | 0.196 | 0.259 |
| 2.794 | 0.257 | 0.335 |
| 2.915 | 0.300 | 0.405 |
| 3.035 | 0.383 | 0.457 |
| 3.156 | 0.380 | 0.475 |
| 3.277 | 0.393 | 0.474 |
| 3.398 | 0.356 | 0.438 |
| 3.519 | 0.290 | 0.357 |
| 3.640 | 0.248 | 0.298 |
| 3.761 | 0.195 | 0.230 |
| 3.882 | 0.155 | 0.157 |
| 4.003 | 0.130 | 0.151 |
| 4.123 | 0.119 | 0.114 |
| 4.244 | 0.109 | 0.117 |

**Continued**

| T (PV) | Br ($C/C_0$) | CNP ($C/C_0$) |
|---|---|---|
| 4.365 | 0.096 | 0.102 |
| 4.486 | 0.083 | 0.095 |
| 4.607 | 0.078 | 0.078 |
| 4.728 | 0.071 | 0.080 |
| 4.849 | 0.069 | 0.078 |
| 4.970 | 0.066 | 0.070 |
| 5.091 | 0.057 | 0.067 |
| 5.211 | 0.055 | 0.060 |
| 5.332 | 0.055 | 0.056 |
| 5.453 | 0.055 | 0.053 |
| 5.574 | 0.046 | 0.049 |
| 5.695 | 0.045 | 0.046 |
| 5.816 | 0.046 | 0.042 |
| 5.937 | 0.040 | 0.038 |
| 6.058 | 0.035 | 0.032 |
| 6.179 | 0.037 | 0.034 |
| 6.299 | 0.037 | 0.034 |
| 6.420 | 0.035 | 0.032 |
| 6.541 | 0.024 | 0.031 |
| 6.662 | 0.026 | 0.031 |
| 6.904 | 0.032 | 0.027 |
| 7.025 | 0.030 | 0.028 |
| 7.146 | 0.029 | 0.025 |
| 7.387 | 0.026 | 0.022 |
| 7.508 | 0.027 | 0.020 |
| 7.750 | 0.030 | 0.024 |
| 7.992 | 0.037 | 0.043 |
| 8.113 | 0.050 | 0.063 |

**Column Type:** Dual-Porosity

**Experiment Name:** Design #1, Pulse Test; Page 2 of 2

**Continued**

| T (PV) | Br ($C/C_0$) | CNP ($C/C_0$) |
|---|---|---|
| 8.234 | 0.056 | 0.088 |
| 8.355 | 0.100 | 0.116 |
| 8.475 | 0.104 | 0.142 |
| 8.596 | 0.121 | 0.166 |
| 8.717 | 0.131 | 0.200 |
| 8.838 | 0.152 | 0.159 |
| 8.959 | 0.155 | 0.229 |
| 9.080 | 0.179 | 0.023 |
| 9.201 | 0.166 | 0.201 |
| 9.322 | 0.118 | 0.191 |
| 9.443 | 0.104 | 0.148 |
| 9.563 | 0.088 | 0.115 |
| 9.684 | 0.049 | 0.086 |
| 9.926 | 0.020 | 0.184 |
| 10.047 | 0.015 | 0.026 |
| 10.168 | 0.008 | 0.016 |
| 10.410 | 0.003 | 0.009 |
| 10.531 | 0.002 | 0.008 |
| 10.772 | 0.001 | 0.005 |
| 10.893 | 0.001 | 0.005 |
| 11.135 | 0.001 | 0.004 |
| 11.256 | 0.001 | 0.004 |
| 11.498 | 0.001 | 0.004 |
| 11.619 | 0.001 | 0.004 |
| 11.739 | 0.001 | 0.004 |
| 11.981 | 0.001 | 0.004 |
| 12.223 | 0.001 | 0.003 |
| 12.344 | 0.001 | 0.003 |
| 12.637 | 0.001 | 0.003 |
| 12.758 | 0.001 | 0.003 |
| 12.879 | 0.000 | 0.003 |
| 13.242 | 0.000 | 0.003 |
| 13.484 | 0.000 | 0.003 |
| 13.605 | 0.000 | 0.003 |
| 13.725 | 0.000 | 0.003 |
| 13.967 | 0.000 | 0.003 |
| 14.330 | 0.000 | 0.003 |

**Continued**

| T (PV) | Br ($C/C_0$) | CNP ($C/C_0$) |
|---|---|---|
| 14.572 | 0.000 | 0.003 |
| 14.693 | 0.000 | 0.003 |
| 14.934 | 0.000 | 0.003 |
| 15.176 | 0.000 | 0.003 |
| 15.297 | 0.000 | 0.003 |
| 15.418 | 0.000 | 0.003 |
| 15.660 | 0.000 | 0.003 |
| 15.901 | 0.000 | 0.003 |
| 16.022 | 0.000 | 0.003 |
| 16.143 | 0.000 | 0.003 |
| 16.385 | 0.000 | 0.003 |
| 16.506 | 0.000 | 0.003 |

**Column Type:** Dual-Porosity
**Experiment Name:** Design #2, Pulse Test; Page 1 of 2
**Experiment Date:** 29-Jan-15
**Media Length (cm):** 30.48
**Mobile Pore Volume (mL):** 13.13
**Design Details / Problems:** 1.27cm diameter core, with frits and baffles
still had flow paths through fines and double peak in BTC
**Tracer Pulse Time (min):** 87.51
**Flow Rate (mL $min^{-1}$):** 0.69
**Application Volume (mL):** 60.68
**Mobile Pore Velocity (m $d^{-1}$):** 23.18

| T (PV) | Br ($C/C_0$) | CNP ($C/C_0$) |
|---|---|---|
| 0.171 | 0.000 | 0.000 |
| 1.340 | 0.005 | 0.000 |
| 2.484 | 0.003 | 0.000 |
| 3.056 | 0.002 | 0.000 |
| 3.628 | 0.002 | 0.000 |
| 4.200 | 0.002 | 0.001 |
| 4.772 | 0.002 | 0.005 |
| 5.344 | 0.016 | 0.032 |
| 5.916 | 0.066 | 0.083 |
| 6.488 | 0.128 | 0.148 |
| 7.060 | 0.179 | 0.210 |
| 7.632 | 0.219 | 0.259 |
| 8.203 | 0.251 | 0.294 |
| 8.775 | 0.289 | 0.326 |
| 9.347 | 0.320 | 0.335 |
| 9.919 | 0.300 | 0.301 |
| 10.491 | 0.263 | 0.237 |
| 11.063 | 0.209 | 0.196 |
| 11.635 | 0.182 | 0.157 |
| 12.207 | 0.158 | 0.136 |
| 12.779 | 0.138 | 0.115 |
| 13.351 | 0.124 | 0.105 |
| 13.923 | 0.115 | 0.094 |
| 14.495 | 0.105 | 0.083 |
| 15.067 | 0.089 | 0.073 |
| 15.639 | 0.088 | 0.070 |
| 16.210 | 0.081 | 0.064 |
| 16.782 | 0.072 | 0.058 |
| 17.354 | 0.066 | 0.053 |

**Continued**

| T (PV) | Br ($C/C_0$) | CNP ($C/C_0$) |
|---|---|---|
| 17.926 | 0.068 | 0.052 |
| 18.498 | 0.067 | 0.048 |
| 19.070 | 0.068 | 0.046 |
| 19.642 | 0.065 | 0.046 |
| 20.214 | 0.058 | 0.045 |
| 20.786 | 0.063 | 0.044 |
| 21.358 | 0.062 | 0.045 |
| 21.930 | 0.068 | 0.046 |
| 22.502 | 0.064 | 0.046 |
| 23.074 | 0.063 | 0.048 |
| 23.646 | 0.065 | 0.047 |
| 24.217 | 0.053 | 0.049 |
| 24.789 | 0.074 | 0.049 |
| 25.361 | 0.066 | 0.049 |
| 25.933 | 0.067 | 0.051 |
| 26.505 | 0.074 | 0.052 |
| 27.077 | 0.073 | 0.055 |
| 27.649 | 0.073 | 0.056 |
| 28.221 | 0.075 | 0.059 |
| 28.793 | 0.074 | 0.057 |
| 29.365 | 0.075 | 0.064 |
| 30.509 | 0.079 | 0.069 |
| 31.081 | 0.082 | 0.071 |
| 32.224 | 0.086 | 0.078 |
| 32.796 | 0.093 | 0.079 |
| 33.368 | 0.095 | 0.084 |
| 34.512 | 0.091 | 0.092 |
| 35.084 | 0.078 | 0.094 |

**Column Type:** Dual-Porosity

**Experiment Name:** Design #2, Pulse Test; Page 2 of 2

**Continued**

| T (PV) | Br ($C/C_0$) | CNP ($C/C_0$) |
|---|---|---|
| 35.656 | 0.094 | 0.094 |
| 36.800 | 0.088 | 0.090 |
| 37.372 | 0.082 | 0.086 |
| 37.944 | 0.089 | 0.082 |
| 38.516 | 0.077 | 0.076 |
| 39.088 | 0.073 | 0.072 |
| 40.231 | 0.059 | 0.060 |
| 40.803 | 0.051 | 0.052 |
| 41.375 | 0.043 | 0.049 |
| 42.519 | 0.029 | 0.038 |
| 43.091 | 0.022 | 0.033 |
| 43.663 | 0.017 | 0.030 |
| 44.235 | 0.010 | 0.026 |
| 45.379 | 0.006 | 0.019 |
| 45.951 | 0.004 | 0.017 |
| 46.523 | 0.004 | 0.014 |
| 47.666 | 0.002 | 0.010 |
| 48.238 | 0.002 | 0.009 |
| 48.810 | 0.001 | 0.008 |
| 49.954 | 0.000 | 0.006 |
| 50.526 | 0.000 | 0.005 |
| 51.098 | 0.000 | 0.005 |
| 52.242 | 0.000 | 0.004 |
| 52.814 | 0.000 | 0.003 |
| 53.386 | 0.000 | 0.003 |
| 53.969 | 0.000 | 0.003 |
| 54.552 | 0.000 | 0.003 |
| 55.696 | 0.000 | 0.002 |
| 56.268 | 0.000 | 0.002 |
| 57.412 | 0.000 | 0.002 |
| 57.984 | 0.000 | 0.002 |
| 59.128 | 0.000 | 0.002 |
| 59.700 | 0.000 | 0.002 |
| 60.844 | 0.000 | 0.001 |
| 61.987 | 0.000 | 0.001 |
| 63.131 | 0.000 | 0.001 |
| 63.703 | 0.000 | 0.001 |

**Continued**

| T (PV) | Br ($C/C_0$) | CNP ($C/C_0$) |
|---|---|---|
| 64.847 | 0.000 | 0.001 |
| 65.991 | 0.000 | 0.001 |
| 66.563 | 0.000 | 0.001 |
| 67.707 | 0.000 | 0.001 |
| 68.851 | 0.000 | 0.001 |
| 69.423 | 0.000 | 0.001 |

**Column Type:** Dual-Porosity
**Experiment Name:** Design #3, Pulse Test #1; Page 1 of 2
**Experiment Date:** 4-Feb-15
**Media Length (cm):** 31.76
**Mobile Pore Volume (mL):** 13.68
**Design Details / Problems:** 1.27cm diameter core, with baffles, no frits

**Tracer Pulse Time (min):** 67.74
**Flow Rate (mL $min^{-1}$):** 0.56
**Application Volume (mL):** 37.77
**Mobile Pore Velocity (m $d^{-1}$):** 18.64

| T (PV) | Br ($C/C_0$) | CNP ($C/C_0$) |
|---|---|---|
| 0.100 | 0.000 | 0.001 |
| 0.601 | 0.000 | 0.002 |
| 1.102 | 0.095 | 0.095 |
| 1.603 | 0.295 | 0.315 |
| 2.104 | 0.421 | 0.441 |
| 2.605 | 0.466 | 0.479 |
| 3.106 | 0.494 | 0.490 |
| 3.607 | 0.506 | 0.517 |
| 4.108 | 0.381 | 0.383 |
| 4.609 | 0.250 | 0.248 |
| 5.109 | 0.196 | 0.192 |
| 5.610 | 0.166 | 0.160 |
| 6.111 | 0.137 | 0.130 |
| 6.612 | 0.127 | 0.115 |
| 7.113 | 0.109 | 0.091 |
| 7.614 | 0.095 | 0.081 |
| 8.115 | 0.083 | 0.069 |
| 8.616 | 0.076 | 0.063 |
| 9.117 | 0.065 | 0.053 |
| 9.617 | 0.062 | 0.048 |
| 10.118 | 0.061 | 0.048 |
| 10.619 | 0.055 | 0.042 |
| 11.120 | 0.054 | 0.038 |
| 11.621 | 0.050 | 0.035 |
| 12.122 | 0.047 | 0.032 |
| 12.623 | 0.042 | 0.031 |
| 13.124 | 0.038 | 0.029 |
| 13.625 | 0.037 | 0.026 |
| 14.126 | 0.035 | 0.025 |

**Continued**

| T (PV) | Br ($C/C_0$) | CNP ($C/C_0$) |
|---|---|---|
| 14.626 | 0.034 | 0.023 |
| 15.628 | 0.032 | 0.019 |
| 16.129 | 0.029 | 0.020 |
| 17.131 | 0.028 | 0.017 |
| 17.632 | 0.029 | 0.019 |
| 18.634 | 0.026 | 0.016 |
| 19.635 | 0.027 | 0.016 |
| 20.136 | 0.021 | 0.014 |
| 20.637 | 0.021 | 0.014 |
| 21.639 | 0.017 | 0.014 |
| 22.140 | 0.018 | 0.013 |
| 23.142 | 0.017 | 0.012 |
| 23.643 | 0.014 | 0.011 |
| 24.644 | 0.014 | 0.010 |
| 25.145 | 0.015 | 0.010 |
| 25.646 | 0.013 | 0.009 |
| 26.648 | 0.014 | 0.009 |
| 27.149 | 0.016 | 0.009 |
| 28.151 | 0.015 | 0.008 |
| 28.651 | 0.016 | 0.009 |
| 29.653 | 0.016 | 0.009 |
| 30.655 | 0.016 | 0.009 |
| 31.156 | 0.016 | 0.009 |
| 31.657 | 0.015 | 0.009 |
| 32.659 | 0.015 | 0.009 |
| 33.660 | 0.015 | 0.008 |
| 34.161 | 0.013 | 0.009 |
| 34.662 | 0.013 | 0.008 |

**Column Type:** Dual-Porosity

**Experiment Name:** Design #3, Pulse Test #1; Page 2 of 2

**Continued**

| T (PV) | Br ($C/C_0$) | CNP ($C/C_0$) |
|---|---|---|
| 35.664 | 0.012 | 0.009 |
| 36.165 | 0.012 | 0.009 |
| 36.666 | 0.012 | 0.009 |
| 37.668 | 0.010 | 0.009 |
| 38.669 | 0.010 | 0.008 |
| 39.170 | 0.009 | 0.008 |
| 39.671 | 0.009 | 0.008 |
| 40.673 | 0.010 | 0.008 |
| 41.675 | 0.009 | 0.008 |
| 42.176 | 0.009 | 0.008 |
| 43.177 | 0.009 | 0.007 |
| 43.678 | 0.008 | 0.008 |
| 44.179 | 0.008 | 0.007 |
| 45.181 | 0.009 | 0.008 |
| 45.682 | 0.008 | 0.008 |
| 46.684 | 0.009 | 0.007 |
| 47.185 | 0.007 | 0.007 |
| 47.685 | 0.008 | 0.007 |
| 48.687 | 0.008 | 0.007 |
| 49.689 | 0.008 | 0.007 |
| 50.190 | 0.008 | 0.006 |
| 51.192 | 0.007 | 0.007 |
| 52.194 | 0.007 | 0.007 |
| 52.694 | 0.006 | 0.006 |
| 53.195 | 0.007 | 0.007 |
| 54.197 | 0.007 | 0.007 |
| 54.698 | 0.007 | 0.007 |
| 55.700 | 0.006 | 0.007 |
| 56.702 | 0.006 | 0.007 |
| 57.202 | 0.007 | 0.006 |
| 57.703 | 0.006 | 0.006 |
| 58.705 | 0.005 | 0.006 |
| 59.707 | 0.005 | 0.006 |
| 60.208 | 0.004 | 0.005 |
| 61.210 | 0.003 | 0.005 |
| 61.711 | 0.003 | 0.005 |
| 62.211 | 0.003 | 0.005 |

**Continued**

| T (PV) | Br ($C/C_0$) | CNP ($C/C_0$) |
|---|---|---|
| 62.712 | 0.003 | 0.005 |
| 63.213 | 0.003 | 0.005 |
| 63.714 | 0.003 | 0.005 |
| 64.716 | 0.003 | 0.005 |
| 65.217 | 0.003 | 0.004 |
| 66.219 | 0.003 | 0.004 |
| 67.220 | 0.002 | 0.004 |
| 68.222 | 0.002 | 0.004 |
| 69.725 | 0.002 | 0.003 |
| 70.226 | 0.002 | 0.003 |
| 70.727 | 0.001 | 0.004 |
| 72.229 | 0.001 | 0.003 |
| 73.732 | 0.000 | 0.003 |
| 74.734 | 0.000 | 0.003 |
| 75.736 | 0.000 | 0.003 |
| 76.737 | 0.000 | 0.003 |
| 77.739 | 0.000 | 0.003 |
| 78.741 | 0.000 | 0.003 |
| 79.743 | 0.000 | 0.003 |
| 80.244 | 0.000 | 0.003 |

**Column Type:** Dual-Porosity
**Experiment Name:** Design #3, Pulse Test #2; Page 1 of 2
**Experiment Date:** 10-Mar-15
**Media Length (cm):** 31.76
**Mobile Pore Volume (mL):** 13.68
**Design Details / Problems:** 1.27cm diameter core, with baffles, no frits

**Tracer Pulse Time (min):** 177.43
**Flow Rate (mL $min^{-1}$):** 0.38
**Application Volume (mL):** 67.89
**Mobile Pore Velocity (m $d^{-1}$):** 12.79

| T (PV) | Br ($C/C_0$) | CNP ($C/C_0$) |
|---|---|---|
| 0.100 | 0.000 | 0.001 |
| 0.654 | 0.000 | 0.001 |
| 1.207 | 0.132 | 0.157 |
| 1.760 | 0.342 | 0.334 |
| 2.313 | 0.410 | 0.403 |
| 2.867 | 0.448 | 0.435 |
| 3.420 | 0.472 | 0.464 |
| 3.973 | 0.493 | 0.486 |
| 4.526 | 0.519 | 0.518 |
| 5.079 | 0.540 | 0.534 |
| 5.633 | 0.563 | 0.558 |
| 6.739 | 0.593 | 0.579 |
| 7.292 | 0.608 | 0.601 |
| 7.845 | 0.569 | 0.512 |
| 8.399 | 0.313 | 0.288 |
| 8.952 | 0.226 | 0.204 |
| 9.505 | 0.198 | 0.176 |
| 10.058 | 0.176 | 0.160 |
| 10.612 | 0.158 | 0.147 |
| 11.165 | 0.143 | 0.133 |
| 11.718 | 0.128 | 0.123 |
| 12.271 | 0.122 | 0.108 |
| 12.824 | 0.112 | 0.097 |
| 13.378 | 0.102 | 0.087 |
| 13.931 | 0.092 | 0.081 |
| 14.484 | 0.085 | 0.073 |
| 15.037 | 0.082 | 0.067 |
| 15.590 | 0.078 | 0.065 |
| 16.144 | 0.072 | 0.061 |

**Continued**

| T (PV) | Br ($C/C_0$) | CNP ($C/C_0$) |
|---|---|---|
| 16.697 | 0.067 | 0.057 |
| 17.250 | 0.064 | 0.056 |
| 17.803 | 0.061 | 0.054 |
| 18.357 | 0.058 | 0.050 |
| 18.910 | 0.055 | 0.048 |
| 20.016 | 0.051 | 0.043 |
| 20.569 | 0.047 | 0.041 |
| 21.676 | 0.044 | 0.038 |
| 22.229 | 0.042 | 0.036 |
| 23.336 | 0.042 | 0.033 |
| 23.889 | 0.040 | 0.030 |
| 24.995 | 0.039 | 0.029 |
| 25.548 | 0.038 | 0.028 |
| 26.655 | 0.037 | 0.026 |
| 27.208 | 0.036 | 0.026 |
| 28.314 | 0.036 | 0.024 |
| 28.868 | 0.035 | 0.023 |
| 29.974 | 0.034 | 0.022 |
| 30.527 | 0.034 | 0.022 |
| 31.634 | 0.035 | 0.019 |
| 32.740 | 0.034 | 0.019 |
| 33.293 | 0.030 | 0.018 |
| 34.400 | 0.030 | 0.017 |
| 34.953 | | 0.017 |
| 36.613 | | 0.017 |
| 37.166 | 0.030 | 0.017 |
| 38.272 | 0.029 | 0.017 |
| 38.826 | | 0.016 |

**Column Type:** Dual-Porosity

**Experiment Name:** Design #3, Pulse Test #2; Page 2 of 2

**Continued**

| T (PV) | Br ($C/C_0$) | CNP ($C/C_0$) |
|---|---|---|
| 40.485 | | 0.016 |
| 41.038 | | 0.016 |
| 42.698 | 0.027 | 0.015 |
| 43.805 | 0.027 | 0.014 |
| 44.911 | | 0.014 |
| 46.571 | | 0.014 |
| 47.677 | | 0.014 |
| 48.783 | 0.025 | 0.013 |
| 49.337 | 0.025 | 0.014 |
| 50.443 | | 0.014 |
| 52.144 | | 0.014 |
| 53.804 | | 0.013 |
| 54.910 | 0.023 | 0.013 |
| 57.123 | 0.021 | 0.012 |
| 58.783 | | 0.012 |
| 60.443 | | 0.012 |
| 61.549 | | 0.011 |
| 63.762 | 0.019 | 0.010 |
| 66.528 | 0.017 | 0.010 |
| 68.741 | | 0.011 |
| 70.400 | | 0.011 |
| 71.507 | | 0.011 |
| 73.720 | 0.016 | 0.011 |
| 75.933 | 0.016 | 0.012 |
| 78.145 | | 0.013 |
| 79.805 | | 0.014 |
| 81.465 | | 0.014 |
| 82.571 | 0.015 | 0.015 |
| 83.678 | 0.016 | 0.016 |
| 84.784 | | 0.016 |
| 85.890 | 0.016 | 0.017 |
| 86.997 | | 0.017 |
| 88.103 | | 0.017 |
| 90.869 | | 0.016 |
| 93.636 | | 0.018 |
| 96.402 | | 0.017 |
| 99.168 | | 0.015 |

**Continued**

| T (PV) | Br ($C/C_0$) | CNP ($C/C_0$) |
|---|---|---|
| 101.934 | | 0.013 |
| 104.700 | | 0.011 |
| 107.466 | | 0.009 |
| 110.232 | | 0.008 |
| 112.998 | | 0.006 |
| 115.764 | | 0.005 |
| 118.530 | | 0.004 |

**Column Type:** Dual-Porosity
**Experiment Name:** Design #4, Pulse Test #1; Page 1 of 2
**Experiment Date:** 9-Feb-15
**Media Length (cm):** 31.76
**Mobile Pore Volume (mL):** 5.43
**Design Details / Problems:** 0.80 cm diameter core, with baffles, no frits
pore velocity too high
**Tracer Pulse Time (min):** 44.29
**Flow Rate (mL $min^{-1}$):** 0.4
**Application Volume (mL):** 17.65
**Mobile Pore Velocity (m $d^{-1}$):** 33.58

| T (PV) | Br ($C/C_0$) | CNP ($C/C_0$) |
|---|---|---|
| 0.074 | 0.007 | 0.002 |
| 1.164 | 0.094 | 0.105 |
| 2.237 | 0.302 | 0.295 |
| 3.309 | 0.367 | 0.363 |
| 4.381 | 0.315 | 0.282 |
| 5.454 | 0.146 | 0.113 |
| 6.526 | 0.113 | 0.091 |
| 7.598 | 0.101 | 0.069 |
| 8.671 | 0.088 | 0.063 |
| 9.743 | 0.076 | 0.055 |
| 10.815 | 0.058 | 0.047 |
| 11.888 | 0.049 | 0.042 |
| 12.960 | 0.045 | 0.033 |
| 14.032 | 0.040 | 0.031 |
| 15.105 | 0.038 | 0.024 |
| 16.177 | 0.034 | 0.021 |
| 17.249 | 0.031 | 0.017 |
| 18.322 | 0.029 | 0.017 |
| 19.394 | 0.027 | 0.016 |
| 20.466 | 0.025 | 0.016 |
| 21.539 | 0.023 | 0.015 |
| 22.611 | 0.023 | 0.014 |
| 23.683 | 0.022 | 0.013 |
| 24.756 | 0.020 | 0.012 |
| 26.900 | 0.019 | 0.011 |
| 27.973 | 0.019 | 0.010 |
| 29.045 | 0.018 | 0.010 |
| 30.117 | 0.017 | 0.009 |
| 32.262 | 0.016 | 0.008 |

**Continued**

| T (PV) | Br ($C/C_0$) | CNP ($C/C_0$) |
|---|---|---|
| 33.334 | 0.016 | 0.008 |
| 34.407 | 0.015 | 0.007 |
| 35.479 | 0.014 | 0.007 |
| 37.624 | 0.014 | 0.007 |
| 38.696 | 0.013 | 0.007 |
| 39.768 | 0.013 | 0.006 |
| 40.841 | 0.013 | 0.006 |
| 42.985 | 0.012 | 0.006 |
| 44.058 | 0.012 | 0.006 |
| 45.130 | 0.012 | 0.006 |
| 46.202 | 0.012 | 0.006 |
| 48.347 | 0.012 | 0.005 |
| 49.419 | 0.012 | 0.006 |
| 50.492 | 0.012 | 0.005 |
| 51.564 | 0.012 | 0.005 |
| 52.636 | 0.011 | 0.005 |
| 54.781 | 0.012 | 0.005 |
| 56.926 | 0.012 | 0.005 |
| 57.998 | 0.012 | 0.005 |
| 60.143 | 0.011 | 0.005 |
| 61.215 | 0.011 | 0.005 |
| 62.287 | 0.012 | 0.005 |
| 65.504 | 0.012 | 0.005 |
| 67.649 | 0.012 | 0.005 |
| 68.721 | 0.011 | 0.005 |
| 70.866 | 0.010 | 0.004 |
| 73.010 | 0.010 | 0.004 |
| 76.227 | 0.009 | 0.004 |

**Column Type:** Dual-Porosity

**Experiment Name:** Design #4, Pulse Test #1; Page 2 of 2

**Continued**

| T (PV) | Br ($C/C_0$) | CNP ($C/C_0$) |
|---|---|---|
| 78.372 | 0.009 | 0.004 |
| 80.517 | 0.009 | 0.004 |
| 81.589 | 0.008 | 0.004 |
| 82.661 | 0.008 | 0.004 |
| 84.806 | 0.008 | 0.004 |
| 86.951 | 0.007 | 0.004 |
| 90.168 | 0.007 | 0.004 |
| 92.312 | 0.007 | 0.004 |
| 94.420 | 0.009 | 0.004 |
| 95.488 | 0.008 | 0.004 |
| 97.632 | 0.007 | 0.004 |
| 99.777 | 0.007 | 0.004 |
| 100.849 | 0.007 | 0.004 |
| 104.066 | 0.007 | 0.004 |
| 106.211 | 0.007 | 0.004 |
| 108.355 | 0.007 | 0.004 |
| 109.428 | 0.007 | 0.004 |
| 111.572 | 0.007 | 0.004 |
| 112.645 | 0.008 | 0.004 |
| 114.789 | 0.008 | 0.004 |
| 116.934 | 0.007 | 0.004 |
| 122.296 | 0.008 | 0.004 |
| 123.368 | 0.008 | 0.004 |
| 125.513 | 0.008 | 0.004 |
| 127.657 | 0.008 | 0.005 |
| 128.730 | 0.008 | 0.005 |
| 129.802 | 0.009 | 0.005 |
| 133.019 | 0.009 | 0.005 |
| 135.164 | 0.009 | 0.005 |
| 137.308 | 0.010 | 0.005 |
| 138.381 | 0.009 | 0.005 |
| 141.598 | 0.009 | 0.006 |
| 143.742 | 0.009 | 0.006 |
| 146.959 | 0.008 | 0.006 |
| 149.104 | 0.008 | 0.006 |
| 150.176 | 0.007 | 0.006 |
| 154.466 | 0.007 | 0.005 |

**Continued**

| T (PV) | Br ($C/C_0$) | CNP ($C/C_0$) |
|---|---|---|
| 157.683 | 0.006 | 0.005 |
| 159.827 | 0.006 | 0.005 |
| 163.044 | 0.006 | 0.005 |
| 165.189 | 0.005 | 0.005 |
| 168.406 | 0.004 | 0.004 |
| 170.550 | 0.004 | 0.004 |
| 172.695 | 0.004 | 0.004 |
| 175.912 | 0.003 | 0.004 |
| 179.129 | 0.003 | 0.003 |
| 181.274 | 0.002 | 0.003 |
| 184.491 | 0.002 | 0.003 |
| 186.635 | 0.002 | 0.003 |
| 188.780 | 0.002 | 0.003 |
| 189.852 | 0.002 | 0.003 |
| 191.997 | 0.002 | 0.003 |
| 193.069 | 0.002 | 0.003 |

**Column Type:** Dual-Porosity
**Experiment Name:** Design #4, Pulse Test #2; Page 1 of 2
**Experiment Date:** 13-Feb-15
**Media Length (cm):** 31.76
**Mobile Pore Volume (mL):** 5.43
**Design Details / Problems:** 0.80 cm diameter core, with baffles, no frits
pore velocity too high
**Tracer Pulse Time (min):** 72
**Flow Rate (mL $min^{-1}$):** 0.4
**Application Volume (mL):** 28.49
**Mobile Pore Velocity (m $d^{-1}$):** 33.34

| T (PV) | Br ($C/C_0$) | CNP ($C/C_0$) |
|---|---|---|
| 0.035 | 0.005 | 0.002 |
| 1.048 | 0.013 | 0.017 |
| 2.043 | 0.181 | 0.198 |
| 3.037 | 0.263 | 0.273 |
| 4.032 | 0.296 | 0.305 |
| 5.027 | 0.330 | 0.333 |
| 6.022 | 0.351 | 0.335 |
| 7.016 | 0.209 | 0.173 |
| 8.011 | 0.145 | 0.119 |
| 9.006 | 0.123 | 0.108 |
| 10.001 | 0.111 | 0.098 |
| 10.995 | 0.102 | 0.085 |
| 11.990 | 0.092 | 0.078 |
| 12.985 | 0.080 | 0.072 |
| 13.980 | 0.071 | 0.063 |
| 14.974 | 0.066 | 0.053 |
| 15.969 | 0.061 | 0.048 |
| 16.964 | 0.056 | 0.042 |
| 17.958 | 0.052 | 0.037 |
| 18.953 | 0.050 | 0.037 |
| 19.948 | 0.050 | 0.036 |
| 20.943 | 0.048 | 0.031 |
| 21.937 | 0.046 | 0.028 |
| 22.932 | 0.043 | 0.025 |
| 23.927 | 0.041 | 0.024 |
| 24.922 | 0.040 | 0.023 |
| 25.916 | 0.038 | 0.021 |
| 26.911 | 0.036 | 0.020 |
| 27.906 | 0.035 | 0.019 |

**Continued**

| T (PV) | Br ($C/C_0$) | CNP ($C/C_0$) |
|---|---|---|
| 28.901 | 0.034 | 0.018 |
| 30.890 | 0.031 | 0.016 |
| 31.885 | 0.031 | 0.015 |
| 33.874 | 0.029 | 0.013 |
| 34.869 | 0.028 | 0.014 |
| 35.864 | 0.027 | 0.013 |
| 37.853 | 0.027 | 0.013 |
| 38.848 | 0.025 | 0.012 |
| 39.843 | 0.024 | 0.012 |
| 40.838 | 0.023 | 0.011 |
| 41.832 | 0.022 | 0.010 |
| 42.827 | 0.021 | 0.010 |
| 43.822 | 0.021 | 0.009 |
| 45.811 | 0.019 | 0.008 |
| 46.806 | 0.019 | 0.008 |
| 47.801 | 0.018 | 0.008 |
| 49.790 | 0.018 | 0.007 |
| 51.780 | 0.017 | 0.007 |
| 52.774 | 0.017 | 0.007 |
| 53.769 | 0.017 | 0.007 |
| 55.759 | 0.017 | 0.006 |
| 57.748 | 0.018 | 0.006 |
| 58.743 | 0.018 | 0.006 |
| 59.738 | 0.018 | 0.006 |
| 60.732 | 0.018 | 0.006 |
| 61.727 | 0.018 | 0.006 |
| 62.722 | 0.018 | 0.006 |
| 64.711 | 0.018 | 0.006 |

**Column Type:** Dual-Porosity

**Experiment Name:** Design #4, Pulse Test #2; Page 2 of 2

**Continued**

| T (PV) | Br ($C/C_0$) | CNP ($C/C_0$) |
|---|---|---|
| 66.701 | 0.019 | 0.006 |
| 67.696 | 0.018 | 0.006 |
| 70.680 | 0.019 | 0.006 |
| 72.669 | 0.020 | 0.006 |
| 73.664 | 0.019 | 0.006 |
| 74.659 | 0.019 | 0.006 |
| 75.653 | 0.018 | 0.006 |
| 77.643 | 0.019 | 0.006 |
| 79.632 | 0.018 | 0.006 |
| 80.627 | 0.018 | 0.006 |
| 82.617 | 0.017 | 0.006 |
| 85.601 | 0.018 | 0.006 |
| 86.596 | 0.018 | 0.006 |
| 87.590 | 0.012 | 0.007 |
| 89.580 | 0.012 | 0.007 |
| 91.569 | 0.012 | 0.007 |
| 93.050 | 0.011 | 0.007 |
| 95.672 | 0.012 | 0.007 |
| 98.656 | 0.012 | 0.007 |
| 100.646 | 0.012 | 0.007 |
| 103.630 | 0.013 | 0.008 |
| 106.614 | 0.013 | 0.010 |
| 107.609 | 0.013 | 0.008 |
| 109.599 | 0.012 | 0.009 |
| 112.583 | 0.013 | 0.009 |
| 113.578 | 0.013 | 0.009 |
| 116.562 | 0.014 | 0.010 |
| 118.551 | 0.014 | 0.010 |
| 121.535 | 0.014 | 0.012 |
| 123.525 | 0.014 | 0.012 |
| 126.509 | 0.014 | 0.013 |
| 128.499 | 0.013 | 0.014 |
| 130.488 | 0.013 | 0.019 |
| 133.472 | 0.012 | 0.013 |
| 135.462 | 0.012 | 0.013 |
| 138.446 | 0.011 | 0.013 |
| 139.441 | 0.011 | 0.011 |

**Continued**

| T (PV) | Br ($C/C_0$) | CNP ($C/C_0$) |
|---|---|---|
| 141.430 | 0.009 | 0.011 |
| 144.414 | 0.009 | 0.010 |
| 147.399 | 0.008 | 0.008 |
| 148.393 | 0.007 | 0.008 |
| 151.378 | 0.005 | 0.008 |
| 153.367 | 0.004 | 0.008 |
| 156.351 | 0.004 | 0.007 |
| 159.336 | 0.002 | 0.006 |
| 162.320 | 0.000 | 0.005 |
| 163.315 | 0.000 | 0.005 |
| 166.299 | 0.000 | 0.005 |
| 168.288 | 0.000 | 0.004 |
| 170.278 | 0.000 | 0.004 |
| 171.272 | 0.000 | 0.004 |
| 174.257 | 0.000 | 0.003 |
| 176.246 | 0.000 | 0.003 |
| 178.236 | 0.000 | 0.003 |
| 179.230 | 0.000 | 0.003 |
| 182.215 | 0.000 | 0.003 |
| 184.204 | 0.000 | 0.003 |
| 185.199 | 0.000 | 0.003 |
| 186.194 | 0.000 | 0.003 |
| 187.188 | 0.000 | 0.003 |
| 188.183 | 0.000 | 0.003 |

**Column Type:** Dual-Porosity
**Experiment Name:** Design #3, Interruption Test
**Experiment Date:** 13-Feb-15
**Media Length (cm):** 31.76
**Mobile Pore Volume (mL):** 13.68
**Design Details / Problems:** 1.27 cm diameter core, with baffles
Interrupt for 6 days at 114.17 min and 305.88 min
**Tracer Pulse Time (min):** 175.17
**Flow Rate (mL $min^{-1}$):** 0.43
**Application Volume (mL):** 76.28
**Mobile Pore Velocity (m $d^{-1}$):** 14.56

| T (PV) | Br ($C/C_0$) | CNP ($C/C_0$) |
|---|---|---|
| 0.087 | 0.000 | 0.000 |
| 0.599 | 0.000 | 0.000 |
| 1.083 | 0.064 | 0.096 |
| 1.567 | 0.267 | 0.334 |
| 2.051 | 0.356 | 0.392 |
| 2.535 | 0.398 | 0.434 |
| 3.019 | 0.425 | 0.462 |
| 3.351 | 0.455 | 0.471 |
| 3.862 | 0.130 | 0.129 |
| 4.359 | 0.136 | 0.134 |
| 4.843 | 0.335 | 0.367 |
| 5.327 | 0.443 | 0.469 |
| 5.810 | 0.500 | 0.519 |
| 6.294 | 0.529 | 0.539 |
| 6.778 | 0.425 | 0.404 |
| 7.262 | 0.270 | 0.267 |
| 7.746 | 0.211 | 0.195 |
| 8.230 | 0.186 | 0.164 |
| 8.714 | 0.168 | 0.149 |
| 9.290 | 0.143 | 0.110 |
| 9.778 | 0.161 | 0.123 |
| 10.262 | 0.162 | 0.126 |
| 10.746 | 0.117 | 0.093 |
| 11.230 | 0.103 | 0.081 |
| 11.714 | 0.093 | 0.073 |
| 12.197 | 0.088 | 0.070 |
| 12.681 | 0.084 | 0.066 |
| 13.165 | 0.079 | 0.063 |
| 13.649 | 0.076 | 0.059 |
| 14.133 | 0.074 | 0.059 |

**Continued**

| T (PV) | Br ($C/C_0$) | CNP ($C/C_0$) |
|---|---|---|
| 14.617 | 0.071 | 0.056 |
| 15.101 | 0.068 | 0.055 |
| 15.605 | 0.067 | 0.056 |
| 16.106 | 0.065 | 0.051 |
| 16.590 | 0.063 | 0.052 |
| 17.074 | 0.061 | 0.051 |
| 18.042 | 0.058 | 0.047 |
| 19.010 | 0.056 | 0.044 |
| 19.978 | 0.055 | 0.044 |
| 20.946 | 0.053 | 0.042 |
| 21.914 | 0.050 | 0.040 |
| 23.850 | 0.047 | 0.038 |
| 25.786 | 0.046 | 0.036 |
| 27.722 | 0.043 | 0.035 |
| 29.657 | 0.042 | 0.033 |
| 31.109 | 0.041 | 0.033 |
| 33.529 | 0.039 | 0.032 |
| 35.949 | 0.038 | 0.032 |
| 38.369 | 0.037 | 0.031 |
| 40.789 | 0.037 | 0.030 |
| 43.209 | 0.033 | 0.027 |
| 45.628 | 0.031 | 0.027 |
| 48.048 | 0.031 | 0.024 |
| 50.468 | 0.029 | 0.025 |
| 52.888 | 0.029 | 0.023 |
| 55.308 | 0.028 | 0.024 |
| 57.728 | 0.027 | 0.024 |
| 60.148 | 0.025 | 0.023 |
| 61.115 | 0.025 | 0.023 |

**Column Type:** Dual-Porosity
**Experiment Name:** Design #3, Long-Term Test; Page 1 of 2
**Experiment Date:** 2-Apr-15 through 17-Apr-15
**Media Length (cm):** 31.76
**Mobile Pore Volume (mL):** 13.68
**Design Details / Problems:** 1.27 cm diameter core, with baffles
Injected tracer for 14 days
**Tracer Pulse Time (min):** 20,162
**Flow Rate (mL $min^{-1}$):** 0.47
**Application Volume (mL):** 9561.01
**Mobile Pore Velocity (m $d^{-1}$):** 15.85

| T (PV) | Br ($C/C_0$) | CNP ($C/C_0$) |
|---|---|---|
| 0.059 | 0.000 | 0.000 |
| 0.512 | 0.000 | 0.000 |
| 0.952 | 0.011 | 0.002 |
| 1.391 | 0.218 | 0.301 |
| 1.831 | 0.413 | 0.574 |
| 2.271 | 0.507 | 0.670 |
| 2.711 | 0.537 | 0.715 |
| 3.150 | 0.584 | 0.769 |
| 3.590 | 0.625 | 0.793 |
| 4.030 | 0.646 | 0.823 |
| 4.469 | 0.658 | 0.831 |
| 4.909 | 0.664 | 0.840 |
| 5.349 | 0.676 | 0.845 |
| 5.788 | 0.687 | 0.848 |
| 6.228 | 0.717 | 0.857 |
| 6.668 | 0.723 | 0.842 |
| 7.108 | 0.737 | 0.812 |
| 7.547 | 0.755 | 0.860 |
| 7.987 | 0.758 | 0.874 |
| 8.427 | 0.779 | 0.880 |
| 8.866 | 0.785 | 0.902 |
| 9.306 | 0.794 | 0.909 |
| 9.746 | 0.799 | 0.917 |
| 10.185 | 0.788 | 0.896 |
| 10.625 | 0.794 | 0.906 |
| 11.065 | 0.802 | 0.895 |
| 11.505 | 0.826 | 0.880 |
| 11.944 | 0.826 | 0.888 |
| 12.384 | 0.811 | 0.876 |

**Continued**

| T (PV) | Br ($C/C_0$) | CNP ($C/C_0$) |
|---|---|---|
| 12.824 | 0.826 | 0.899 |
| 13.703 | 0.841 | 0.903 |
| 14.582 | 0.847 | 0.931 |
| 15.462 | 0.861 | 0.957 |
| 16.341 | 0.873 | 0.964 |
| 17.221 | 0.867 | 0.965 |
| 18.100 | 0.876 | 0.964 |
| 18.979 | 0.858 | 0.955 |
| 19.859 | 0.894 | 0.949 |
| 20.738 | 0.906 | 0.951 |
| 21.618 | 0.912 | 0.934 |
| 23.816 | 0.926 | 0.938 |
| 26.015 | 0.941 | 0.953 |
| 28.213 | 0.956 | 0.969 |
| 30.411 | 0.962 | 1.001 |
| 32.610 | 0.965 | 1.020 |
| 34.808 | 0.973 | 1.016 |
| 37.007 | 0.991 | 1.029 |
| 39.205 | 0.956 | 1.020 |
| 41.404 | 0.941 | 1.002 |
| 99.131 | 1.015 | 1.050 |
| 191.159 | 1.000 | 1.018 |
| 340.116 | 0.980 | 1.007 |
| 500.576 | 0.971 | 0.978 |
| 589.399 | 0.966 | 1.009 |
| 698.803 | 1.003 | 1.045 |
| 699.321 | 1.000 | 1.071 |
| 699.770 | 0.997 | 1.087 |

**Column Type:** Dual-Porosity

**Experiment Name:** Design #3, Long-Term Test; Page 2 of 2

**Continued**

| T (PV) | Br ($C/C_0$) | CNP ($C/C_0$) |
|---|---|---|
| 700.219 | 0.940 | 1.051 |
| 700.668 | 0.825 | 0.979 |
| 701.117 | 0.761 | 0.927 |
| 701.566 | 0.718 | 0.873 |
| 702.015 | 0.652 | 0.830 |
| 702.464 | 0.621 | 0.798 |
| 702.913 | 0.601 | 0.764 |
| 703.362 | 0.578 | 0.719 |
| 703.811 | 0.563 | 0.679 |
| 704.261 | 0.534 | 0.684 |
| 704.710 | 0.517 | 0.688 |
| 705.159 | 0.503 | 0.657 |
| 705.608 | 0.500 | 0.640 |
| 706.057 | 0.483 | 0.622 |
| 706.506 | 0.457 | 0.605 |
| 706.955 | 0.443 | 0.600 |
| 707.404 | 0.434 | 0.572 |
| 708.302 | 0.422 | 0.525 |
| 709.200 | 0.394 | 0.514 |
| 710.098 | 0.374 | 0.533 |
| 710.996 | 0.353 | 0.498 |
| 711.894 | 0.351 | 0.504 |
| 712.793 | 0.342 | 0.470 |
| 713.691 | 0.328 | 0.465 |
| 714.589 | 0.307 | 0.446 |
| 715.487 | 0.299 | 0.427 |
| 716.385 | 0.293 | 0.415 |
| 717.283 | 0.290 | 0.402 |
| 718.181 | 0.283 | 0.385 |
| 719.079 | 0.265 | 0.364 |
| 719.977 | 0.261 | 0.346 |
| 720.875 | 0.258 | 0.319 |
| 723.121 | 0.244 | 0.299 |
| 725.366 | 0.218 | 0.277 |
| 727.611 | 0.202 | 0.271 |
| 729.857 | 0.193 | 0.246 |
| 732.102 | 0.179 | 0.235 |

**Continued**

| T (PV) | Br ($C/C_0$) | CNP ($C/C_0$) |
|---|---|---|
| 734.347 | 0.170 | 0.220 |
| 735.694 | 0.159 | 0.201 |
| 736.198 | 0.161 | 0.213 |
| 738.947 | 0.145 | 0.177 |
| 741.192 | 0.138 | 0.170 |
| 743.438 | 0.127 | 0.149 |
| 745.683 | 0.117 | 0.134 |
| 747.928 | 0.103 | 0.115 |
| 750.173 | 0.092 | 0.108 |
| 752.419 | 0.074 | 0.089 |
| 754.664 | 0.065 | 0.069 |
| 756.909 | 0.052 | 0.052 |
| 759.154 | 0.042 | 0.038 |
| 761.400 | 0.031 | 0.027 |
| 763.645 | 0.023 | 0.019 |
| 765.890 | 0.018 | 0.012 |
| 768.135 | 0.013 | 0.009 |
| 770.381 | 0.010 | 0.005 |
| 772.626 | 0.007 | 0.004 |
| 774.871 | 0.006 | 0.002 |
| 777.117 | 0.004 | 0.002 |
| 778.464 | 0.004 | 0.001 |

**Column Type:** Reactive Porous Media
**Experiment Name:** Design #1 Pulse Test; Page 1 of 2
**Experiment Date:** 19-Feb-15
**Media Length (cm):** 30.48
**Mobile Pore Volume (mL):** 179.16
**Design Details / Problems:** 25% SMZ by weight, 75% coarse sand
Br almost completely sorbed, fluorescence affected by surfactant
**Tracer Pulse Time (min):** 526.32
**Flow Rate (mL $min^{-1}$):** 0.40
**Application Volume (mL):** 212.69
**Pore Velocity (m $d^{-1}$):** 0.99

| T (PV) | Br ($C/C_0$) | CNP ($C/C_0$) |
|---|---|---|
| 0.008 | 0.002 | 0.000 |
| 0.132 | 0.002 | 0.000 |
| 0.298 | 0.002 | 0.000 |
| 0.506 | 0.003 | 0.000 |
| 0.714 | 0.002 | 0.000 |
| 0.921 | 0.003 | 0.001 |
| 1.046 | 0.003 | 0.015 |
| 1.129 | 0.003 | 0.038 |
| 1.254 | 0.003 | 0.091 |
| 1.337 | 0.003 | 0.144 |
| 1.420 | 0.003 | 0.210 |
| 1.503 | 0.003 | 0.289 |
| 1.545 | 0.003 | 0.358 |
| 1.586 | 0.003 | 0.415 |
| 1.669 | 0.003 | 0.440 |
| 1.752 | 0.003 | 0.620 |
| 1.877 | 0.003 | 0.718 |
| 1.918 | 0.003 | 0.806 |
| 1.960 | 0.003 | 0.742 |
| 2.043 | 0.003 | 0.830 |
| 2.085 | 0.003 | 0.883 |
| 2.126 | 0.003 | 1.005 |
| 2.168 | 0.003 | 1.026 |
| 2.251 | 0.004 | 0.986 |
| 2.292 | 0.004 | 0.981 |
| 2.334 | 0.004 | 0.911 |
| 2.417 | 0.004 | 0.781 |
| 2.458 | 0.004 | 0.760 |
| 2.541 | 0.004 | 0.629 |

**Continued**

| T (PV) | Br ($C/C_0$) | CNP ($C/C_0$) |
|---|---|---|
| 2.624 | 0.004 | 0.543 |
| 2.708 | 0.004 | 0.436 |
| 2.791 | 0.004 | 0.350 |
| 2.832 | 0.004 | 0.326 |
| 2.874 | 0.004 | 0.297 |
| 2.942 | 0.004 | 0.248 |
| 3.009 | 0.004 | 0.206 |
| 3.051 | 0.004 | 0.189 |
| 3.134 | 0.003 | 0.149 |
| 3.176 | 0.003 | 0.133 |
| 3.259 | 0.003 | 0.115 |
| 3.342 | 0.003 | 0.097 |
| 3.383 | 0.003 | 0.092 |
| 3.466 | 0.003 | 0.097 |
| 3.508 | 0.003 | 0.070 |
| 3.549 | 0.003 | 0.066 |
| 3.591 | 0.003 | 0.062 |
| 3.632 | 0.003 | 0.054 |
| 3.674 | 0.003 | 0.055 |
| 3.716 | 0.003 | 0.052 |
| 3.765 | 0.005 | 0.048 |
| 3.806 | 0.005 | 0.045 |
| 3.889 | 0.004 | 0.039 |
| 4.014 | 0.004 | 0.031 |
| 4.097 | 0.004 | 0.030 |
| 4.222 | 0.003 | 0.028 |
| 4.388 | 0.003 | 0.023 |
| 4.471 | 0.003 | 0.021 |

**Column Type:** Reactive Porous Media

**Experiment Name:** Design #1 Pulse Test; Page 2 of 2

**Continued**

| T (PV) | Br ($C/C_0$) | CNP ($C/C_0$) |
|---|---|---|
| 4.679 | 0.003 | 0.016 |
| 4.720 | 0.003 | 0.019 |
| 4.845 | 0.003 | 0.018 |
| 4.928 | 0.003 | 0.017 |
| 5.136 | 0.003 | 0.015 |
| 5.302 | 0.002 | 0.016 |
| 5.468 | 0.002 | 0.014 |
| 5.592 | 0.002 | 0.014 |
| 5.634 | 0.002 | 0.014 |
| 5.759 | 0.002 | 0.013 |
| 5.966 | 0.002 | 0.013 |
| 6.008 | 0.002 | 0.013 |
| 6.132 | 0.002 | 0.013 |
| 6.215 | 0.002 | 0.012 |
| 6.382 | 0.002 | 0.011 |
| 6.506 | 0.002 | 0.010 |
| 6.589 | 0.002 | 0.010 |
| 6.714 | 0.002 | 0.012 |
| 6.755 | 0.002 | 0.012 |
| 6.963 | 0.002 | 0.011 |
| 7.046 | 0.002 | 0.011 |
| 7.212 | 0.002 | 0.010 |
| 7.337 | 0.002 | 0.009 |
| 7.503 | 0.002 | 0.009 |
| 7.669 | 0.002 | 0.009 |
| 7.794 | 0.002 | 0.008 |
| 7.960 | 0.002 | 0.009 |
| 8.209 | 0.002 | 0.008 |
| 8.375 | 0.002 | 0.007 |
| 8.666 | 0.002 | 0.007 |
| 8.874 | 0.002 | 0.007 |
| 9.082 | 0.002 | 0.006 |
| 9.289 | 0.002 | 0.006 |
| 9.497 | 0.002 | 0.005 |
| 9.705 | 0.002 | 0.005 |
| 9.746 | 0.002 | 0.005 |
| 9.912 | 0.002 | 0.005 |

**Continued**

| T (PV) | Br ($C/C_0$) | CNP ($C/C_0$) |
|---|---|---|
| 10.120 | 0.002 | 0.005 |
| 10.286 | 0.002 | 0.005 |
| 10.328 | 0.002 | 0.005 |
| 10.535 | 0.002 | 0.004 |
| 10.743 | 0.002 | 0.004 |

**Column Type:** Reactive Porous Media
**Experiment Name:** Design #2, Pulse Test #1; Page 1 of 3
**Experiment Date:** 27-Feb-15
**Media Length (cm):** 15.24
**Mobile Pore Volume (mL):** 89.58
**Design Details / Problems:** 12.5% SMZ by weight, 87.5% coarse sand

**Tracer Pulse Time (min):** 930.23
**Flow Rate (mL $min^{-1}$):** 0.43
**Application Volume (mL):** 398.62
**Pore Velocity (m $d^{-1}$):** 1.05

| T (PV) | Br ($C/C_0$) | CNP ($C/C_0$) |
|---|---|---|
| 0.235 | 0.003 | 0.000 |
| 0.390 | 0.003 | 0.000 |
| 0.544 | 0.003 | 0.000 |
| 0.699 | 0.003 | 0.000 |
| 0.854 | 0.003 | 0.000 |
| 1.009 | 0.003 | 0.000 |
| 1.164 | 0.003 | 0.008 |
| 1.319 | 0.003 | 0.062 |
| 1.396 | 0.004 | 0.118 |
| 1.474 | 0.004 | 0.235 |
| 1.551 | 0.004 | 0.347 |
| 1.629 | 0.004 | 0.441 |
| 1.706 | 0.004 | 0.575 |
| 1.783 | 0.004 | 0.685 |
| 1.861 | 0.005 | 0.801 |
| 1.938 | 0.005 | 0.868 |
| 2.016 | 0.005 | 0.797 |
| 2.093 | 0.005 | 0.897 |
| 2.171 | 0.005 | 0.941 |
| 2.248 | 0.005 | 1.000 |
| 2.326 | 0.005 | 1.018 |
| 2.403 | 0.005 | 1.026 |
| 2.558 | 0.005 | 0.984 |
| 2.635 | 0.006 | 1.010 |
| 2.713 | 0.006 | 1.011 |
| 2.868 | 0.006 | 0.972 |
| 2.945 | 0.006 | 0.967 |
| 3.022 | 0.006 | 0.912 |
| 3.177 | 0.006 | 0.863 |

**Continued**

| T (PV) | Br ($C/C_0$) | CNP ($C/C_0$) |
|---|---|---|
| 3.332 | 0.006 | 0.917 |
| 3.410 | 0.006 | 0.950 |
| 3.487 | 0.006 | 1.004 |
| 3.642 | 0.006 | 1.074 |
| 3.719 | 0.006 | 1.092 |
| 3.797 | 0.006 | 1.087 |
| 3.952 | 0.006 | 1.089 |
| 4.029 | 0.006 | 1.113 |
| 4.107 | 0.006 | 1.056 |
| 4.274 | 0.006 | 0.987 |
| 4.441 | 0.006 | 0.930 |
| 4.596 | 0.006 | 0.877 |
| 4.674 | 0.015 | |
| 4.751 | 0.021 | |
| 4.829 | 0.030 | 0.892 |
| 4.906 | 0.042 | 0.948 |
| 4.983 | 0.057 | |
| 5.061 | 0.072 | 0.972 |
| 5.138 | 0.089 | |
| 5.216 | 0.114 | 0.999 |
| 5.293 | 0.139 | 1.016 |
| 5.371 | 0.169 | 1.026 |
| 5.448 | 0.192 | |
| 5.525 | 0.233 | 1.022 |
| 5.603 | 0.262 | 0.974 |
| 5.680 | 0.293 | 0.899 |
| 5.758 | 0.328 | 0.773 |
| 5.835 | 0.361 | 0.662 |

**Column Type:** Reactive Porous Media

**Experiment Name:** Design #2, Pulse Test #1; Page 2 of 3

**Continued**

| T (PV) | Br ($C/C_0$) | CNP ($C/C_0$) |
|---|---|---|
| 5.913 | 0.399 | 0.514 |
| 5.990 | 0.402 | 0.454 |
| 6.068 | 0.402 | 0.405 |
| 6.145 | 0.405 | 0.359 |
| 6.222 | 0.408 | 0.299 |
| 6.300 | 0.396 | 0.246 |
| 6.455 | 0.349 | 0.148 |
| 6.610 | 0.317 | 0.100 |
| 6.687 | 0.296 | 0.087 |
| 6.764 | 0.288 | 0.075 |
| 6.919 | 0.262 | 0.058 |
| 6.997 | 0.250 | 0.052 |
| 7.074 | 0.243 | 0.045 |
| 7.229 | 0.228 | 0.038 |
| 7.307 | 0.223 | 0.035 |
| 7.461 | 0.211 | 0.030 |
| 7.539 | 0.207 | 0.029 |
| 7.694 | 0.200 | 0.026 |
| 7.771 | 0.203 | 0.024 |
| 7.926 | 0.196 | 0.022 |
| 8.003 | 0.187 | 0.021 |
| 8.158 | 0.184 | 0.018 |
| 8.236 | 0.181 | 0.017 |
| 8.313 | 0.177 | 0.017 |
| 8.468 | 0.174 | 0.016 |
| 8.546 | 0.171 | 0.015 |
| 8.700 | 0.167 | 0.014 |
| 8.778 | 0.167 | 0.014 |
| 8.933 | 0.163 | 0.013 |
| 9.010 | 0.162 | 0.011 |
| 9.088 | 0.159 | 0.012 |
| 9.242 | 0.157 | 0.011 |
| 9.397 | 0.152 | 0.011 |
| 9.475 | 0.150 | 0.011 |
| 9.630 | 0.148 | 0.009 |
| 9.707 | 0.149 | 0.010 |
| 9.862 | 0.143 | 0.009 |

**Continued**

| T (PV) | Br ($C/C_0$) | CNP ($C/C_0$) |
|---|---|---|
| 10.017 | 0.144 | 0.008 |
| 10.172 | 0.144 | 0.009 |
| 10.249 | 0.141 | 0.009 |
| 10.404 | 0.139 | 0.008 |
| 10.481 | 0.138 | 0.008 |
| 10.636 | 0.137 | 0.008 |
| 10.791 | 0.137 | 0.008 |
| 11.024 | 0.137 | 0.007 |
| 11.256 | 0.132 | 0.007 |
| 11.411 | 0.124 | 0.007 |
| 11.528 | 0.122 | 0.007 |
| 11.607 | 0.121 | 0.006 |
| 11.762 | 0.118 | 0.006 |
| 11.994 | 0.117 | 0.006 |
| 12.149 | 0.119 | 0.006 |
| 12.381 | 0.116 | 0.006 |
| 12.536 | 0.114 | 0.006 |
| 12.768 | 0.112 | 0.006 |
| 12.923 | 0.112 | 0.006 |
| 13.078 | 0.112 | 0.006 |
| 13.310 | 0.112 | 0.006 |
| 13.543 | 0.111 | 0.005 |
| 13.698 | 0.109 | 0.005 |
| 13.930 | 0.106 | 0.005 |
| 14.162 | 0.106 | 0.005 |
| 14.394 | 0.105 | 0.005 |
| 14.472 | 0.103 | 0.005 |
| 14.627 | 0.103 | 0.005 |
| 14.782 | 0.101 | 0.005 |
| 15.014 | 0.100 | 0.004 |
| 15.246 | 0.101 | 0.004 |
| 15.324 | 0.100 | 0.004 |
| 15.556 | 0.100 | 0.004 |
| 15.711 | 0.098 | 0.004 |
| 15.943 | 0.097 | 0.004 |
| 16.098 | 0.097 | 0.003 |
| 16.253 | 0.095 | 0.004 |

**Column Type:** Reactive Porous Media

**Experiment Name:** Design #2, Pulse Test #1; Page 3 of 3

**Continued**

| T (PV) | Br ($C/C_0$) | CNP ($C/C_0$) |
|---|---|---|
| 16.485 | 0.094 | 0.004 |
| 16.640 | 0.093 | 0.004 |
| 16.795 | 0.092 | 0.004 |
| 16.950 | 0.093 | 0.003 |
| 17.105 | 0.091 | 0.004 |
| 17.182 | 0.093 | 0.003 |
| 17.415 | 0.088 | 0.003 |
| 17.569 | 0.094 | 0.003 |
| 17.724 | 0.090 | 0.003 |
| 17.957 | 0.090 | 0.003 |
| 18.034 | 0.090 | 0.003 |
| 18.189 | 0.093 | 0.003 |
| 18.266 | 0.092 | 0.003 |
| 18.344 | 0.091 | 0.003 |
| 18.499 | 0.089 | 0.003 |
| 18.557 | 0.083 | 0.003 |
| 18.685 | 0.093 | 0.003 |
| 19.084 | 0.091 | 0.003 |
| 19.471 | 0.089 | 0.003 |
| 19.859 | 0.088 | 0.003 |
| 20.246 | 0.087 | 0.003 |
| 20.633 | 0.086 | 0.003 |
| 21.020 | 0.084 | 0.003 |
| 21.407 | 0.083 | 0.003 |
| 21.795 | 0.082 | 0.003 |
| 22.182 | 0.083 | 0.003 |
| 22.569 | 0.082 | 0.003 |
| 22.956 | 0.080 | 0.003 |
| 23.343 | 0.080 | 0.003 |
| 23.731 | 0.079 | 0.003 |
| 24.118 | 0.079 | 0.003 |
| 24.505 | 0.079 | 0.003 |
| 24.892 | 0.079 | 0.003 |
| 25.279 | 0.079 | 0.003 |
| 25.666 | 0.079 | 0.003 |
| 26.058 | 0.079 | 0.003 |
| 26.446 | 0.078 | 0.003 |

**Continued**

| T (PV) | Br ($C/C_0$) | CNP ($C/C_0$) |
|---|---|---|
| 26.833 | 0.077 | 0.003 |
| 27.220 | 0.076 | 0.003 |
| 27.607 | 0.075 | 0.003 |
| 27.994 | 0.074 | 0.002 |
| 28.382 | 0.072 | 0.002 |
| 28.769 | 0.072 | 0.002 |
| 29.156 | 0.071 | 0.002 |
| 29.543 | 0.070 | 0.002 |
| 29.930 | 0.070 | 0.002 |
| 30.317 | 0.069 | 0.002 |
| 30.705 | 0.068 | 0.002 |
| 31.092 | 0.068 | 0.002 |
| 31.479 | 0.068 | 0.002 |
| 31.866 | 0.068 | 0.002 |
| 32.253 | 0.067 | 0.002 |
| 32.563 | 0.066 | 0.001 |

**Column Type:** Reactive Porous Media
**Experiment Name:** Design #2, Pulse Test #2; Page 1 of 2
**Experiment Date:** 28-Apr-15
**Media Length (cm):** 15.24
**Mobile Pore Volume (mL):** 89.58
**Design Details / Problems:** 12.5% SMZ by weight, 87.5% coarse sand

**Tracer Pulse Time (min):** 983
**Flow Rate (mL $min^{-1}$):** 0.44
**Application Volume (mL):** 434.46
**Pore Velocity (m $d^{-1}$):** 1.08

| T (PV) | Br ($C/C_0$) | CNP ($C/C_0$) |
|---|---|---|
| 0.103 | 0.002 | 0.000 |
| 0.356 | 0.002 | 0.000 |
| 0.608 | 0.002 | 0.000 |
| 0.861 | 0.002 | 0.000 |
| 1.029 | 0.002 | 0.005 |
| 1.198 | 0.002 | 0.032 |
| 1.282 | 0.002 | 0.061 |
| 1.366 | 0.002 | 0.135 |
| 1.451 | 0.002 | 0.241 |
| 1.535 | 0.002 | 0.368 |
| 1.619 | 0.002 | 0.514 |
| 1.703 | 0.002 | 0.662 |
| 1.787 | 0.002 | 0.797 |
| 1.872 | 0.002 | 0.844 |
| 1.956 | 0.003 | 0.913 |
| 2.040 | 0.003 | 1.000 |
| 2.124 | 0.003 | 1.053 |
| 2.209 | 0.004 | 1.069 |
| 2.293 | 0.004 | 1.086 |
| 2.377 | 0.004 | 1.040 |
| 2.461 | 0.004 | 1.060 |
| 2.545 | 0.004 | 1.054 |
| 2.630 | 0.004 | 1.029 |
| 2.714 | 0.004 | 0.985 |
| 2.798 | 0.004 | 0.981 |
| 2.882 | 0.004 | 0.946 |
| 2.967 | 0.005 | 0.940 |
| 3.051 | 0.005 | 0.987 |
| 3.135 | 0.006 | 0.986 |

**Continued**

| T (PV) | Br ($C/C_0$) | CNP ($C/C_0$) |
|---|---|---|
| 3.219 | 0.015 | 1.067 |
| 3.303 | 0.024 | 1.067 |
| 3.388 | 0.033 | 1.052 |
| 3.472 | 0.044 | 1.052 |
| 3.556 | 0.056 | 1.049 |
| 3.725 | 0.081 | 1.028 |
| 3.893 | 0.107 | 0.956 |
| 3.977 | 0.123 | 0.988 |
| 4.146 | 0.160 | 0.915 |
| 4.230 | 0.180 | 0.883 |
| 4.314 | 0.196 | 0.905 |
| 4.398 | 0.214 | 0.931 |
| 4.483 | 0.230 | 0.981 |
| 4.567 | 0.251 | 0.972 |
| 4.651 | 0.269 | 0.944 |
| 4.738 | 0.283 | 0.961 |
| 4.824 | 0.304 | 0.971 |
| 4.909 | 0.331 | 0.941 |
| 4.993 | 0.355 | 0.898 |
| 5.077 | 0.378 | 0.898 |
| 5.161 | 0.402 | 0.860 |
| 5.246 | 0.435 | 0.813 |
| 5.330 | 0.468 | 0.831 |
| 5.414 | 0.508 | 0.873 |
| 5.498 | 0.529 | 0.886 |
| 5.583 | 0.565 | 0.894 |
| 5.667 | 0.607 | 0.882 |
| 5.751 | 0.634 | 0.881 |

**Column Type:** Reactive Porous Media

**Experiment Name:** Design #2, Pulse Test #2; Page 2 of 2

**Continued**

| T (PV) | Br ($C/C_0$) | CNP ($C/C_0$) |
|---|---|---|
| 5.835 | 0.667 | 0.873 |
| 5.919 | 0.718 | 0.868 |
| 6.004 | 0.736 | 0.791 |
| 6.088 | 0.754 | 0.792 |
| 6.172 | 0.775 | 0.705 |
| 6.256 | 0.784 | 0.599 |
| 6.341 | 0.784 | 0.514 |
| 6.425 | 0.781 | 0.454 |
| 6.509 | 0.760 | 0.397 |
| 6.593 | 0.724 | 0.330 |
| 6.677 | 0.688 | 0.264 |
| 6.762 | 0.658 | 0.212 |
| 6.846 | 0.607 | 0.164 |
| 6.930 | 0.565 | 0.129 |
| 7.014 | 0.538 | 0.104 |
| 7.099 | 0.505 | 0.081 |
| 7.183 | 0.480 | 0.064 |
| 7.267 | 0.426 | 0.059 |
| 7.351 | 0.396 | 0.051 |
| 7.435 | 0.366 | 0.045 |
| 7.520 | 0.348 | 0.041 |
| 7.604 | 0.327 | 0.038 |
| 7.688 | 0.303 | 0.036 |
| 7.772 | 0.289 | 0.032 |
| 7.857 | 0.281 | 0.031 |
| 7.941 | 0.269 | 0.030 |
| 8.025 | 0.260 | 0.028 |
| 8.109 | 0.250 | 0.027 |
| 8.194 | 0.244 | 0.025 |
| 8.278 | 0.235 | 0.024 |
| 8.362 | 0.231 | 0.024 |
| 8.446 | 0.223 | 0.023 |
| 8.530 | 0.214 | 0.023 |
| 8.699 | 0.204 | 0.021 |
| 8.867 | 0.198 | 0.020 |
| 9.036 | 0.191 | 0.018 |
| 9.204 | 0.182 | 0.017 |

**Continued**

| T (PV) | Br ($C/C_0$) | CNP ($C/C_0$) |
|---|---|---|
| 9.373 | 0.179 | 0.016 |
| 9.541 | 0.170 | 0.016 |
| 9.710 | 0.167 | 0.015 |
| 9.878 | 0.164 | 0.015 |
| 10.046 | 0.163 | 0.014 |
| 10.215 | 0.154 | 0.013 |
| 10.383 | 0.151 | 0.012 |
| 10.552 | 0.148 | 0.012 |
| 10.720 | 0.144 | 0.012 |
| 11.141 | 0.139 | 0.011 |
| 11.547 | 0.134 | 0.010 |
| 11.957 | 0.129 | 0.009 |
| 12.378 | 0.122 | 0.008 |
| 12.799 | 0.118 | 0.007 |
| 13.220 | 0.116 | 0.007 |
| 13.641 | 0.113 | 0.007 |
| 14.063 | 0.109 | 0.006 |
| 14.484 | 0.107 | 0.006 |
| 14.905 | 0.106 | 0.006 |
| 15.326 | 0.102 | 0.006 |
| 15.747 | 0.099 | 0.006 |
| 16.168 | 0.097 | 0.005 |
| 16.589 | 0.096 | 0.005 |
| 17.010 | 0.095 | 0.005 |
| 17.432 | 0.092 | 0.005 |
| 17.853 | 0.091 | 0.005 |
| 18.274 | 0.089 | 0.005 |
| 18.695 | 0.087 | 0.005 |
| 19.116 | 0.086 | 0.004 |
| 19.537 | 0.085 | 0.004 |

APPENDIX B: GRAPHS AND CXTFIT PARAMETERS

**Column Type:** Homogeneous Porous Media
**Experiment Name:** Pulse Test #1

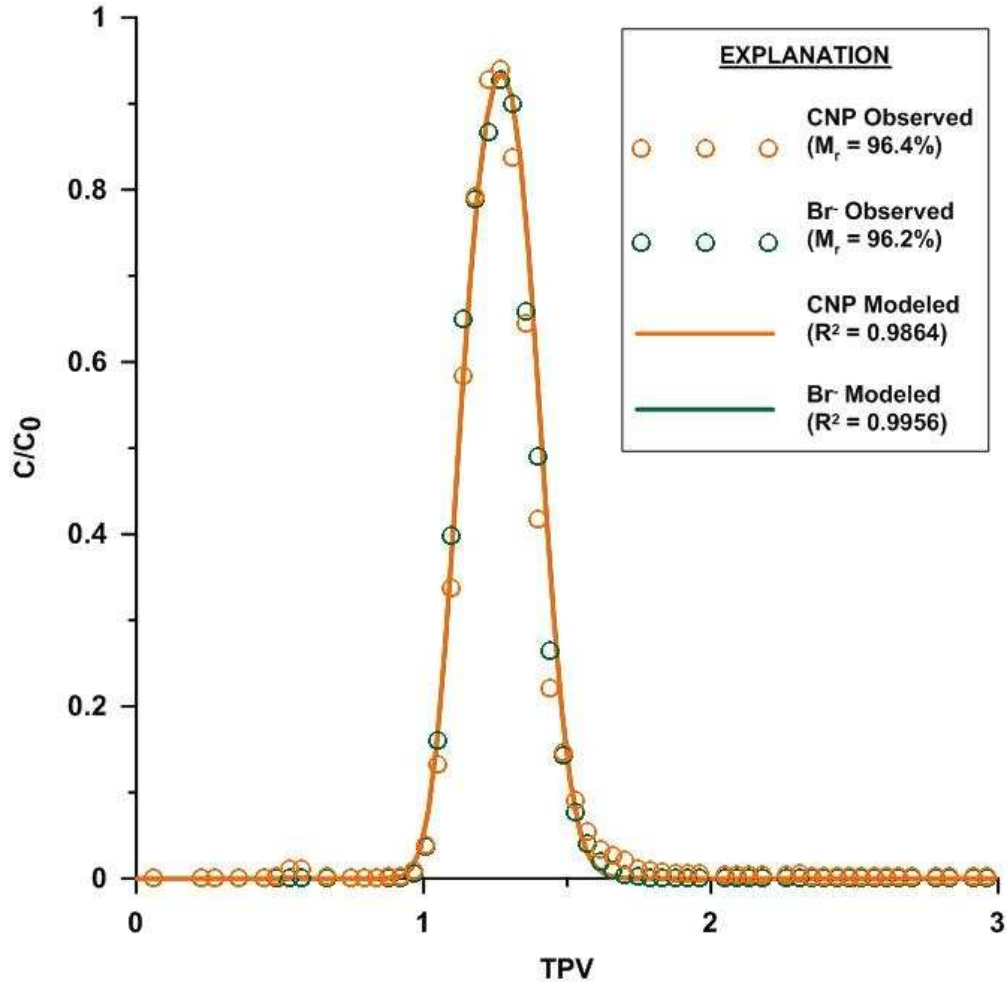


| Fitting Parameters | CNP | | | Br | | |
|---|---|---|---|---|---|---|
| | Value | 95% Confidence Interval | | Value | 95% Confidence Interval | |
| **Dispersion Coefficient, D ($cm^2/s$)** | $2.18X10^{-4}$ | $1.86X10^{-4}$ | $2.49X10^{-4}$ | $2.18X10^{-4}$ | $2.00X10^{-4}$ | $2.37X10^{-4}$ |
| **Retardation Factor, R** | 1.11 | 1.11 | 1.12 | 1.11 | 1.11 | 1.12 |

**Column Type:** Homogeneous Porous Media
**Experiment Name:** Pulse Test #2

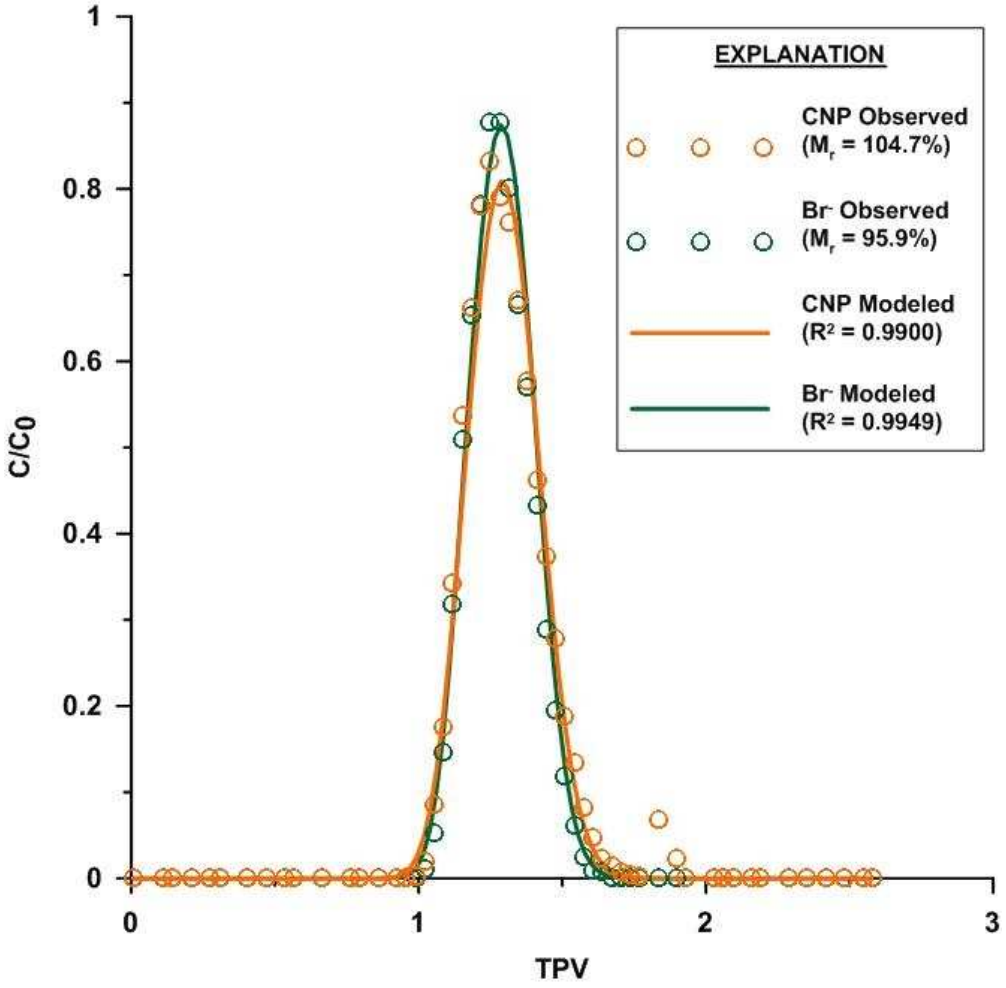


| Fitting Parameters | CNP | | | Br | | |
|---|---|---|---|---|---|---|
| | Value | 95% Confidence Interval | | Value | 95% Confidence Interval | |
| Dispersion Coefficient, D ($cm^2/s$) | $2.36X10^{-4}$ | $2.13X10^{-4}$ | $2.58X10^{-4}$ | $1.74X10^{-4}$ | $1.60X10^{-4}$ | $1.87X10^{-4}$ |
| Retardation Factor, R | 1.16 | 1.15 | 1.16 | 1.15 | 1.15 | 1.16 |

**Column Type:** Homogeneous Porous Media
**Experiment Name:** Step Test

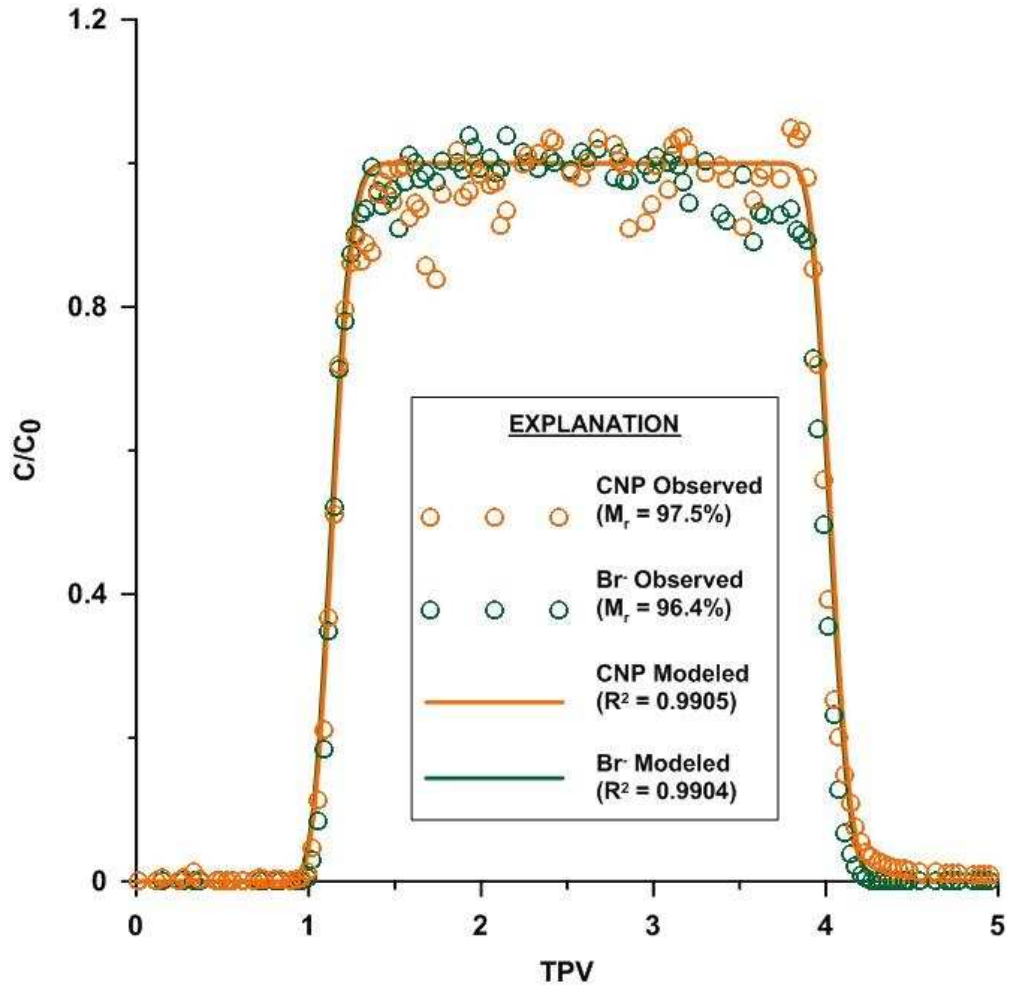


| Fitting Parameters | CNP | | | Br | | |
|---|---|---|---|---|---|---|
| | Value | 95% Confidence Interval | | Value | 95% Confidence Interval | |
| Dispersion Coefficient, D ($cm^2/s$) | $2.89X10^{-4}$ | $2.30X10^{-4}$ | $3.47X10^{-4}$ | $2.85X10^{-4}$ | $2.26X10^{-4}$ | $3.44X10^{-4}$ |
| Retardation Factor, R | 1.14 | 1.13 | 1.14 | 1.13 | 1.12 | 1.14 |

**Column Type:** Dual-Porosity

**Experiment Name:** Design #1, Pulse Test

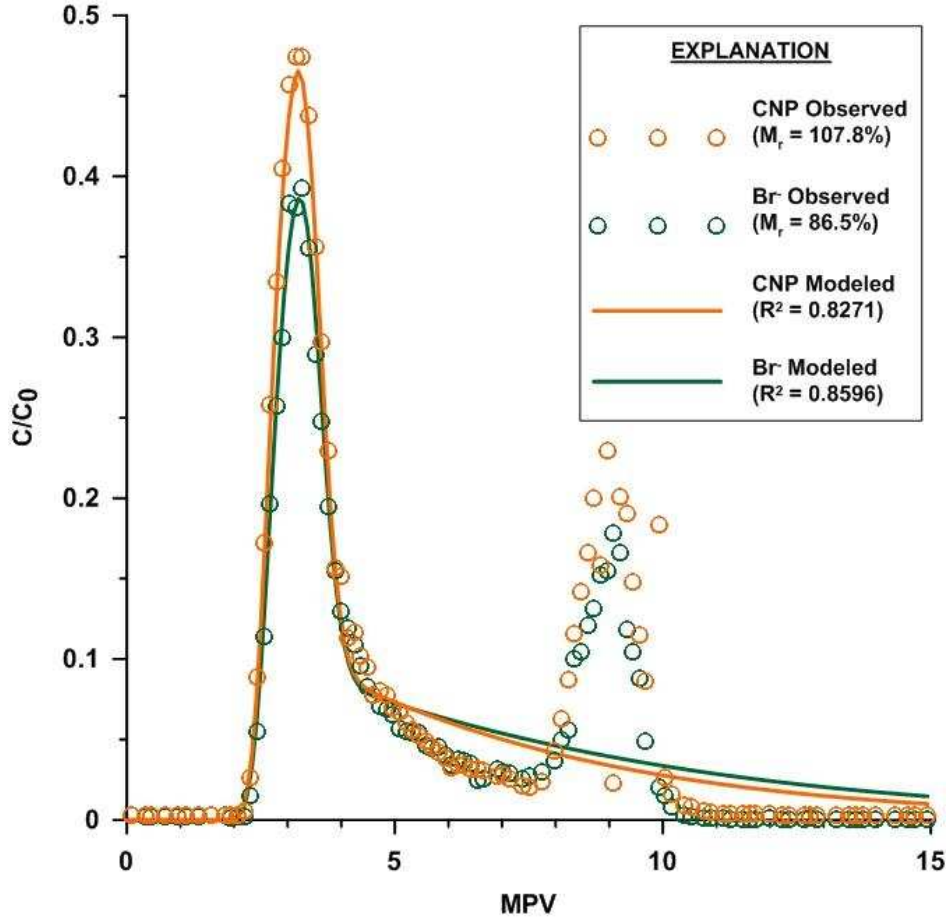


| Fitting Parameters | CNP | | | Br | | |
|---|---|---|---|---|---|---|
| | Value | 95% Confidence Interval | | Value | 95% Confidence Interval | |
| Velocity, v (m/d) | 1.47* | 1.21 | 1.72 | 1.23 | 1.06 | 1.40 |
| Dispersion Coefficient, D ($cm^2/s$) | $2.63X10^{-4}$ | $8.35X10^{-5}$ | $4.42 X10^{-4}$ | $2.37X10^{-4}$ | $1.01X10^{-4}$ | $1.62X10^{-3}$ |
| Retardation Factor, R | 1.00** | --- | --- | 1.00** | --- | --- |
| Partitioning Coefficient, β | 0.50* | 0.42 | 0.58 | 0.42 | 0.37 | 0.48 |
| Mass Transfer Coefficient, ω | 0.80 | 0.66 | 0.94 | 1.00 | 0.88 | 1.13 |

* Could not converge on a reasonable solution without allowing β and v to vary for each

** Set equal to 1 since both CNP and Br were demonstrated to be non-reactive with the silica.

**Column Type:** Dual-Porosity

**Experiment Name:** Design #2, Pulse Test

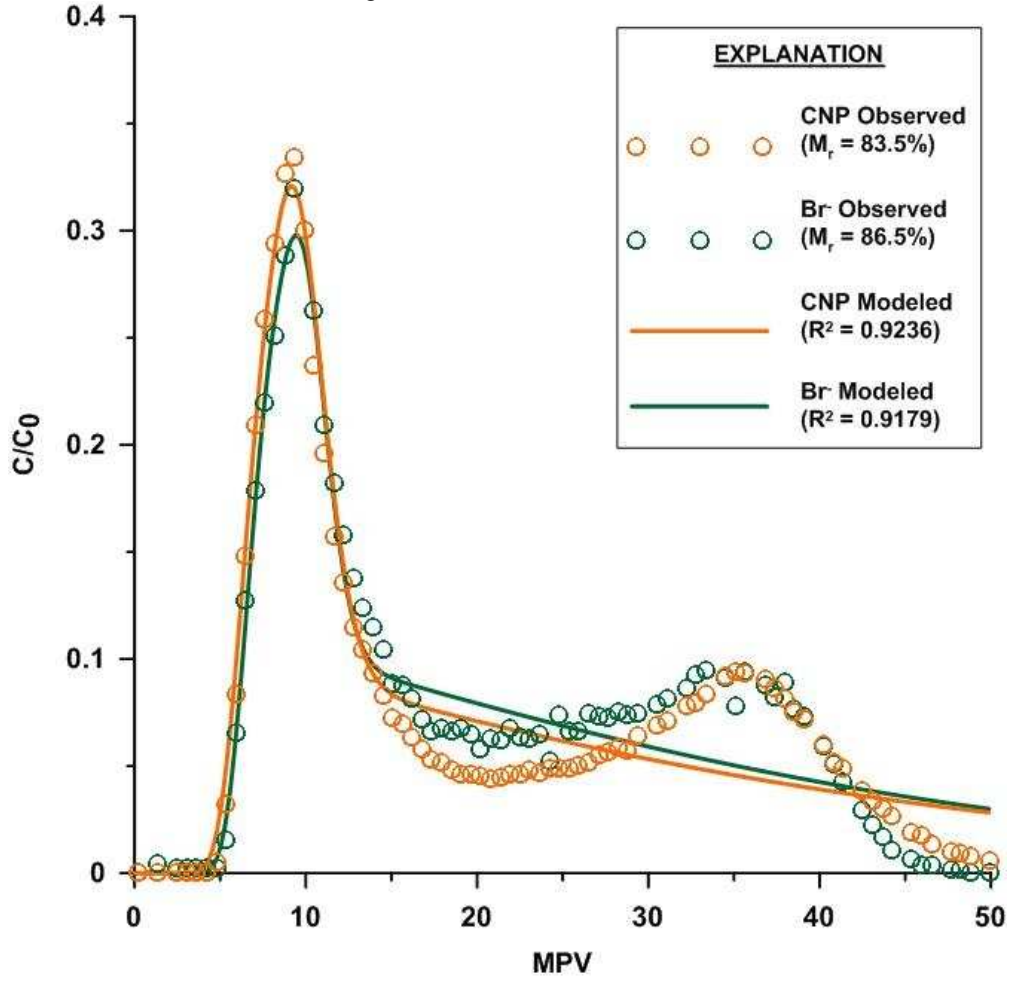


| Fitting Parameters | CNP | | | Br | | |
|---|---|---|---|---|---|---|
| | Value | 95% Confidence Interval | | Value | 95% Confidence Interval | |
| Dispersion Coefficient, D ($cm^2/s$) | $6.95X10^{-4}$ | $5.24X10^{-4}$ | $8.66X10^{-4}$ | $4.76X10^{-4}$ | $3.17X10^{-4}$ | $6.35X10^{-4}$ |
| Retardation Factor, R | 1.00* | --- | --- | 1.00* | --- | --- |
| Partitioning Coefficient, β | 0.26** | --- | --- | 0.26** | --- | --- |
| Mass Transfer Coefficient, ω | 1.20 | 1.13 | 1.27 | 1.37 | 1.29 | 1.44 |

* Set equal to 1 since both CNP and Br were demonstrated to be non-reactive with the silica.

** Converged values of CNP and Br were averaged and set as known for subsequent runs.

**Column Type:** Dual-Porosity

**Experiment Name:** Design #3, Pulse Test #1

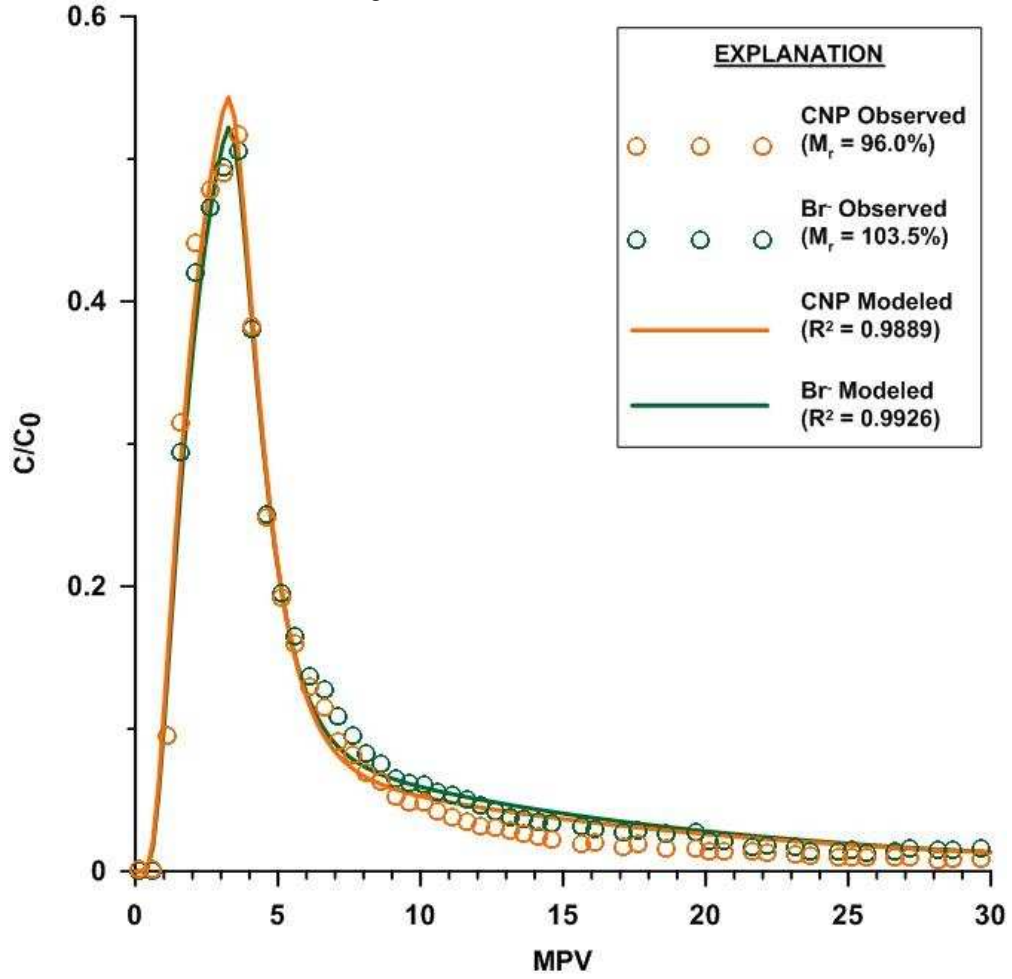


| Fitting Parameters | CNP | | | Br | | |
|---|---|---|---|---|---|---|
| | Value | 95% Confidence Interval | | Value | 95% Confidence Interval | |
| Dispersion Coefficient, D ($cm^2/s$) | $1.87X10^{-2}$ | $1.75X10^{-2}$ | $2.00X10^{-2}$ | $1.76X10^{-2}$ | $1.66X10^{-2}$ | $1.86X10^{-2}$ |
| Retardation Factor, R | 1.00* | --- | --- | 1.00* | --- | --- |
| Partitioning Coefficient, β | 0.29** | --- | --- | 0.29** | --- | --- |
| Mass Transfer Coefficient, ω | 0.58 | 0.55 | 0.61 | 0.65 | 0.63 | 0.68 |

* Set equal to 1 since both CNP and Br were demonstrated to be non-reactive with the silica.

** Converged values of CNP and Br were averaged and set as known for subsequent runs.

**Column Type:** Dual-Porosity

**Experiment Name:** Design #3, Pulse Test #2

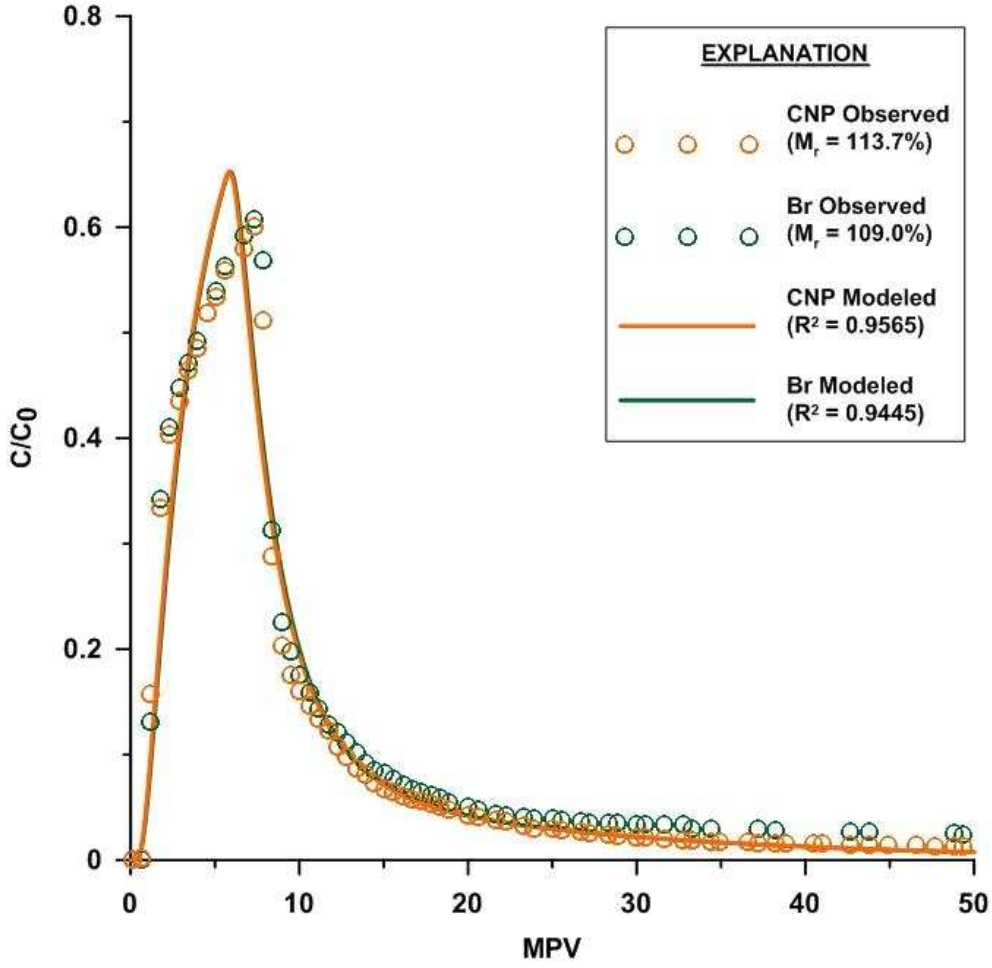


| Fitting Parameters | CNP | | | Br | | |
|---|---|---|---|---|---|---|
| | Value | 95% Confidence Interval | | Value | 95% Confidence Interval | |
| **Dispersion Coefficient, D ($cm^2/s$)** | $2.61X10^{-2}$ | $2.26X10^{-2}$ | $2.96X10^{-2}$ | $2.42X10^{-2}$ | $2.03X10^{-2}$ | $2.81X10^{-2}$ |
| **Retardation Factor, R** | 1.00* | --- | --- | 1.00* | --- | --- |
| **Partitioning Coefficient, β** | 0.53** | --- | --- | 0.53** | --- | --- |
| **Mass Transfer Coefficient, ω** | 0.29 | 0.20 | 0.38 | 0.28 | 0.18 | 0.39 |

* Set equal to 1 since both CNP and Br were demonstrated to be non-reactive with the silica.

** Converged values of CNP and Br were averaged and set as known for subsequent runs.

**Column Type:** Dual-Porosity

**Experiment Name:** Design #4, Pulse Test #1

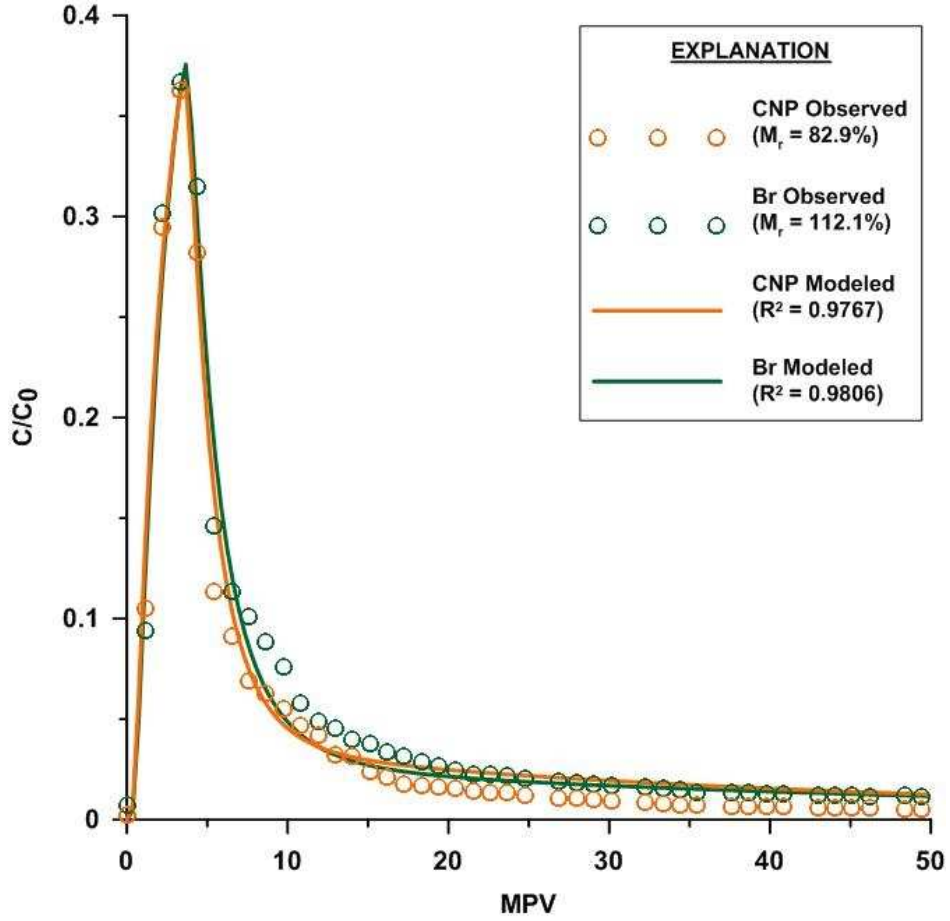


| Fitting Parameters | CNP | | | Br | | |
|---|---|---|---|---|---|---|
| | Value | 95% Confidence Interval | | Value | 95% Confidence Interval | |
| Dispersion Coefficient, D ($cm^2/s$) | $4.50X10^{-2}$ | $4.20X10^{-2}$ | $4.80X10^{-2}$ | $4.02X10^{-2}$ | $3.78X10^{-2}$ | $4.25X10^{-2}$ |
| Retardation Factor, R | 1.00* | --- | --- | 1.00* | --- | --- |
| Partitioning Coefficient, β | 0.21** | --- | --- | 0.21** | --- | --- |
| Mass Transfer Coefficient, ω | 1.63 | 1.43 | 1.83 | 1.24 | 1.10 | 1.39 |

* Set equal to 1 since both CNP and Br were demonstrated to be non-reactive with the silica.

** Converged values of CNP and Br were averaged and set as known for subsequent runs.

**Column Type:** Dual-Porosity

**Experiment Name:** Design #4, Pulse Test #2

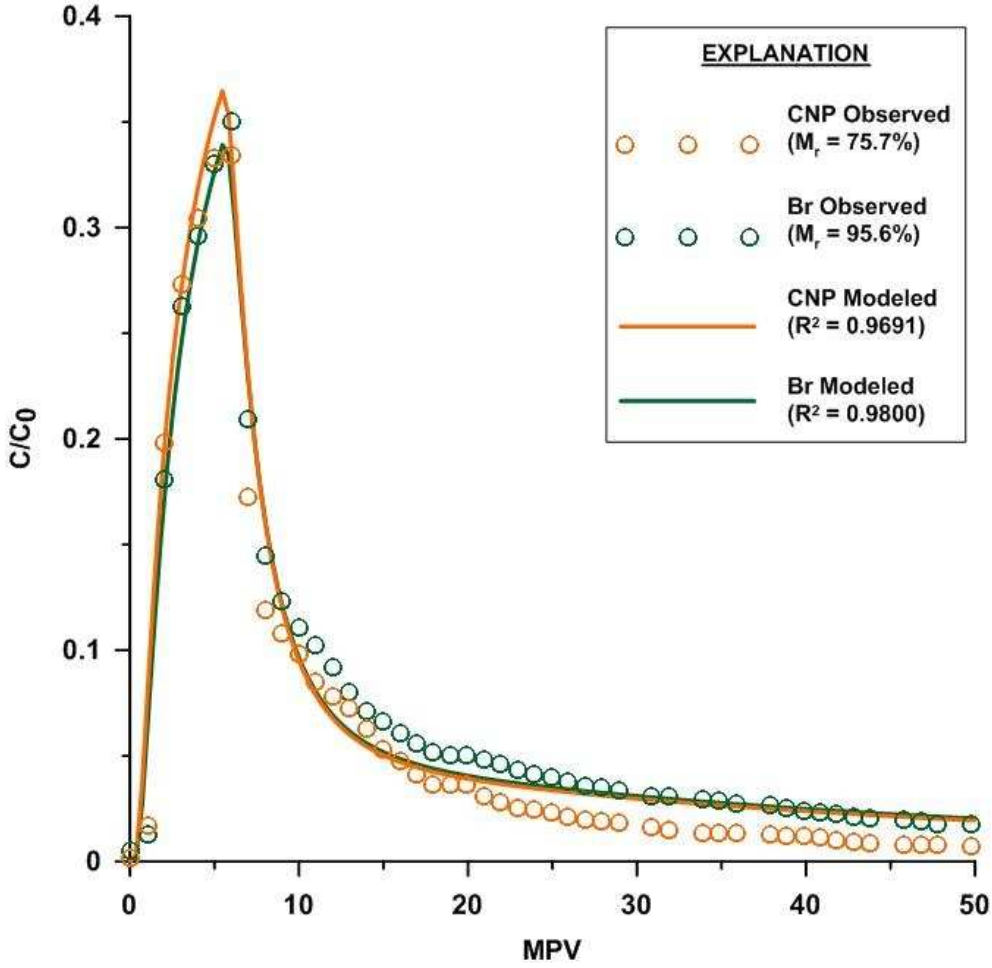


| Fitting Parameters | CNP | | | Br | | |
|---|---|---|---|---|---|---|
| | Value | 95% Confidence Interval | | Value | 95% Confidence Interval | |
| **Dispersion Coefficient, D ($cm^2/s$)** | $4.93X10^{-2}$ | $4.54X10^{-2}$ | $5.31\ X10^{-2}$ | $4.38X10^{-2}$ | $4.11X10^{-2}$ | $4.64X10^{-2}$ |
| **Retardation Factor, R** | 1.00* | --- | --- | 1.00* | --- | --- |
| **Partitioning Coefficient, β** | 0.26** | --- | --- | 0.26** | --- | --- |
| **Mass Transfer Coefficient, ω** | 4.46 | 3.70 | 5.21 | 4.59 | 4.00 | 5.18 |

* Set equal to 1 since both CNP and Br were demonstrated to be non-reactive with the silica.

** Converged values of CNP and Br were averaged and set as known for subsequent runs.

**Column Type:** Dual-Porosity
**Experiment Name:** Design #3, Interruption Test

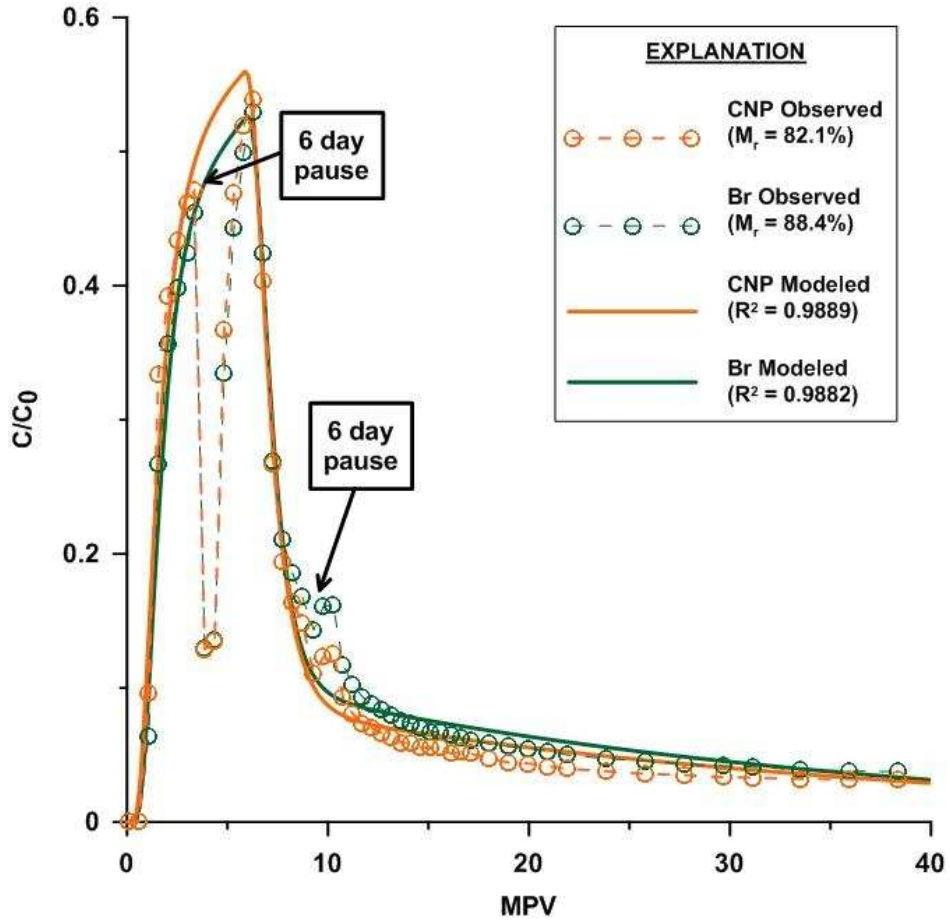


| Fitting Parameters | CNP | | | Br | | |
|---|---|---|---|---|---|---|
| | Value | 95% Confidence Interval | | Value | 95% Confidence Interval | |
| Dispersion Coefficient, D ($cm^2/s$) | $6.86X10^{-3}$ | $6.11X10^{-3}$ | $7.60X10^{-3}$ | $5.23X10^{-3}$ | $4.61X10^{-3}$ | $5.86X10^{-3}$ |
| Retardation Factor, R | 1.00* | --- | --- | 1.00* | --- | --- |
| Partitioning Coefficient, β | 0.13** | --- | --- | 0.13** | --- | --- |
| Mass Transfer Coefficient, ω | 0.77 | 0.73 | 0.81 | 0.86 | 0.82 | 0.90 |

* Set equal to 1 since both CNP and Br were demonstrated to be non-reactive with the silica.
** Converged values of CNP and Br were averaged and set as known for subsequent runs.

**Column Type:** Dual-Porosity

**Experiment Name:** Design #3, Long-Term Test

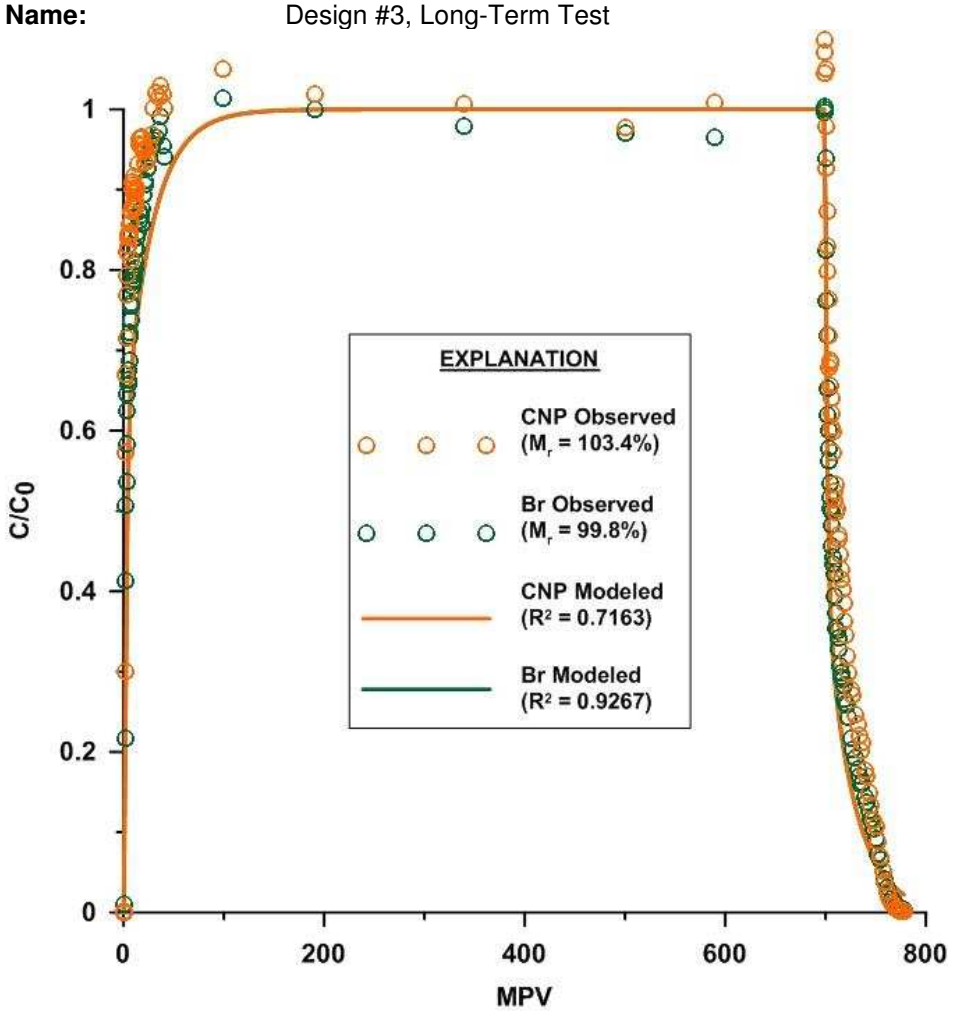


| Fitting Parameters | CNP | | | Br | | |
|---|---|---|---|---|---|---|
| | Value | 95% Confidence Interval | | Value | 95% Confidence Interval | |
| **Dispersion Coefficient, D ($cm^2/s$)** | $1.72X10^{-2}$ | $4.15X10^{-3}$ | $3.01X10^{-2}$ | $1.69X10^{-3}$ | $1.08X10^{-2}$ | $2.31X10^{-2}$ |
| **Retardation Factor, R** | 1.00* | --- | --- | 1.00* | --- | --- |
| **Partitioning Coefficient, β** | 0.13** | --- | --- | 0.13** | --- | --- |
| **Mass Transfer Coefficient, ω** | 0.51 | 0.26 | 0.76 | 0.50 | 0.38 | 0.61 |

* Set equal to 1 since both CNP and Br were demonstrated to be non-reactive with the silica.

** Converged values of CNP and Br were averaged and set as known for subsequent runs.

**Column Type:** Reactive Porous Media
**Experiment Name:** Design #1, Pulse Test

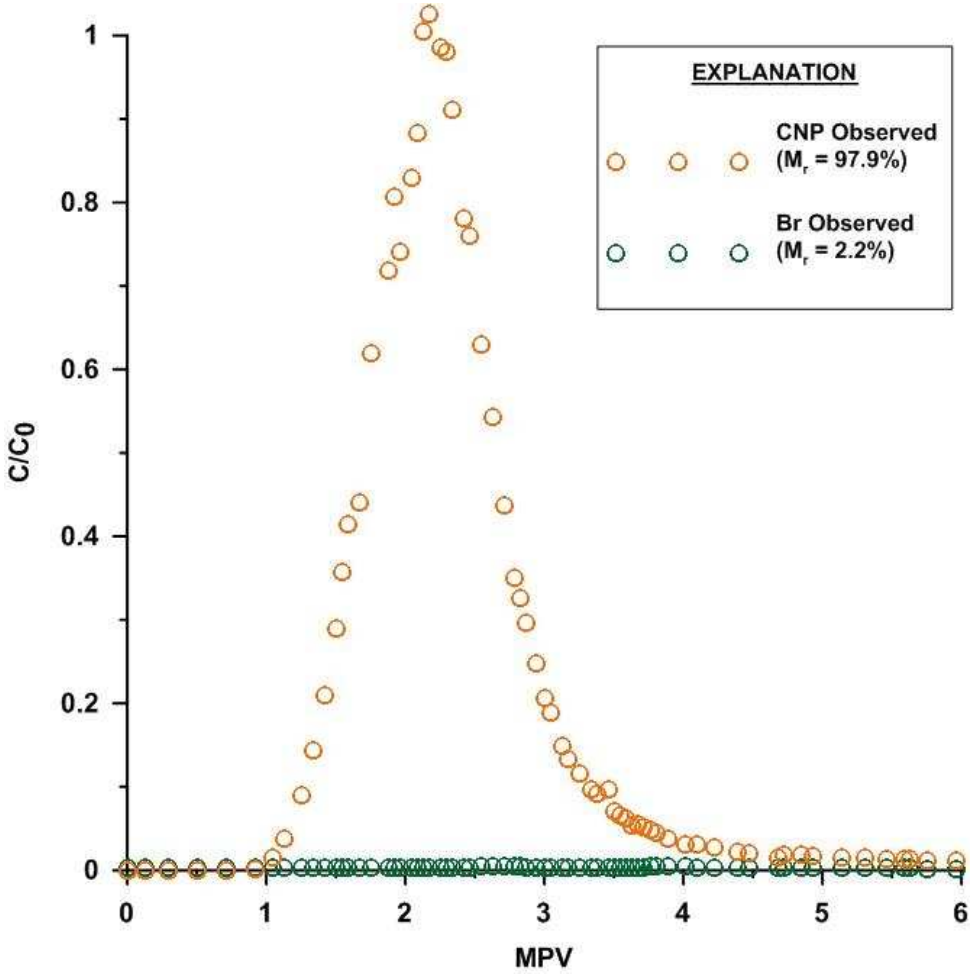


Could not be modeled

**Column Type:** Reactive Porous Media

**Experiment Name:** Design #2, Pulse Test #1

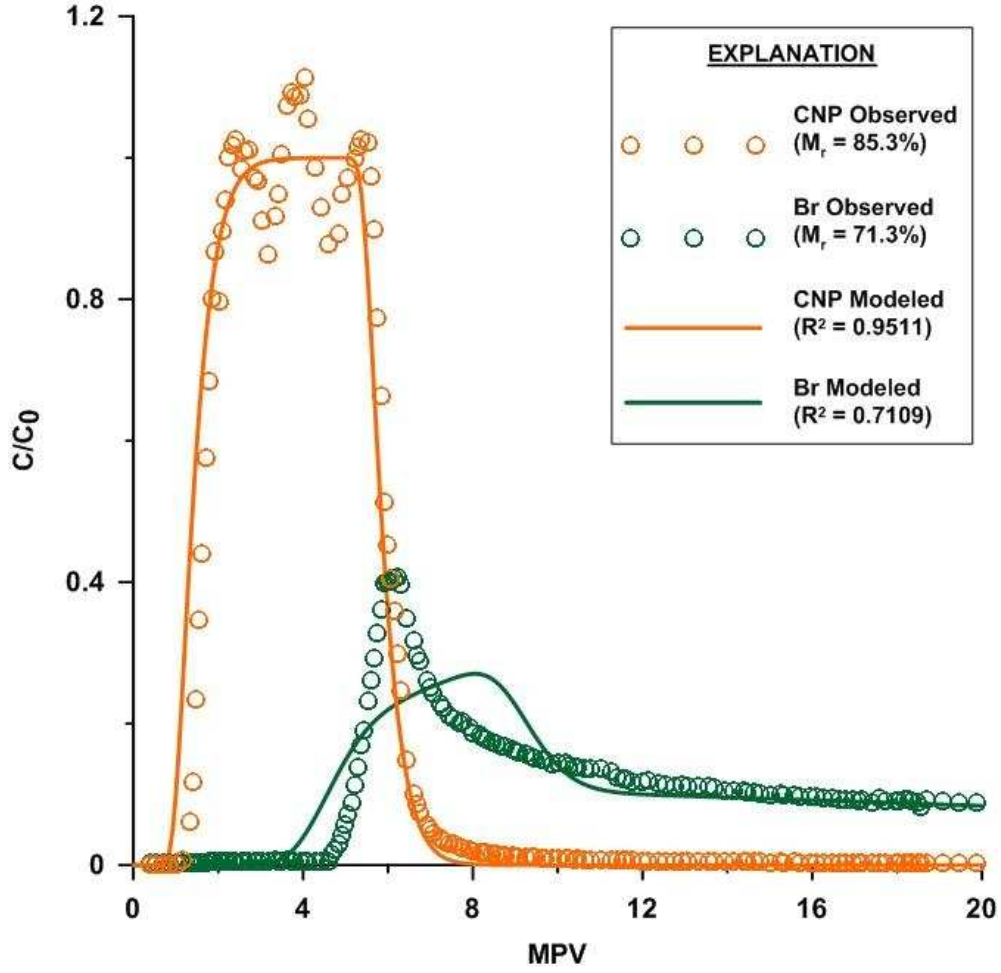


| Fitting Parameters | CNP | | | Br | | |
|---|---|---|---|---|---|---|
| | Value | 95% Confidence Interval | | Value | 95% Confidence Interval | |
| Dispersion Coefficient, D ($cm^2/s$) | $1.95X10^{-4}$* | --- | --- | $1.95X10^{-4}$* | --- | --- |
| Retardation Factor, R | 1.13 | 1.09 | 1.17 | 20.76 | 18.31 | 23.21 |
| Partitioning Coefficient, β | 0.77** | --- | --- | 0.18 | 0.16 | 0.20 |
| Mass Transfer Coefficient, ω | 1.72 | 0.87 | 2.57 | 1.65 | 1.54 | 1.75 |

* Set equal to the average of D from the homogeneous tests multiplied the factor of $\theta_m/\theta$.

** Value was set equal to the calculated β (as $\theta_m/\theta$) since CNP was shown to be non-reactive

**Column Type:** Reactive Porous Media

**Experiment Name:** Design #2, Pulse Test #2

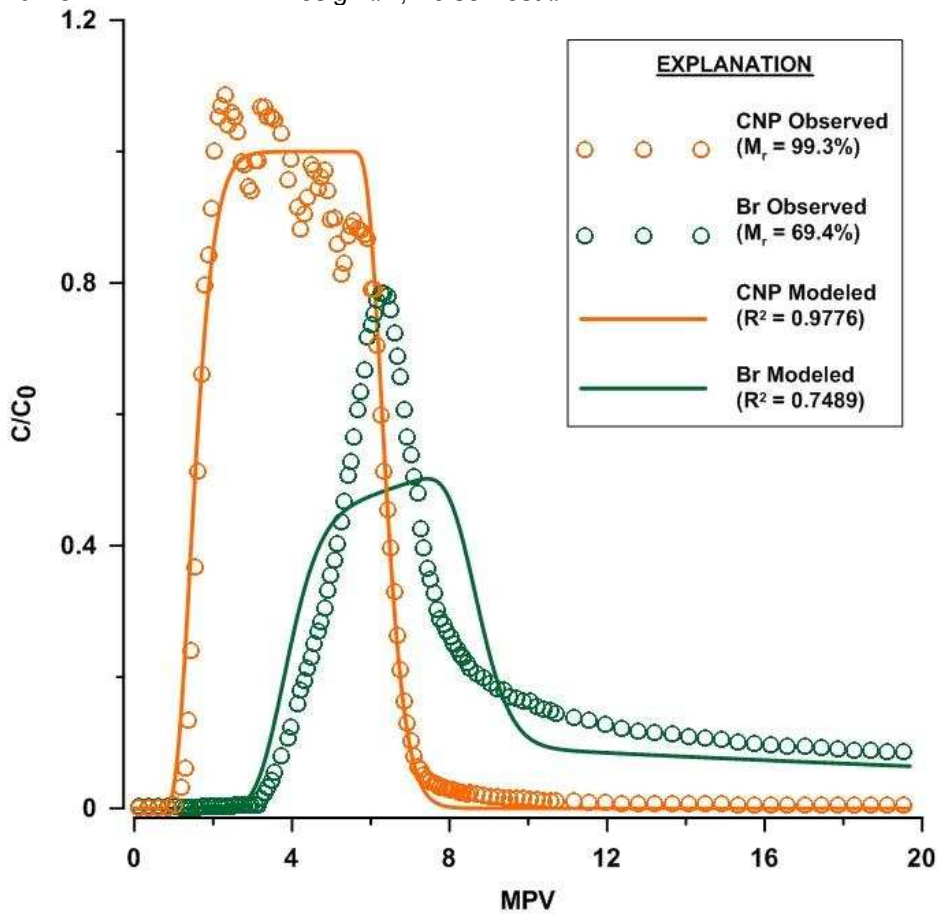


| Fitting Parameters | CNP | | | Br | | |
|---|---|---|---|---|---|---|
| | Value | 95% Confidence Interval | | Value | 95% Confidence Interval | |
| **Dispersion Coefficient, D ($cm^2/s$)** | $1.95X10^{-4}$* | --- | --- | $1.95X10^{-4}$* | --- | --- |
| **Retardation Factor, R** | 1.21 | 1.19 | 1.24 | 13.87 | 7.69 | 20.06 |
| **Partitioning Coefficient, β** | 0.77** | --- | --- | 0.22 | 0.13 | 0.31 |
| **Mass Transfer Coefficient, ω** | 3.00*** | 1.71 | 4.29 | 0.85 | 0.73 | 0.96 |

* Set equal to the average of D from the homogeneous tests multiplied the factor of $\theta_m/\theta$.

** Value was set equal to the calculated β (as $\theta_m/\theta$) since CNP was shown to be non-reactive

*** Value arbitrary (defaulted to the maximum allowed ω, but model was insensitive to ω)

# LIST OF ABBREVIATIONS

| | |
|---|---|
| ADE | advection-dispersion equation |
| Ag | silver |
| Br | bromide |
| BTCs | breakthrough curves |
| CNP | carbon nanospheres |
| DI | deionized |
| $Fe^0$ | zero-valent iron |
| ID | inner diameter |
| ISE | ion selective electrode |
| KBr | potassium bromide |
| MPV | mobile pore volumes |
| NP | nanoparticles |
| NPT | National Pipe Thread |
| OD | outer diameter |
| PTFE | polytetrafluoroethylene |
| PV | pore volumes |
| TPV | total pore volumes |
| Zn | zinc |